SCUOLA DI DOTTORATO

UNIVERSITÀ DEGLI STUDI DI MILANO-BICOCCA

Department of

Environmental and Earth Science

PhD program Chemical, Geological and Environmental Science Cycle XXXI

Curriculum in Chemical Science

FROM HIGH-PRESSURE TO IN-SITU POLYMERIZATION: DESIGN AND SYNTHESIS, NEW CHALLENGING OF POROUS MATERIALS

Surname Piga Name Daniele

Registration number 770771

Tutor: Prof. Angiolina Comotti

Coordinator: Prof. Maria Luce Frezzotti

ACADEMIC YEAR 2018/2019

Contents

Introduction 1

1| Porous Materials 4

1.1| A brief history 4

1.2| Classification 5

1.3| Inorganic porous materials 7

1.3.1| Zeolites 7

1.3.2| Mesoporous silica 10

1.4| Hybrid organic-inorganic porous materials 11

1.4.1| Organosilica 11

1.4.2| Metal Organic Frameworks (MOFs) 14

1.5| Organic porous materials 17

1.5.1| Porous carbons 17

1.5.2| Porous Organic Polymers (POPs) 19

1.5.3| Porous organic molecules 26

References 29

2| Porous Materials for gas adsorption and storage 33

2.1| Definitions 34

2.2| Isotherms 35

2.3| Surface area 38

2.3.1| Langmuir model 39

2.3.2| BET model 40
2.4| Density Functional Theory (DFT) 42
2.5| Isosteric heat of adsorption 43
2.6| Selectivity 44
2.7| High-pressure adsorption 46
2.8| Porous materials for methane storage 47
2.8.1| Experimental 49
2.8.2| Results and discussion 53
2.9| Porous materials for gas adsorption 72
2.9.1| Experimental 73
2.9.2| Result and discussion 76
2.10| Conclusion 87
References 89
3| Porous Materials for confined polymerization 92
3.1| An overview to confined polymerization 93
3.1.1| Confined polymerization in porous organic molecules 93
3.1.2| Polymerization in mesoporous silica 95
3.1.3| Confined polymerization in Zeolites 97
3.1.4| Polymerization in MOFs 97
3.1.5| Confined polymerization in PAFs 99
3.2| Anionic polymerization in PAFs 99
3.2.1| No-anchored polymerization 101

3.2.2| Anchored polymerization.....107

3.3| Thermal evolution of polyacrylonitrile in nanochannels MOFs 118

3.3.1| Experimental part.....120

3.3.2| Results and discussion 122

3.4| Conclusion.....136

References.....139

Conclusion 142

Introduction

In the field of materials science, the properties and possible applications of many materials depend on the structure. A category of materials in which the structure is of fundamental importance is that of porous systems; such systems have very high surface areas and pores with diameters of the order of the nanometer, these characteristics give the structures interesting properties.

Studies on this type of material have been carried out for several decades and it have mainly focused on obtaining porous structures of different nature having geometries and dimensions that are sought based on the applicative purposes of interest. The porous materials are possible applications in many fields: in the purification of the water, in the heterogeneous catalysis, in the capture, separation and storage of gas; in the delivery of drugs; in modern batteries or as matrices for confined state reactions and preparation of composites/nanocomposites.

In particular, the interaction of these materials with gaseous species is one of the studies widely pursued and consists of one of the objectives of great importance, as it concerns environmental and energy issues and problems. In recent years, there has been a lot of talk about global warming due to greenhouse gases and in particular, the decrease in carbon dioxide emissions or the use of alternative sources with low environmental impact or low carbon dioxide emissions. Being a current topic, the researchers has focused on these aspects, and porous systems can be good materials for selective CO_2 capture or for the storage of combustible gases that reduce emissions such as H_2 and CH_4.

Another aspect that has interested scientists in recent years is the search for systems that can control the progress of reactions without the use of catalysts, as occurs in living organisms thanks to enzymes. This field of research is quite wide, since the ways to control the reactions are many. However, even in this sector the porous materials are catching on for their ability to contain the molecules inside them, forcing them into narrow spaces that decrease the degrees of freedom by preventing some movements that they would otherwise have in solution, in the same way that enzymes intervene in organisms.

In particular, it has been widely studied how porous materials can affect the growth and the final properties of the polymers. This is because polymeric materials have found more applications from their discovery until today and this has led to the development of the science of such materials. The use of porous materials as reactors for controlled growth of polymers precludes the use of catalysts, which are expensive and not recyclable unlike porous materials. Furthermore, the confinement of polymer chains allows the study and modification of polymers in conditions that would not occur with conventional techniques.

After having made these premises, the work developed on porous materials in two different areas, gas adsorption and confined polymerizations will be described below. In particular, porous materials will be explained in a general way with their differences and their characteristics. Subsequently, some basic concepts will be described in the study of porous materials for the adsorption of gas and the first part of the work will be presented. Which consists in the development of low-cost porous materials for the storage of high-pressure CH_4 and the structural modification of porous materials in order to increase affinity with different gases. In a second part, the use of porous materials for the control of the growth and properties of polymers will be described. With the development of a new and innovative technique that has never been studied before and how porous materials can also be used as fillers inside of the polymer or as a support for the structural modification

of the polymer chains in order to obtain innovative and more performing materials than the existing ones.

1| Porous Materials

1.1| A brief history

The history of porous materials began from the discovery of the first zeolite mineral in 1756 by the Swedish mineralogist Axel F. Cronstedt; he was the first scientist to describe the distinctive property of zeolites. In the 1756 a paper titled “Observation and description of an unknown mineral species, called zeolite” [1] by Cronstedt described a new type of hydrated mineral showing unique frothing features when heated in a blow-pipe flame was described and a novel name recalling this property, *zeolite*, was coined for it, from the Greek zéō (boil) and lìthos (stone). In this paper, Cronstedt described three zeolite types named in Latin: *particulis impalpabilibus*, *spatosus* and *crystallisatus* [2].

In 1862, the French chemist Sainte-Claire Deville studied the composition of natural alkaline silicates and aluminosilicates; he published a paper entitled “Reprodution of the Lévyne” [3], in this paper he found that mixing sodium or potassium aluminate and silicate provided alkaline aluminosilicates analogous to natural zeolites.

In 1896 Friedel developed the idea that the structure of dehydrated zeolites consists of open spongy frameworks after observing that various liquids were occluded by dehydrated zeolites [4]. In

1910 Grandjean observed that dehydrated chabazite adsorbs ammonia, air, hydrogen and other molecules [5], and in 1925 Weigel and Steinhoff reported the first molecular sieve effect [6]. They noted that dehydrated chabazite rapidly adsorbed various liquids such as water, methanol, ethanol and formic acid but essentially excluded acetone ether or benzene. In the 1932, McBain established the term "molecular sieve" to define porous solid materials that act as sieves on a molecular scale [7].

Thus, by the mid-1930s the literature described the ion exchange, adsorption, molecular sieving and structural properties of zeolite minerals as well as a number of reported syntheses of zeolites.

From 1930 until today, the world of porous materials has expanded, especially through the applications that such systems have found with the industrialization and development of new technologies. Consequently, the researchers have focused their interests on porous materials, placing attention to the study and design of different materials in terms of both the chemical and the structural, to meet different needs and expand the use of porous systems.

1.2| Classification

Porous systems can be divided into various groups based on the average diameter or type of pore structure and based on the chemical nature of the pore wall. The different classifications focus on one aspect in particular and are therefore independent of each other.

The IUPAC nomenclature subdivides the nanoporous materials [8], i.e. with pores between 1 nm and 100 nm, in:

- microporous materials (pore diameter less than 2 nm);
- mesoporous materials (pores diameter between 2 nm and 50 nm);

- macroporous materials (pore diameter greater than 50 nm).

The pores of the material may have different types of accessibility and shape, as regards the accessibility, a pores can be distinguished in closed, open, blind and through pores, instead as regards the shape, a pores can be cylindrical open, cylindrical blind, ink-bottle shaped, funnel shaped and roughness.

The voids of the material can be structured according to different geometries: they can be isolated cavities, parallel channels or three-dimensional structure containing interconnected pores. Considering the spatial extension of the empty spaces, it is possible to classify the materials as:

- zero-dimensional systems: confined on a nanometer scale in all three dimension. Generally, they have spherical cavities connected to each other by accessible channels.
- mono-dimensional systems: they have one of the three directions of greater than nanometer order.
- bi-dimensional systems: they have only one dimension on a nanometric scale.
- three-dimensional systems: they not have a confinement on a nanometric scale. The systems of pores are extended in all directions.

A further subdivision is that which differentiates systems with permanent and non-permanent porosity. To the first belong those materials that maintain the ordered and porous structure after the removal of the templating agent or the solvent. The materials with non-permanent porosity if crystallized in suitable conditions have polymorphic structures containing solvent the removal of the guest generate a collapse of the porous structure.

Porous materials can also be classified into crystalline and amorphous, crystalline systems have a high order regarding shape, spatial distribution and pore shape, but crystalline is not a necessary condition for a high porosity; in fact, there are several examples of amorphous systems that possess a high porosity.

The porous materials can also be classified in according to the chemical nature of the walls of materials:

- Inorganic systems (mesoporous silica, zeolites);
- Hybrid systems (organosilica, metal organic frameworks);
- Organic systems (porous carbons, porous organic polymers).

Then the various types of porous materials will be described, dividing them according to this last type of classification.

1.3| Inorganic porous materials

1.3.1| Zeolites

As previously mentioned, the zeolites are the first porous materials discovered and studied. The zeolites are a class of crystalline aluminosilicates based on rigid anionic frameworks with well-defined pores, which intersect at cavities. These cavities contain exchangeable metal cations. The general formula for the composition of zeolite is $M_{x/n}\left[(AlO_2)_x(SiO_2)_y\right] mH_2O$ where cations M of valence n neutralize the negative charge on the aluminosilicate frameworks.

The primary building units of zeolites are $[SiO_4]^{4-}$ and $[AlO_4]^{5-}$ tetrahedral linked together by corner sharing, forming oxygen bridges. The Si/Al—O—Si/Al linkage is very flexible and the angle can vary between 120° and 180°. The presence of Al in the tetrahedral linked creates an electrical imbalance compensated by cations in the cavities. The possibility for the tetrahedral to link by two, three, or all corners generate a variety of different structures. The linked tetrahedral are

simply represented by a hexagon (called 6-ring), where the sides are the unit Si/Al—O—Si/Al (Fig. 1.1).

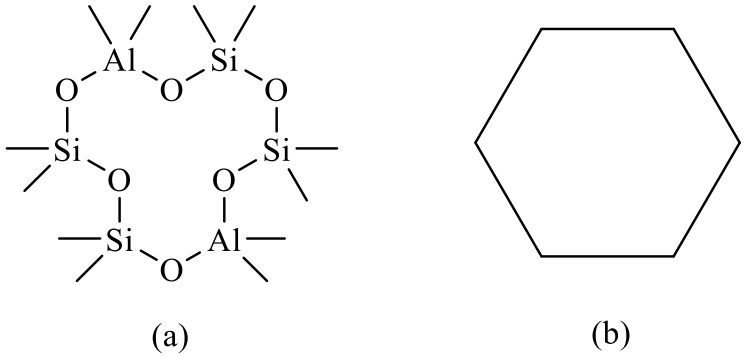

Figure 1.1 (a) 6-ring containing two Al and four Si atoms, (b) hexagonal rapresentation.

The secondary building units of zeolites consists of 24 silica or alumina tetrahedral linked together, in this structure are present 4- and 6-rings linked together to form a basket-like structure called the sodalite unit (also known as the β-cage), with the shape of a truncated octahedron (Fig. 1.2). Several of the most important zeolite structures are based on the sodalite unit.

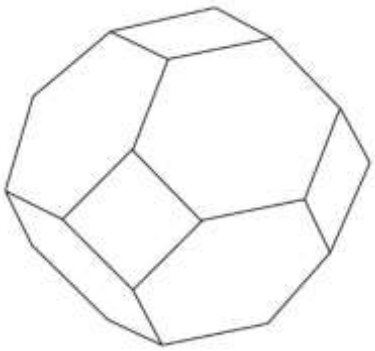

Figure 1.2. Sodalite unit or β-cage.

The name sodalite unit from to the mineral sodalite, this mineral is composed of these units, where each 4-ring shared directly by two β-cage (Fig. 1.3). In this three-dimensional structure, the tetrahedral is situated at the intersection of four lines because oxygen bridges are made by corner sharing from all four vertices of the tetrahedron. Sodalite is a highly symmetrical structure and the cavities link together to form channels and pores, which is parallel to all three cubic crystal axes. This is the simplest zeolites structure; in other zeolites, the sodalite units are stacked in a primitive array,

but they are linked by oxygen bridges between the 4-rings or 6-rings. A three-dimensional framework of linked cavities each with a truncated cuboctahedron shape, as in the zeolites A, X and Y (Fig. 1.4).

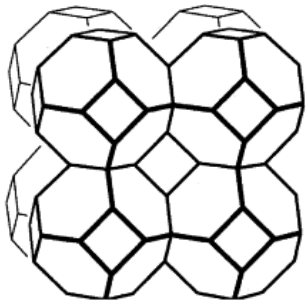

Figure 1.3. Sodalite zeolite.

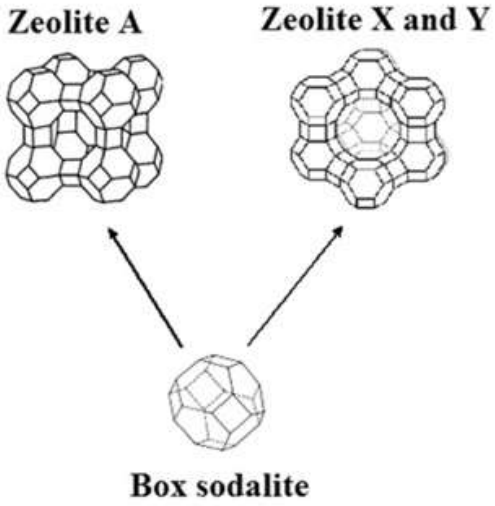

Figure 1.4. Structure of zeolites A, X and Y.

The zeolite structure obtained is determined by the synthesis conditions, such as temperature, pH, time and mechanical movement. This was discovered through the pioneering work of Barrer [9], in a systematic study Barrer prepared the zeolites using reactive silica and alumina reagents, under hydrothermal conditions, at high pH. A gel forms by a process of copolymerization of the silicate and aluminate ions, then the gel is heated gently in an autoclave for several days, generating a condensed zeolite.

The formation of novel zeolites was performed by the use of templates, such as quaternary ammonium salt, the aluminosilicate framework condenses around this large cation, which can subsequently be removed by thermal composition.

1.3.2| Mesoporous silica

In early 1990's, mesoporous silica has attracted special attention after the discovery of a new family of molecular sieves as MCM-41, but the first mesoporous silica was patented around 1970 [10]. The common mesoporous silica materials have a pore size ranging from 2 – 10 nm and 2D-hexagonal and 3D-cubic structural characteristics [11]. The manageable synthesis protocol, outstanding mesoporous structure and surface with silanol groups make mesoporous silica have unique properties, as high pore volume, large surface area, low mass density, easily modified of surface, biocompatibility, uniform and tunable pore size varying the surfactants [12].

The mesoporous silica is synthetized in the presence of assembled cationic surfactant micelle templates, which serve as structure-directing agents for polymerizing silica constituent by electrostatic interactions. The rate of hydrolysis, the level of interaction between assembled template and silica polymer and the condensation of silica source are the variables to control the size and morphology of mesoporous silica, through the controlling of pH, using different templates and co-solvent [13]. The pore size are control of amount of silica source and surfactant and of packing capacity of surfactant. The aggregation of surfactant in solution depend on pH, concentration of the solution and temperature (Fig. 1.5), the mesoporous materials are synthetized at both acid and basic solution with different pore structure. The selection of surfactant with different hydrophobic chain length plays an important role in production of desired pore size [14].

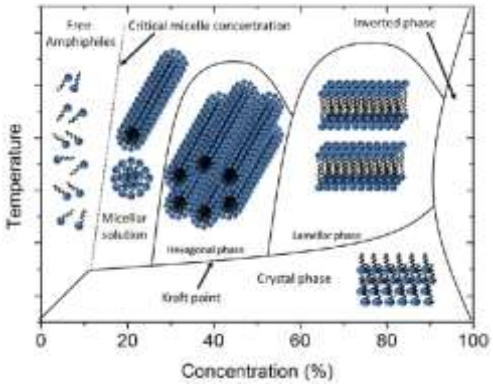

Figure 1.5. Phase diagram of surfactant.

1.4| Hybrid organic-inorganic porous materials

1.4.1| Organosilica

The combination of the properties of organic and inorganic systems in a single material is particularly attractive from the scientists, because is possible to combine the enormous functional variation of organic chemistry with the advantages of thermal stability and robust substrate. The symbiosis of organic and inorganic components can lead to materials whose properties differ significantly from those of their individual and isolated components.

Adjustment of the polarity of surfaces of an inorganic matrix by addition of organic component extends the range which can be used the materials, equally interesting is the modification with organic functionalization.

Three pathways are available for the synthesis of porous organosilica [15]:

- grafting, where the pores surface of mesoporous silica is modification with organic molecules;
- co-condensation, where the simultaneous condensation of corresponding silica and organosilica precursors;
- preparation of periodic mesoporous organosilica (PMOs), where the organic groups is incorporated as bridging components directly into the pore walls by using of bissilyl organo compounds.

The grafting and co-condensation generating hybrid materials where the organic compounds are inside to the pores. Instead, in the case of the PMOs the organic compounds are incorporated in the walls of the materials.

The grafting is a post-synthetic functionalization of the walls of mesoporous silica, this process is carried out primarily by reaction of organosilanes, chlorosilanes or silazanes with the free

silanol groups of the pore surfaces (Fig. 1.6). The method it can be used for functionalize with a variety of organic groups and has the benefit that the structure of the silica is retained, but with a reduction of the porosity. The problem of this technique is the diffusion into the centre of the pores, which can in turn lead to a nonhomogeneous distribution of the organic groups [15].

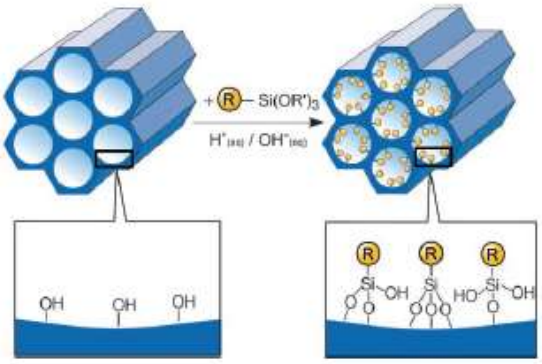

Figure 1.6. Grafting for organic functionalization. R = organic functional group.

The co-condensation method is an alternative method to synthetize organosilica materials, with this method is possible to prepare mesostructured silica by the co-condensation of tetra-alkoxysilanes (such as TEOS or TMOS) with terminal tri-alkoxyorganosilanes in the presence of templates leading to materials with organic residues anchored covalently to pore walls (Fig. 1.7). This method of synthesis is similar at the methods synthesis for produce mesoporous silica and use the same template agents.

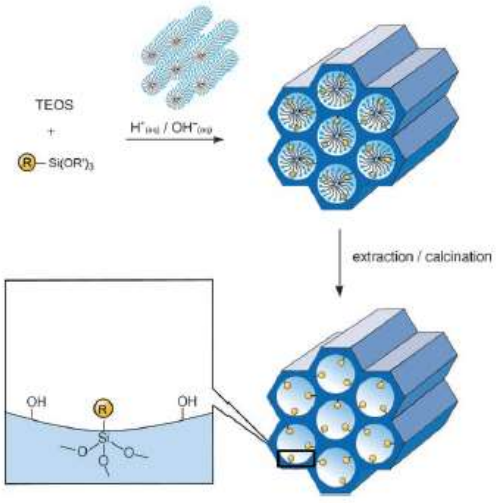

Figure 1.7. Co-condensation method for the organic modification of mesoporous silica phases. R = organic functional group.

Since, the organic functionalities are direct components of the silica matrix and the pore blocking is not a problem. Moreover, the organic units are more generally homogeneously distributed than in materials synthetized with the grafting. However, this method also has of disadvantages, in general, the degree of the order decreases with the increasing of the concentration of tri-alkoxyorganosilanes in the reaction mixture, so the content of organic functionalities does not exceed the 40 mol%. In addition, the proportion of terminal organic groups that are incorporated is generally lower than would correspond to the starting concentration, because in the reaction mixture the homocondensation is favourite, this problem cannot have guaranteed a homogeneous distribution of different organic functionalities in the framework [15].

The synthesis of organic-inorganic hybrid materials by hydrolysis and condensation reactions of bridged organosilica precursors has been known for a long time from sol-gel chemistry [16]. In contrast to the organically functionalized silica, which are obtained by post-synthetic or direct synthesis, the organic units are incorporated in the network structure of the silica matrix through covalent bonds and consequently distributed homogeneously in the pore walls. These materials commonly exhibit completely disordered pore systems with a moderately wide distribution of pore radii. The transfer of the concept of the structure-directed synthesis of pure silica by surfactants to the bissilylated organosilica precursors allows the construction of the PMOs in which the organic bridges are integral components of the silica network (Fig. 1.8).

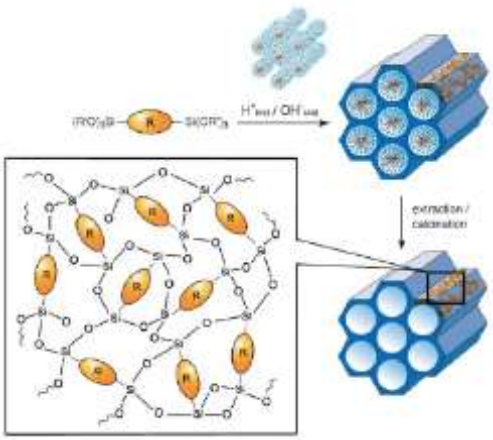

Figure 1.8. General synthesis to PMOs that are constructed from bissilylated organic bridging units. R = organic functional group.

The hydrocarbon chain of the organosilica precursors can be at most just two carbon atoms long to produce a periodic system, this is an indication that the organic bridge must not be too flexible otherwise the hybrid materials obtain are disordered. This condition is fulfilled by the aromatic compounds, the materials synthetized by aromatic precursors show a crystallinity of pore walls (Fig. 1.9).

The first synthesis of PMO materials with aromatic groups was reported by Yoshina-Ishii et al. [17] in the 1999, they used 1,4-bis(triethoxysilyl)benzene and 2,5-bis(triethoxysilyl)thiophene as precursors in the presence of template.

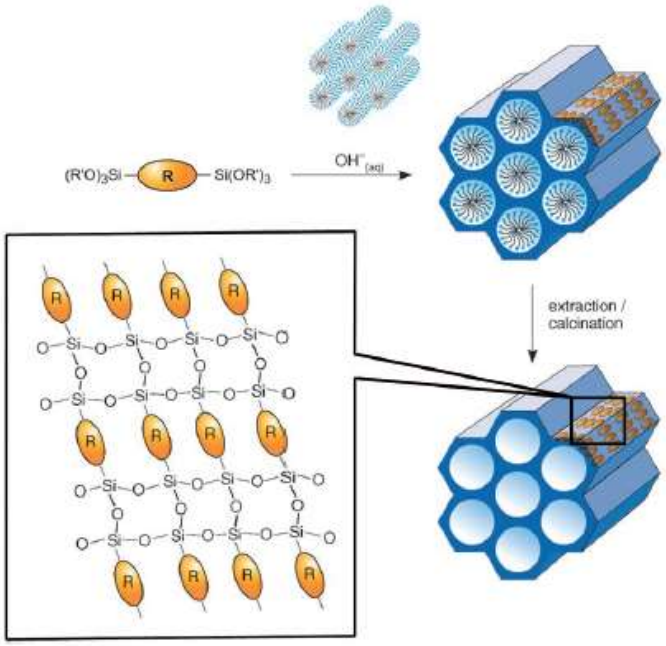

Figure 1.9. Synthesis of PMOs with a crystal-like arrangement of the bridging organic units (R) in the pore walls.

1.4.2| Metal Organic Frameworks (MOFs)

The MOFs are a subclass of coordination polymers, with organic ligand containing potential voids. More specifically, the IUPAC defined the MOF as a coordination network; for the IUPAC a

coordination network is a coordination compound extending in one dimension, but with crosslink between two or more individual chains or a coordination compound extending through repeating coordination entities in two or three dimensions (Fig 1.10) [18].

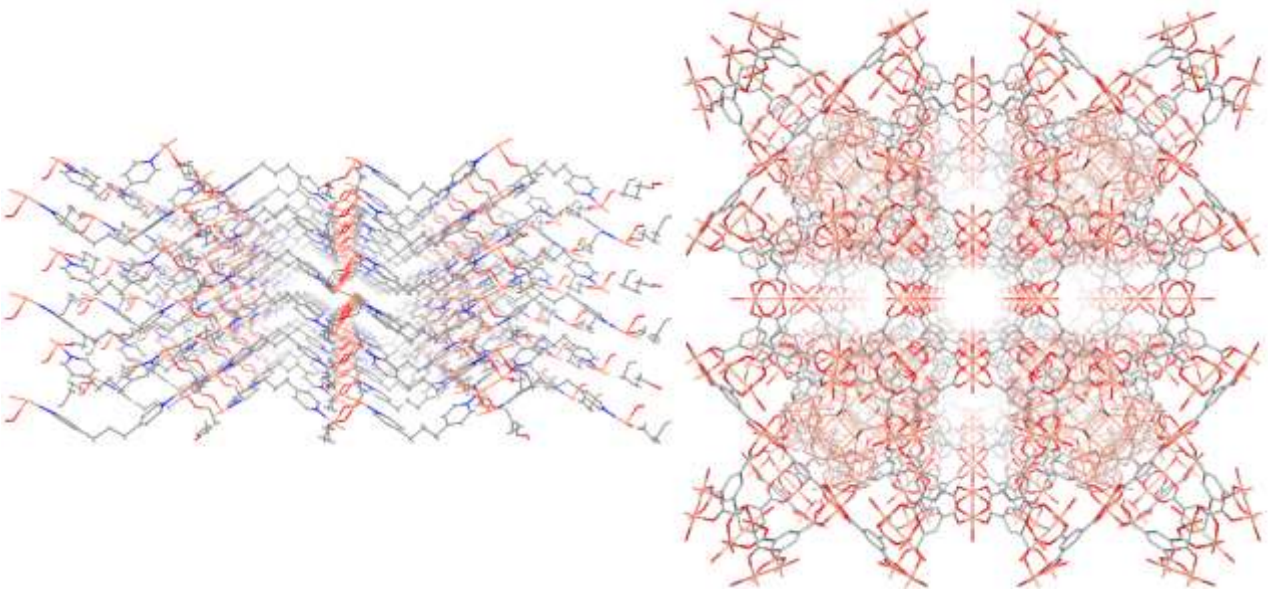

Figure 1.10. Structure of bidimensional and tridimensional MOF. At left the 2D $[Cu_2(Glu)_2(\mu\text{-bpa})]$ and at right the 3D $[Cu_3(BTC)_2]$ (commonly called HKUST-1).

The MOFs are formed by two components: the organic units and the inorganic units. The organic units called linkers consist of organic anions, such as carboxylates, sulfonate and phosphate, or heterocyclic compounds and they are typically di-, tri, or tetravalent ligand. The inorganic units are the metal ions or clusters called secondary building units (SBUs). MOFs are formed by coordination between metal ions or SBU with organic linkers. Their geometry is determined by the number and geometry of coordination of the metal ions, and the nature of the functional groups. A variety of SBU geometries with different number of points of extension such as octahedron, square paddle-wheel, trigonal prism and triangle have been observed in MOF structures (Fig 1.11). These modulation possibilities allow obtaining a large number of different architectures; currently the Cambridge database reports over 60000 different MOF structures.

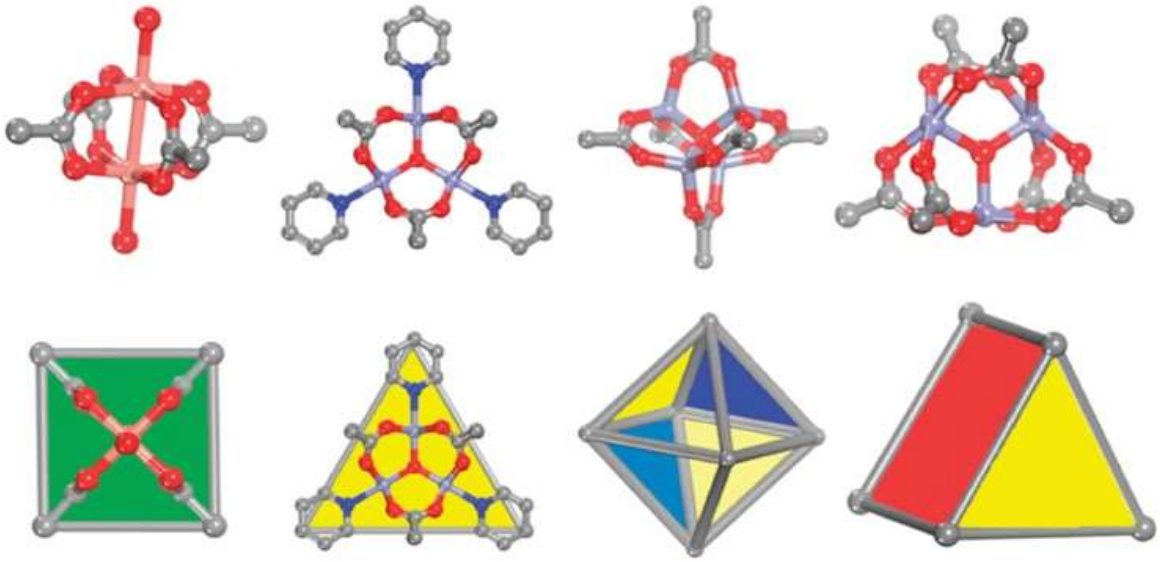

Figure 1.11. Different kind of SBUs geometries observed in MOFs. From the left square paddle-wheel, triangle, octahedron and trigonal prism.

The MOFs are produced almost exclusively by hydrothermal or solvothermal techniques and the crystal are slowly growth form the solution. Unlike zeolites, where a templating agent is used, in the synthesis of MOF the templating action is performed by the metallic ions or SBUs and the organic ligands [19]. The coordination between linkers and SBU/ions is generally reversible; this involves the slow growth of the crystals leading to give a material with crystal in millimetric scale and a density of defect near equilibrium. Using the solvothermal synthesis it is possible obtain crystals that can be used to determine the structure of the material, since growth takes place over hours or days, but for the industrial application is necessary a faster production and a scale-up. Scale-up has not been widely studied, but several groups have demonstrated the possibility to use the microwaves for nucleated MOF crystals rapidly from solution. This technique, called "microwave-assisted solvothermal synthesis" produces micron-crystal in few minutes, in the same yields to the solvothermal synthesis [20].

Another fast synthesis technique is the solvent-free technique, in this one the metal salts and the organic ligands are mixed and ground up with a ball mill, the metal salts usually used is the acetate. In the 2008 James at al. [21] synthesised H-KUST1 in this way, the synthesis is quickly and

in quantitative yield and the resulting materials had the same morphology and characteristic as the industrial one. A recent advancement in the solvent-free preparation of MOF films is their synthesis by chemical vapour deposition; this synthetic way consists in two steps. The first step is the deposition of metal oxide layers; in the second step, these layers are exposed at sublimed linkers, this one induce a phase transformation to the MOF crystal [22].

1.5| Organic porous materials

1.5.1| Porous carbons

Porous carbons or activated carbons have been used for thousands of years and are now versatile materials of major industrial significance. The development of micro and mesopores is of importance because only such pores allow the adsorption of a large amount of chemicals. For the development of the pores, usually these carbons must be activated by gasification processes or by reaction with appropriate chemical agents. However, the complexity of the structure prevents these processes the preparation of specific porous structure. The development of industrial technology provides new applications for porous carbons but it requires carbon with specific pore structure. For this, new approaches have been developed to control the structure of pores [23]. Whereby the porous carbons can be divided into two categories: activated carbons consisting of porous carbons with added active surface chemical group and carbons with desired architecture of pores.

Activate carbons are manufactured by the pyrolysis of carbonaceous materials of vegetable or synthetic polymers origin followed by activation. The pyrolysis of carbonaceous materials in an inert atmosphere allow the degradation of the organic molecules to give a porous carbonaceous solid, these

solids contain predominantly macropores connected to mesopores and micropores [24]. The pore structure depends on the type of precursors used for pyrolysis.

During carbonisation process, the non-carbon elements are removed by pyrolytic decomposition of the starting materials and the carbon atoms are grouped in elementary graphite crystallites. The arrangement of the crystallite is irregular; which generated free interstices between them [25]. The resulting carbonised materials has a very small adsorption capacity, probably a part of carbon precursor remains in the pores and on their surfaces. These carbons can be activated through the removal of precursor by heating in steam or under gas or by extraction with a solvent or by chemical reaction [24], leading to an enlargement of the porous created during the carbonization process and creating a new porosity [26].

The micro and mesoporosity can be controlled through a different kind of technique. For the control of microporosity, there are two methods, the carbonization of suitable carbon precursor, in particularly in the presence of metal ions and the modification of existing porosity. The first method used an ion-exchange resin as the precursor and Miura et al. demonstrated that using some different cations is possible to change the average pore diameter [27]. The second method is a chemical modification of micropore walls Kaneko et al. introduced nitrogen into the pores and they carried out pyridine by CVD [28]. The mesoporosity can be controlled acting both on the activation process and on the carbonization process. In the activation, process is possible to use same organo-rare earth metal complexes as an additive to have an extremely large mesoporosities [29]. The control during the carbonization process provides the carbonization of preformed mesoporous materials as mesoporous aerogels [30] or the carbonization of polymer blends, where the two polymers have different degrees of thermal stability [31].

A desired pore architecture can be produced through the carbonization of carbon precursors with some template agents. In the 1986, Knox et al. reported that silica gel can be impregnated with polymer precursor and after the polymerization it is formed a continuous network surrounding the

silica particles, the carbonization and the subsequent dissolution of the silica template rendered a mesoporous carbon with rigid structure featuring also some micropores [32]. This work gave rise to the development of new types of porous carbons. In particular, the carbons of the family known as CMKs. CMKs are synthesized using mesoporous silica as templates, the silica templates were impregnated with sucrose in the presence of sulphuric acid and the resulting mixture was dried and subsequently they were carbonized and finally the silica templates were dissolved (Fig. 1.12) [33].

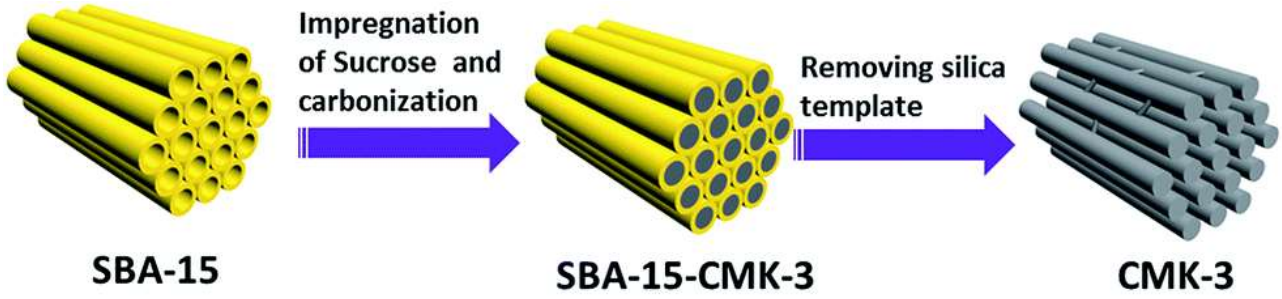

Figure 1.12. Synthetic procedure of CMK-3.

1.5.2| Porous Organic Polymers (POPs)

These compounds are predominantly amorphous materials based on strong covalent bonds (C—C, C—O and C—N prevalently) and on light atoms. Such they are based on strong covalent bonds, they show high thermal and chemical stability, some important parameters in industrial applications. The amorphous materials do not allow a precise control of pore size distribution and the physical characteristic of the materials could be changed by choosing precise building units, synthetic pathways and reaction conditions. High porosity is obtained by using rigid building units; the rigidity of the structure prevents the collapse after guest removal and generated free space inside the structures [34].

1.5.2.1| Hyper-Crosslinked Polymers (HCPs)

HCPs are amorphous materials endued of high surface areas, microporosity and low density. They are synthetized using much different reactions from other polymer materials or single molecules. From the synthetic point of view, these materials render certain advantages, such as mild reaction conditions, inexpensive reagents and monolithic products; this allows easy scale-up in industrial production [35]. There are three different techniques for the synthesis of HCPs: the post-crosslinking of polymers, direct one-step polycondensation, and using external crosslinkers. The latter led to the diversification of HCPs.

The post-crosslinking technique is a post modification of polymers. The polymers precursors was dissolved in a solvent, after swelling the polymer chains separate and the space between them was occupied by the solvent, the polymer chains are thereafter subjected to cross-linking by an external crosslink agent, after the solvent was removed the polymer chains are held apart by the crosslink generating the porosity (Fig. 1.13). The development of this technique it is to attributed a Davankov and co-worker, they continued to synthetize HCPs adopting polystyrene as a precursor and using a different kind crosslinkers molecules [36].

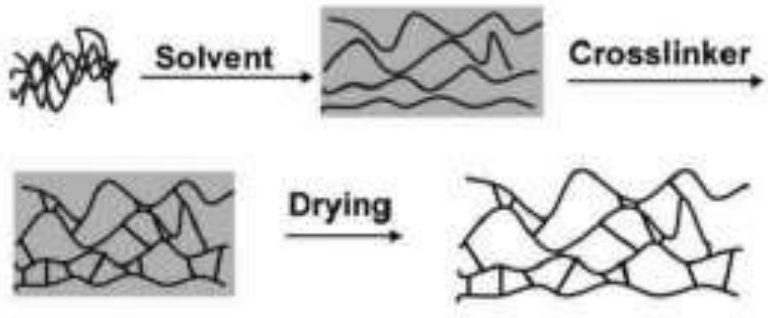

Figure 1.13. Schematic of post-crosslinking technique.

The direct one-step polycondensation technique involves through the use of multifunctional small organic molecules (Fig. 1.14) for obtaining rigid open framework structure which share similar properties with the HCP polystyrene networks. The Cooper group adopted this technique to

synthesize HCPs as monolithic blocks that helped to subside the volumetric methane storage concerns of HCPs pertaining to the packing of porous particulate materials [35].

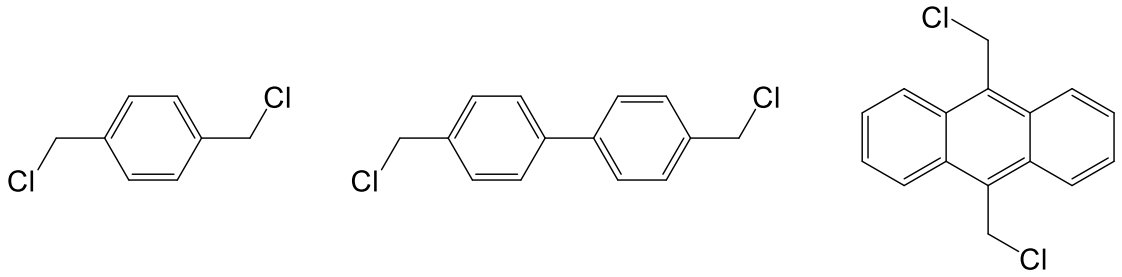

Figure 1.14. Monomer using by Copper group for synthesis HCPs by polycondensation.

In 2011, Tan and co-worker introduced a novel approach to synthesize HCPs using external cross-linkers [37]. Aromatic ring containing in small organic molecules were crosslinked through methylene bonds by formaldehyde dimethylacetate (FDA) as an external crosslinker, via the Friedel-Craft alkylation mechanism by the catalysis of a Lewis acid $FeCl_3$ (Fig. 1.15). The resulting network showed high thermal stability and microporous structure. Moreover, this technique allows using monomers with different structures that contain aromatic rings. Other than FDA, 1,4-dimethoxybenzene [38], formaldehyde glyoxylic acid [39], and dibromo-*p*-xylene [40] could all be used as the external crosslinker.

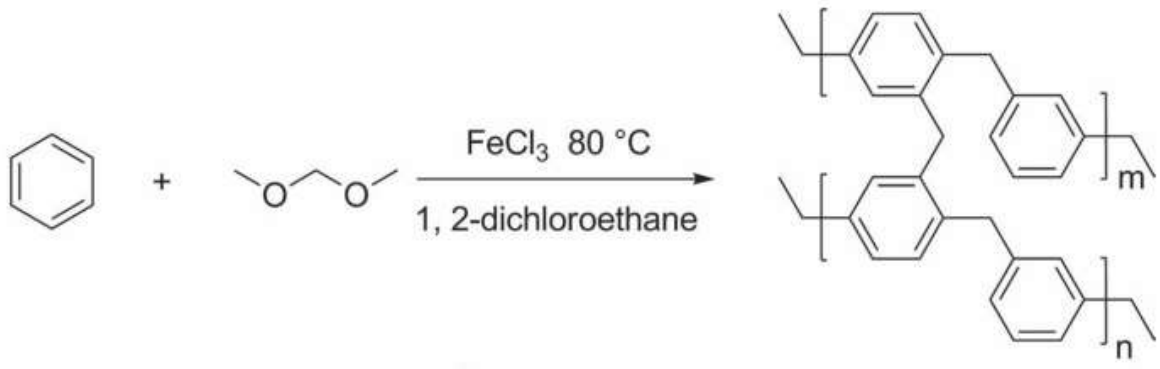

Figure 1.15. Schematic synthesis of HCP by benzene.

1.5.2.2| Polymers of Intrinsic Microporosity (PIMs)

PIMs are amorphous microporous polymers with rigid polymer chains. They resemble a series of interclasped aromatic rings put together like a chain with contorted sites, thereby dispossessing them of the ability to pack efficiently. Some these materials are soluble in organic solvents and it is possible created of films, these two properties have enabled their application to fabricate membranes for gas separation.

The first PIMs was development by McKeown and co-worker in the 2002 [41] and the design evolved 4 years before that they reported the design of a porous polymer from phthalocyanines. Generally, phthalocyanines network polymers show a strong propensity to aggregate into columnar stacks due the π–π stacking of aromatic components, resulting in nonporous solids [42]. Therefore, it was deemed essential to use a highly rigid and contorted linker composed of fused rings that would ensure a space inefficient packing of the macrocycles and prevent structural relaxation and loss of microporosity.

1.5.2.3| Covalent Organic Frameworks (COFs)

Endowed with crystallinity as well as porosity, COFs comprise molecular building blocks linked via covalent bonds. The crystallinity of the COFs is related by the reversible character of the polymerization reactions adopted to synthetize COFs, which favours the formation of thermodynamically controlled polymers. The variety of molecular building blocks and custom-made attributes have enabled the adoption of COFs for a wide range of applications including gas adsorption and storage, catalysis, energy storage, and others applications.

The first work on COFs was reported in 2005 by Yaghi group, the earliest documented two COF were synthetized, one by the self-condensation reaction of 1,4-benzenediboronic acid and one by the co-condensation reaction of 1,4-benzenediboronic (COF-1) acid with 2,3,6,7,10,11-hexahydroxytriphenylene (COF-5) respectively [43]. The solvent for the reaction is more important because is necessary that the monomer is not completely soluble as enables the slow condensation of boronic groups, thereby facilitating the nucleation and growth of crystalline COFs. The structure of these two COFs is graphene-like (Fig. 1.16), the frameworks are extended in two-dimensional, the layer are packed and the pores are channels, but the COF-1 is staggered networks. In 2007, the Yaghi group reported the synthesis of three-dimensional COFs synthetized by using some three-dimensional molecules [44].

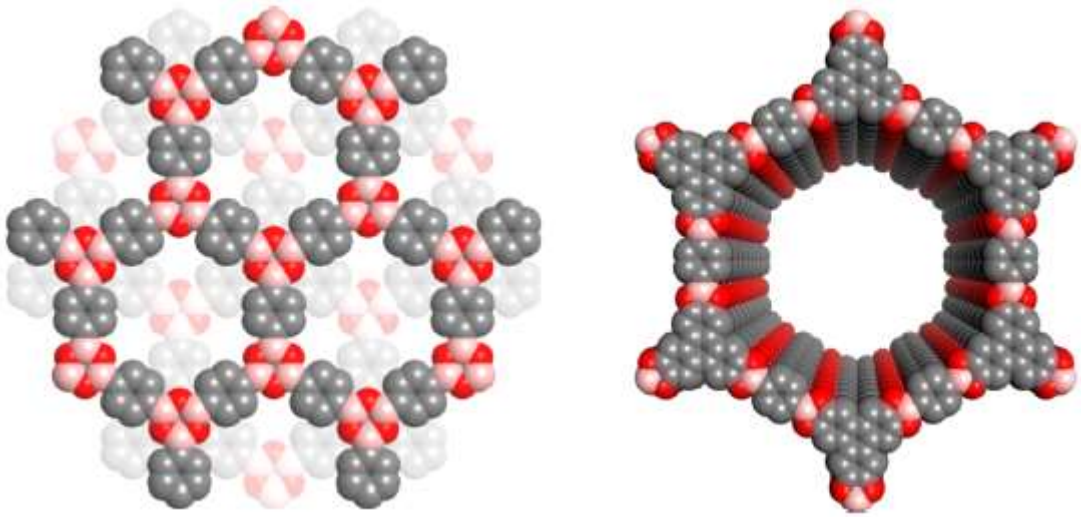

Figure 1.16. Structural models of COF-1 (left) and COF-5 (right).

COFs materials could be constructed from a variety of rigid organic building blocks with different structural configuration. The formation of strong covalent bonds through diverse synthetic organic reactions between the building units provides the COF materials with well-defined 2D or 3D structures. In principle, all the synthetic methodologies for the covalent-bond formation developed in organic synthesis are of potential interest for the construction of organic polymers. However, in order to construct the polymeric structure with both structural regularity and porosity, many limitations still

exist. Indeed, the structural regularity of COF materials is much difficult to control due the strong covalent bonds. It is by far believed that only the reversible reactions [45] are applicable for the possible construction of crystalline COF structures.

The reaction that successfully applied for the COFs synthesis are six. The first two are those used by Yaghi in first article on COFs, in particularly, the reaction used for the synthesis of COF-1 is based on the reversible formation of boronate anhydride from the dehydratation of boronic acid. Instead, for the COF-5 the reaction is an analogous dehydratation reaction between boronic acid and catechol derivate results in the reversible formation of boronate esters [43]. Similarly, the dehydratation reaction of boronic acid and silanol results in the formation of borosilicate reaction [46]. The covalent triazine-based frameworks were synthetized by the nitrile cyclotrimerization and this procedure represents a unique method to synthetize this kind of COFs [47]. The last two methods are based on the reversible formation of imine bonds, the dehydratation of aldehyde and amine gives rise to the Schiff-base type linkage [48], while that of aldehyde and hydrazide affords the hydrazone formation [49].

1.5.2.4| Conjugated Microporous Polymers (CMPs)

CMPs refers to a macromolecule that possesses a microporous network that has building blocks within the system that give rise to π-conjugation [50]. The alternation of π and σ bonds throughout the network readily allows their structure to be utilized electronically. Together with efficient molecular packing, CMPs offer properties for not only electronic but also porous applications. These materials are amorphous due to the freedom of rotation about the *s* bonds formed between building blocks. These structural features are unique and are not available in other porous materials, which are typically not π-conjugated, or conventional conjugated polymers, which are non-

porous. Subsequently the discovery of the first CMP by Cooper [51], many scientists have joined this field of study and contributed to the rapid growth of the CMP family.

The most characteristic feature of CMPs is the rather broad diversity of π units. Building blocks ranging from simple phenyl units to extended arenes, heterocyclic aromatic units and large macrocycles have been successfully exploited for the synthesis of CMPs. Because there is a less limitation on size, geometry and functional groups, CMPs can systematically, tune their π-conjugated porous architecture and allow for the optimization of the skeleton and properties.

To construct a conjugated skeleton, the synthetic reaction must covalently link building blocks with a π-conjugated bond. Chemical reaction utilized for the preparation of linear conjugated polymers can also be employed for the synthesis of CMPs. The Suzuki cross-coupling reaction [52], Yamamoto reaction [53], Sonogashira-Haginara reaction [51], oxidative coupling reaction [54], phenazine ring fusion reaction [55] and triple bond cyclotrimerization [47] have been well established for the synthesis of CMPs. Because building blocks can have different geometries, reactive group and πsystems, this structural diversity significantly enhances the flexibility of the design of both skeletons and pores.

1.5.2.5| Porous Aromatic Frameworks (PAFs)

PAFs are open framework porous polymers bearing outstanding surface area and top-notch stability. They owe their outstanding to the monomer structure and reaction conditions. The superb stability of PAFs can be ascribed to its covalent bonds and rigid phenyl framework [56]. PAFs can be readily functionalized to extend their scope of application. PAFs present commendable performance in the selective adsorption of greenhouse gases.

The first PAFs was published in 2009 by Ben group [57] and was synthetized by Yamamoto coupling. This reaction provides a direct method for the homocoupling of monomers, offering a simple synthetic technique for large networks. The differing factor between PAFs and CMPs is that PAFs lose their framework conjugation inasmuch as the conjugation is broken by the central atom of tetrahedral monomers, whereas CMPs maintain the conjugation that originates from the monomers. The crystalline structure of diamond acted as the cue for the design of PAF-1 wherein it was reasonably speculated that substituting phenyl groups for C—C covalent bonds of diamond would sustain the stability in the structure besides indulging in ample exposure of the phenyl groups, which might help expand the internal surface area.

In addition to the contemplative design of PAF-1, which show a phenomenally high surface area supported by the reaction using for the synthesis. This particular coupling reaction is more efficient for the removal of complete terminal groups, which are responsible for reductions in surface area, than other coupling reactions [56].

1.5.3| Porous organic molecules

Most microporous materials are extended networks, the micropore structure in networks is stabilized by the extended directional covalent or coordination bonding, which is absent in molecular solids. Consequently, permanent porosity is much rarer in discrete molecules, as they tend to pock efficiently to form solids with minimal void volume. The design of porosity in molecules that requires therefore a different but related set of strategies to those used for porous networks.

The problems associated with defining porosity in molecular crystals were recently highlighted [58]. For example, the “virtual porosity” is sometimes created by removing guests from a crystal structure, or by representing the structure in a potentially misleading way. For this one, the

porosity was defined as the ability to adsorb guests, independently of whether formally interconnected pore channel exists. This definition takes into account the phenomenon of porosity "without pores" [58], where molecular solids with disconnected void volume nonetheless adsorb considerable quantities of guest by cooperative diffusion mechanisms [59].

It is possible to classify porous molecules as either intrinsically or extrinsically porous. The intrinsic porosity is defining as the porosity that results from the structure of the discrete molecule as viewed in isolation. In contrast, extrinsically porous molecules are those packs together to form porous structures in the solid state, but the porosity is not intrinsic to the isolated molecules.

As regards the extrinsic porosity, a number of organic molecules that pack inefficiently in the solid state and are stable to dessolvation, thus forming permanently porous molecular crystal, have been reported. The Dianin's compound formed by 4-hydroxyphenyl-2,3,4-trimethylchroman, relatively simple molecule, features a bent structure that packs inefficiently to form one-dimensional channels within the crystals [60]. Another extrinsically porous molecule is *tris-o*-phenylenedioxycyclotriphosphazene (TPP); this molecular crystallizes to form a structure with one-dimensional hexagonal pores [61]. Moreover, even biological molecules can pack themselves in an orderly manner to give porous systems; it is the case of dipeptides crystal. Indeed, some dipeptide crystal showed a one-dimensional channel motif generate by the hexagonal crystal that the molecules created [62]. Recently, a new type of extrinsic organic porous crystal has been development, these new materials have been generated by the packing of organic salt, the lattice wall is formed by organic cations and anions and the nodes was formed by the electrostatic interaction between positive and negative charges [63].

The simplest porous materials with intrinsic porosity are characterized to possess a prefabricated hole; this is the case of Calix[*n*]arenes molecules. Calix[n]arenes are a family of oligomeric macrocycles where *n* is the repeat units. In particular, four-membered are molecules with a permanent cone-shaped molecular cavity [64]. Atwood and co-worker focused initially on formally

nonporous crystalline materials, which nonetheless adsorb large amount of various guest by cooperative diffusion mechanisms [64]. More reports that are recent have also demonstrated permanent microporosity in calixarene crystals [65]. Another family of molecular with intrinsic porosity is the cucurbit[*n*]urils in particularly the cucurbit[6]uril (called CB[6]), which is a tubular six-membered macrocycle comprising methylene-bridge glycouril units. The hydrophobic cavity is accessible through two polar carbonyl portals. The synthesis using HCl generate a new polymorph featuring the hexagonal arrangement of one-dimensional channels [66]. A new class of porous molecular are described by Cooper and co-worker, these materials called porous organic cages are tetrahedral imine-linked cage molecules synthetized by [4+6] condensation of 1,3,5-triformylbenzene with three different vicinal diamines: 1,2-ethylenediamine, 1,2-propylendiamine and (R,R)-1,2-diaminocyclohexane [67]. The nature of the resulting porosity depends on the degree of alignment of the cage windows between molecules, which is in turn determined by the cage vertex functionality [67].

References

[1] A. F. Cronstedt, *Kongl Vetenskaps Academiens Handlingar Stockholm,* vol. 17, p. 120, **1756**.

[2] A. F. Cronstedt, Försök till Mineralogie eller Mineral-Rikets Upställning, Stockholm: Wildiska, **1578**, p. 99.

[3] H. S. C. Deville, *C. R. Acad. Sci.,* vol. 54, p. 324, **1862**.

[4] G. Friedel, *C. R. Acad. Sci.,* vol. 122, p. 948, **1896**.

[5] F. Grandjean, *C. R. Acad. Sci.,* vol. 149, p. 866, **1910**.

[6] O. Weigel and E. Steinhoff, *Z. Kristallogr.,* vol. 61, p. 125, **1925**.

[7] J. W. McBain, "The Sorption of Gases and Vapors by Solids," London, Rutledge and Sons, **1932**.

[8] D. H. Everett, "Manual of symbols and terminology for physicochemical quantities and units," in *IUPAC council*, **1971**.

[9] R. Barrer, *J. Chem. Soc.,* vol. 0, p. 2158, **1948**.

[10] V. Chiola, J. E. Ritsko and C. D. Vanderpool.US Patent 3556125D, 26 Feb **1969**.

[11] C. Kresge, M. Leonowicz, W. Roth, J. Vartuli and J. Beck, *Nature,* vol. 359, p. 710, **1992**.

[12] Y. Liu, W. Zhang and T. Pinnavaia, *Angew. Chem. Int. Ed.,* vol. 40, p. 1255, **2001**.

[13] D. Zhao, J. Sun, Q. Li and G. D. Stucky, *Chemistry of Materials,* vol. 12, p. 275, **2000**.

[14] J. Beck, J. Vartuli, W. Roth, M. Leonowicz and C. Kresge, *J. Am. Chem. Soc.,* vol. 114, p. 10834, **1992**.

[15] F. Hoffmann, M. Cornelius, J. Morell and M. Froba, *Angew. Chem. Int. Ed.,* vol. 45, p. 3216, **2006.**

[16] D. Loy and K. Shea, *Chem. Mater.,* vol. 95, p. 3306, **2001**.

[17] C. Yoshina-Ishii, T. Asefa, N. Coombs, M. J. MacLachlan and G. A. Ozin, *Chem. Comm.,* vol. 0, p. 2539, **1999**.

[18] S. Batten, N. Champness, X. M. Chen, J. Garcia-Martinez, S. Kitagawa, L. Ohrstrom, M. O'Keeffe, M. P. Suh and J. Reedijk, *Pure and Applied Chemistry,* vol. 85, p. 1715, **2013**.

[19] D. K. Bucar, G. S. Papaefstathiou, T. D. Hamilton, Q. L. Chu, I. G. Georgiev and L. R. MacGillivary, *European Journal of Inorganic Chemistry,* vol. 29, p. 4559, **2007**.

[20] Z. Ni and R. I. Masel, *J. Am. Chem. Soc.*, vol. 128, p. 12394, **2006**.

[21] A. Pichon and S. L. James, *CrystEngComm*, vol. 10, p. 1839, **2008**.

[22] I. Stassen, M. Styles, G. Grenci, H. V. Gorp, W. Vanderlinden, S. D. Feyter, P. Falcaro, D. D. Vos, P. Vereecken and R. Ameloot, *Nature Materials*, vol. 15, p. 304, **2015**.

[23] T. Kyotani, "Porous Carbon," in *Carbon Alloys Novel Concepts to Develop Carbon Science and Technology*, E. Yasuda, M. Inagaki, K. Kaneko, M. Endo, A. Oya, Y. Tanabe, **2003**, p. 109.

[24] R. C. Bansal, Active carbon, New York: Dekker, **1998**.

[25] F. Derbyshier, Porosity in carbons "Characterization and applications", London: J. W. Patrick, **1995**.

[26] S. M. Manocha, *Sadhana*, vol. 28, p. 335, **2003**.

[27] H. Nakagawa, K. Watanabe, Y. Harada and K. Miura, *Carbon*, vol. 37, p. 1455, **1999**.

[28] C. M. Yang and K. Kaneko, *Carbon*, vol. 39, p. 1075, **2001**.

[29] H. Tamai, T. Kakii, Y. Hirota, T. Kumamoto and H. Yasuda, *Chem Materials*, vol. 8, p. 454, **1996**.

[30] R. W. Pekala, C. T. Alviso, F. M. Kong and S. S. Hulsey, *J. Non-Cryst. Solids*, vol. 145, p. 90, **1992**.

[31] J. Ozaki, N. Endo, W. Ohizumi, K. Igarashi, M. Nakahara, A. Oya, S. Yoshida and T. Iizuka, *Carbon*, vol. 35, p. 1031, **1997**.

[32] J. H. Knox, B. Kaur and G. R. Millward, *J. Chromatogr.*, vol. 3, p. 352, **1986**.

[33] R. Ryoo, S. H. Joo and S. Jun, *J. Phys. Chem. B*, vol. 103, p. 7743, **1999**.

[34] R. Dawson, A. I. Cooper and D. J. Adams, *Progress in Polymer Science*, vol. 37, p. 530, **2012**.

[35] C. D. Wood, B. Tan, A. Trewin, F. Su, D. B. M. J. Rosseinsky, Y. Sun, L. Zhou and A. I. Cooper, *Adv. Mater.*, vol. 20, p. 1916, **2008**.

[36] V. A. Davankov, M. M. Ilyn, M. P. Tsyurupa, G. I. Timofeeva and L. V. Dubrovina, *Macromolecules*, vol. 29, p. 8398, **1996**.

[37] B. Li, R. Gong, W. Wang, X. Huang, W. Zhang, H. Li, C. Hu and B. Tan, *Macromolecules*, vol. 44, p. 2410, **2011**.

[38] L. Tan, B. Li, X. Yang, W. Wang and B. Tan, *Polymer*, vol. 70, p. 336, **2015**.

[39] H. Wang, L. Pan, W. Deng, G. Yang and X. Liu, *Polym. J.*, vol. 48, p. 787, **2016**.

[40] S. Bhunia, B. Banerjee and A. Bhaumik, *Chem. Commun;*, vol. 51, p. 5020, **2015**.

[41] N. B. McKeown, S. Makhseed and P. M. Budd, *Chem. Commun.*, vol. 0, p. 2780, **2002**.

[42] N. B. McKeown, *J. Mater. Chem.*, vol. 10, p. 1979, **2000**.

[43] A. P. Coté, A. I. Benin, N. W. Ockwig, M. O'Keeffe, A. J. Matzger and O. M. Yaghi, *Science*, vol. 50, p. 13825, **2005**.

[44] H. M. El-Kaderi, J. R. Hunt, J. L. Mendoza-Cortés, A. P. Coté, R. E. Taylor, M. O'Keeffe and O. M. Yaghi, *Science*, vol. 316, p. 268, **2007**.

[45] S. J. Rowan, S. J. Cantrill, G. R. L. Cousins, J. K. M. Sanders and J. F. Stoddart, *Angew. Chem. Int. Ed.*, vol. 41, p. 898, **2002**.

[46] J. R. Hunt, J. D. L. C. J. Doonan, A. P. Coté and O. M. Yaghi, *J. Am. Chem. Soc.*, vol. 130, p. 11872, **2008**.

[47] P. Kuhn, M. Antonietti and A. Thomas, *Angew. Chem. Int. Ed.*, vol. 47, p. 3450, **2008**.

[48] F. J. Uribe-Romo, J. R. Hunt, H. Furukawa, C. Klock, M. O'Keeffe and O. M. Yaghi, *J. Am. Chem. Soc.*, vol. 131, p. 4570, **2009**.

[49] F. J. Uribe-Romo, C. J. Doonan, H. Furukawa, K. Oisaki and O. M. Yaghi, *J. Am. Chem. Soc.*, vol. 133, p. 11478, **2011**.

[50] F. Vilela, K. Zhang and M. Antonietti, *Energy Environ. Sci.*, vol. 5, p. 7819, **2012**.

[51] J. X. Jiang, F. B. Su, A. Trewin, C. D. Wood, N. L. Campbell, H. J. Niu, C. Dickinson, A. Y. Ganin, M. J. Rosseinsky, Y. Z. Khimyak and A. I. Cooper, *Angew. Chem. Int. Ed.*, vol. 46, p. 8574, **2007**.

[52] L. Chen, Y. Honsho, S. Seki and D. Jiang, *J. Am. Chem. Soc.*, vol. 132, p. 6742, **2010**.

[53] J. X. Jiang, A. Trewin, D. J. Adams and A. I. Cooper, *Chem. Sci.*, vol. 2, p. 1777, **2011**.

[54] J. X. Jiang, F. Su, H. Niu, C. D. Wood, N. L. Campbell, Y. Z. Khimyak and A. I. Cooper, *Chem. Commun.*, vol. 0, p. 486, **2009**.

[55] Y. Kou, Y. Xu, Z. Guo and D. Jiang, *Angew. Chem. Int. Ed.*, vol. 50, p. 8753, **2011**.

[56] T. Ben and S. Qiu, *CrystEngComm*, vol. 15, p. 17, **2013**.

[57] T. Ben, H. Ren, S. Ma, D. Cao, J. Lan, X. Jing, W. Wang, J. Xu, F. Deng, J. M. Simmons, S. Qiu and G. Zhu, *Angew. Chem. Int. Ed.*, vol. 48, p. 9457, **2009**.

[58] L. J. Barbour, *Chem. Commun.*, vol. 0, p. 1163, **2006**.

[59] J. L. Atwood, L. J. Barbour, A. Jerga and B. L. Schottel, *Science*, vol. 298, p. 1000, **2002**.

[60] R. M. Barrer and V. H. Shanson, *J. Chem. Soc. Chem. Commun.*, vol. 0, p. 333, **1976**.

[61] P. Sozzani, S. Bracco, A. Comotti, L. Ferretti and R. Simonutti, *Angew. Chem. Int. Ed.*, vol. 44, p. 1816, **2005**.

[62] A. Comotti, S. Bracco, G. Distefano and P. Sozzani, *Chem. Commun.*, vol. 0, p. 284, **2009**.

[63] T. Miyano, N. Okada, R. Nishida, A. Yamamoto, I. Hisaki and N. Tohnai, *Chem. Eur. J. A*, vol. 22, p. 15430, **2016**.

[64] S. J. Dalgarno, P. K. Thallapally, L. J. Barbour and J. L. Atwood, *Chem. Soc. Rev.*, vol. 36, p. 236, **2007**.

[65] P. K. Thallapally, B. P. McGrail, J. L. Atwood, C. Gaeta, C. Tedesco and P. Neri, *Chem. Mater.*, vol. 19, p. 3355, **2007**.

[66] S. Lim, H. Kim, N. Selvapalam, K. J. Kim, S. J. Cho, G. Seo and K. Kim, *Angew. Chem. Int. Ed.*, vol. 47, p. 3352, **2008**.

[67] T. Tozawa, J. T. A. Jones, S. I. Swamy, S. Jiang, D. J. Adams, S. Shakespeare, R. Clowes, D. Bradshaw, T. Hasell, S. Y. Chong, C. Tang, S. Tomphson, J. Parker, A. Trewin, J. Bacsa, A. M. Z. Slawin, A. Steiner and A. I. Cooper, *Nature Mat.*, vol. 8, p. 973, **2009**.

2| Porous Materials for gas adsorption and storage

Speaking about porous materials, the first applications that comes to mind is gas adsorption. In particular, in recent years the researchers have engaged in the use of porous materials in the environmental and energy fields. In the environmental field, the idea is to design and build materials that can selectively capture CO_2 or store it inside them, to clean the air and reduce the greenhouse effect, and in material ones that can adsorb and convert CO_2 in other synthetically and industrially useful substances. On the energy side, instead, porous materials are idealized for the storage of combustible gases such as H_2 and CH_4, to have alternative energy sources to oil that lower CO_2 emissions.

A part of my research has focused on these assumptions, exploring a series of porous materials that can be effective for the storage of methane and that, with small changes to the structure, can change the affinities with different gases.

In order to deal with these topics, some basic concepts will be introduced in the field of porous materials and their use for the adsorption of gas, the methods on which the fundamental parameter calculations of porous materials for example the surface area are based will be explained. In the end, my work will be described divided into two sections: storage and adsorption of gas.

2.1| Definitions

In 1985, the International Union of Pure and Applied Chemistry (IUPAC) [1] published a Recommendation regarding the definitions and terminology to be apply in describing the properties of porous materials. In this Recommendation, the IUPAC distinguishes two different types of gas/liquid phenomena with a surface; in particular, it distinguishes between absorption and adsorption. The first describes a diffusion of the fluid within the surface, while the second describes an interaction between the fluid and the surface.

The process of adsorption consist in enriching one or more components in an interfacial layer. The phase on which adsorption occurs is defined as adsorbent, while the adsorbed substance is the adsorbate, before the process takes place it is called adsorb or adsorptive. The term adsorption also indicates the process in which the adsorptive molecules form the interfacial layer; it is distinguished from the term desorption which indicates the inverse process (Fig. 2.1). This terminology is used to indicate the direction of the measured experiment values (adsorption curve and desorption curve).

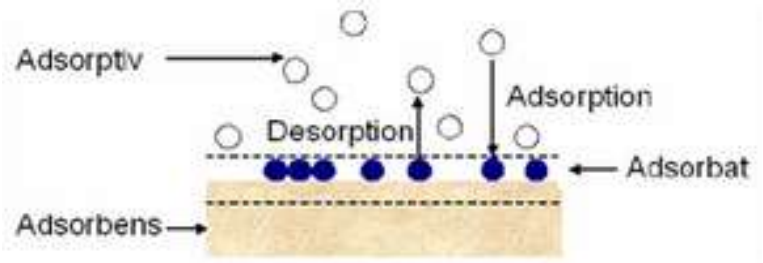

Figure 2.1. Scheme for adsorption and desorption system.

The interactions between adsorbate and adsorbent can be subdivides in two categories depends of energy interaction values, the adsorption process is distinguished in physisorption and chemisorption. In physisorption, adsorbate and adsorbent have physical interactions; the energies involved are of the order of 20-40 kJ/mol, the adsorbate is relatively free to spread on the surface and rotate, the forces involved include both attractive dispersion and short-rage repulsive interactions, for

which in this type of process is quickly established an equilibrium. Instead, in the chemisorption the energy values involved are of the order of 100-400 kJ/mol, are formed new chemical bonds, the adsorbate has no freedom and not an equilibrium is established for which the molecules cannot desorb.

The increase in the molecules of gas adsorbed on the surface involves the formation of a multilayer followed by the pore filling. The pore filling mechanism depends on the pore shape and it is influenced by the adsorptive properties and adsorbent-adsorbed interactions. The total volume accessible in the micropores is considered as an adsorption space and the physisorption is a pore filling process called micropore filling. This classification serves to distinguish it from the modalities with which the physisorption takes place within the mesopores and the macropores. In pores larger than 2 nm, adsorption occurs in two or more steps such as mono-multilayer adsorption and capillary condensation.

In the adsorption of the monolayer, all the adsorbed molecules are in contact with the surface of the adsorbent. The formation of the multilayer consists of the formation of several layers within the available space, so not all the molecules will be in contact with the surface. Capillary condensation involves the occupation of the remaining empty space with the condensed phase of the adsorptive separated from the gaseous phase by a meniscus; capillary condensation is often accompanied by hysteresis.

2.2| Isotherms

The adsorption isotherms are the method to evaluate if porous materials have good characteristics for gas adsorption and storage. In particular, the isotherms is a relation, at constant

temperature, between the quantity adsorbed of materials and the equilibrium pressure of gasses [2]. It is experimental evaluate and it is describe by a function such as:

$$\Gamma = f(p,T)\ [2] \qquad \text{Eq. 2.1}$$

This relation is based on the assumption that all adsorption sites are equivalent that the capacity of the site's ability to adsorb molecules is independent of the location of the site and it is around and finally that the gas molecules are in dynamic equilibrium on each other's, in according on the relation:

$$A_{(g)} + M_{(surface)} \underset{K_d}{\overset{K_a}{\rightleftarrows}} AM_{(surface)}\ [2] \qquad \text{Eq. 2.2}$$

here K_a and $K_d$are the kinetic coefficient of the adsorption and desorption processes:

$$v_a = K_a p_a N(1-\theta)\ [2] \qquad \text{Eq. 2.3}$$

$$v_d = K_d N\theta\ [2] \qquad \text{Eq. 2.4}$$

here θ is the degree of covering; it is defined as the ratio between the amount of gas adsorbed and the monolayer capacity. At the equilibrium $K_a = K_d$ and define $K = K_a/K_d$ is obtained:

$$\theta = \frac{Kp}{(1+KP)}\ [2] \qquad \text{Eq. 2.5}$$

K is an index of affinity between adsorbate and adsorbent and it is in relation with temperature through the Arrenhius equation:

$$K = K^o e^{-\frac{E}{RT}} \qquad \text{Eq. 2.6}$$

The IUPAC divided the experimental isotherms in six categories (Fig. 2.2) [3].

The type I is the Langmuir isotherm, this isotherm is concave and the quantity adsorbed achieve a limit value at $p/p^0 \rightarrow 1$, it is typical of microporous systems and it is described by the relation written in Eq. 2.5.

The type II is the Freundlich isotherm, this isotherm is typical for macroporous systems or of solids having different adsorption sites. Point B (Fig. 2.2) indicates the relative pressure at which the

monolayer coverage ends and the multilayer adsorption begins. It is described by the following equation:

$$\Gamma = K_f p^q \qquad \text{Eq. 2.7}$$

here K_f and q are a constants.

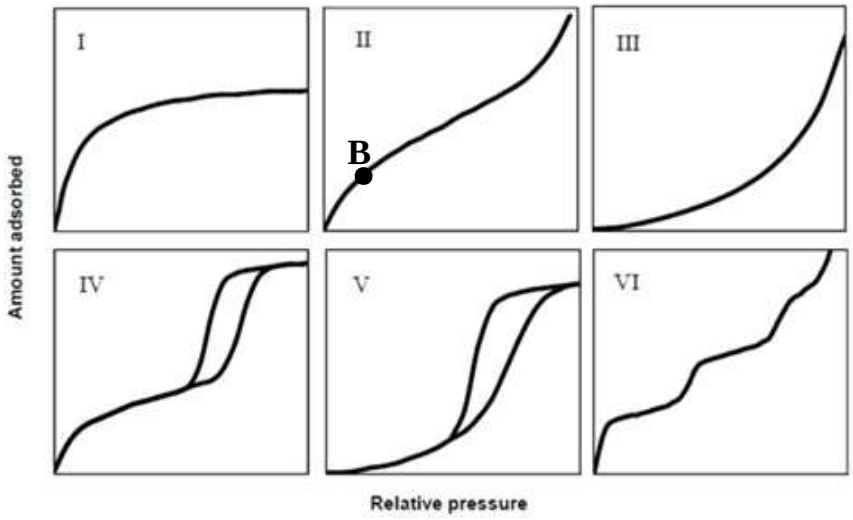

Figure 2.2. Types of physisorption isotherms according to the IUPAC classification.

The type III is convex along the whole axis of the relative pressures; therefore, it does not show any point where the multilayer adsorption begins. It is not a common model and is typical of systems where monolayer interactions are weaker than multilayer ones.

The type IV is the Brunauer-Emmett-Teller isotherms or BET isotherms, it is typical of mesoporous systems. The initial concave part describes the formation of the first adsorbed layer followed by the formation of the multilayer. The hysteresis, characteristic of these curves, is associated with the capillary condensation phenomena.

The type V is uncommon and indicates the presence of cooperation effects. A gaseous molecule binds to the surface more easily if it can interact with another molecule adsorbed. Condensation is due to this type of interactions.

The type VI is characterized by a series of steps that depend on the system and temperature. Represents a multilayer adsorption on a uniform non-porous surface. The height of the single steps indicates the capacity of each single layer adsorbed.

In many cases, at low levels of coverage, the isotherms are reduced to a linear form, described by the equation of Henry's isotherms:

$$\Gamma = K_H \left(\frac{p}{p^0}\right)_T \qquad \text{Eq. 2.8}$$

this trend is a fundamental point for the calculation of the surface area of porous materials.

The isotherms are a powerful means to understand many properties of the porous materials, indeed, with isotherms is possible evaluated the total surface area can be calculated by different methods, of which the most important and used are the Langmuir and the BET models. The pore distribution can be evaluated using a computational calculate on the isotherms. The isotherms a different temperature for the same gas can be allowed the calculation of the heat of interaction between the gas and porous materials, and the isotherms of different gas at the same temperature can be predicted the affinity of the porous materials on a gas in a mixture.

2.3| Surface area

An important parameter for the characterization and comparison of porous materials is the surface area; this one can be distinguished between external and internal. The first one is given by the outer surface of discrete or agglomerated particles; it is often difficult to define it due to the atomic scale roughness of the solid surfaces. Instead, the second one includes the walls of fractures, pores and deeper cavities that wide and accessible to gas. Since, the accessibility of the pores depends on

the shape and size of the gas molecule, the internal surface will also depend on the size of the gaseous molecules and this is the molecular sieves effect.

2.3.1| Langmuir model

In 1916 Irving Langmuir published a paper when was presented his model for the adsorption of fluids onto a simple surfaces [4]. In this paper, he hypothesized that the surface has a certain number of equivalent sites to which a molecule of fluid can stick, by either chemisorption or physisorption. He postulated that gaseous molecules do not rebound elastically from the surface, but are held by it in a similar way of molecules in solids.

This model explains adsorption by assuming an adsorbate behaves as an ideal gas at isothermal conditions. In these conditions, the partial pressure of the gas is related at the volume, adsorbed onto a solid adsorbent. The Langmuir model is based on some assumptions that are valid specifically for the simplest case in which the adsorption of a single adsorbate onto a series of equivalent sites on the surface of the solid. The assumptions are [2]:

- the surface is homogeneous, i.e. containing the adsorbing sites and it is a perfectly flat plane;
- the gas once adsorbed has no mobility;
- all sites are equivalent;
- each site interacts with at most one gas molecule;
- there are no interactions between adsorbate molecules on adjacent sites.

The adsorbate binding is treated as a chemical reaction between the adsorbate molecule and an empty site on surface; this one allowed to obtain an equation for this model by a kinetic derivation;

the kinetic derivation it previously described (Eq. 2.2 – 2.5) where the final equation is the Langmuir isotherm equation.

For evaluate the surface area is necessary to explicitly the Langmuir equation into linear form:

$$\frac{p}{Q} = \frac{1}{K \cdot Q_{max}} + \frac{p}{Q_{max}} \qquad \text{Eq. 2.9}$$

here the Q_{max} is the maximum amount of adsorbed gas for the monolayer formation, is known as the monolayer capacity. If this equation was plotted as p/Q in function of p, is possible evaluated the Q_{max} and through the followed equation is possible obtain the surface area by Langmuir model:

$$Surface\ area = \frac{Q_{max} \cdot N \cdot S}{V_m} \qquad \text{Eq. 2.10}$$

here N is the Avogadro's number, S is the contact surface are by each molecules called molecular cross-section area and V_m is the molar volume of the adsorbate.

2.3.2| BET model

In 1938 Stephen Brunauer, Paul Hugh Hemmett and Edward Teller published an article in which they explained the principle for the BET theory [5]. The BET theory applies to systems of multilayer adsorption and usually utilizes probing gases that do not chemically react with material surfaces as adsorbate to quantify specific surface area. This theory is an extension of the Langmuir theory to multilayer adsorption, the theory was derived on the following assumption:

- the Langmuir equation applies to each adsorbed layer;
- the adsorption and desorption occur only onto and from the exposed layer surface;
- at solid-vapour equilibrium the rate of adsorption onto the ith layer is balanced by the rate of desorption from the $(i + 1)$th layer;

- the molar heat of adsorption for the first layer is considered to be higher than for the succeeding layers;
- the layer not interacted;

These consideration lead to an isotherm of the form:

$$\frac{Q}{Q_{max}} = \frac{C \cdot \frac{p}{p^0}}{\left(1 - \frac{p}{p^0}\right)\left[1 + (C-1)\frac{p}{p^0}\right]} \qquad \text{Eq. 2.11}$$

where p^0 is the saturation pressure of the vapour at the system temperature, and C is a constant related to the difference between the heat of adsorption in the first layer and the heat of liquefaction of the vapour through the following equation:

$$C = \exp\left(\frac{E_1 - E_L}{RT}\right) \qquad \text{Eq. 2.12}$$

where E_1 and E_L is the heat of adsorption for the first layer and the heat of liquefaction of the vapour respectively. The Eq 2.11 may be transformed into

$$\frac{1}{Q\left[\left(\frac{p^0}{p} - 1\right)\right]} = \frac{C-1}{Q_{max} \cdot C}\left(\frac{p}{p^0}\right) + \frac{1}{Q_{max} \cdot C} \qquad \text{Eq. 2.13}$$

a plot of this equation yield a straight line, usually at $0.05 < p/p^0 < 0.30$, and does not go beyond at value higher than 0.30, because the multilayer adsorption does not proceed indefinitely as the theory contends. From the BET plot Q_{max} is determined and by the Eq. 2.10 may be possible calculated the specific surface area.

2.4| Density Functional Theory (DFT)

The most method used for determined the pore size distribution (PSD) is based on the DFT. This theory allow describing the property of material taking into account the energetic heterogeneity that characterized the adsorption phenomena. The gas adsorption is an equilibrium and the density of molecules will be higher in the proximity of the surface, for which it is possible describe an equilibrium distribution of gas in function of pressure e molecular property of the system through the DFT. The DFT is based on the thermodynamic principle for which a system in equilibrium have a minimum of energy and it described the interaction energy with the Lennard-Jones potential.

For evaluated of PSD the DFT considers that each pore is independent, therefore each pore provides a contribution on the total adsorption and this contribution is proportional to the total area of the sample. The relation that explain this assumption is:

$$Q(p) = \int dH q(p,H) f(H)$$ [6] Eq. 2.14

where $Q(p)$ is the experimental quantity adsorbed at the pressure p, $q(p,H)$ is the quantity adsorbed for unit area at the same p in an ideal pore of dimension H called Kernel function, and $f(H)$ is the total pore area of dimension H.

The model consist in a pore represented by two walls at a distance H, this pore is open and immersed in a fluid at pressure and temperature fixed. The fluid interact with the wall and reaches the equilibrium, in this condition, the chemical potential is the same in each point of the system and it is equal at the chemical potential of the bulk fluid. While the bulk fluid is a homogeneous system of constant density whose chemical potential can be determined by the pressure of the system, the fluid near the walls has no constant density. It is possible to define a distribution as density profile $\rho(r)$, expressed as a function of the distance r from the pore wall. This distribution is obtained by minimizing the Helmotz energy of the system. Once the density profile has been obtained for a given pressure value, it is possible to calculate the quantity of gas adsorbed by a particular pore by

integrating the area under the curve. By repeating this procedure for a series of pressure value, the adsorption isotherm for the model is constructed and the PSD is obtained.

2.5| Isosteric heat of adsorption

As previously mentioned, an adsorption process involves the formation of interaction between the adsorbent and adsorbate. This process is exothermic and is associated with a quantity of heat released, which is called isosteric heat of adsorption (ΔH_{iso}). Therefore, the isosteric heat of adsorption is an energy value that indicates the affinity between adsorbent and adsorbate system. It is very important to know the interaction energies involved in a certain adsorption process, certain application energies, because some applications require high values of ΔH_{iso}, while others require lower values.

Experimentally the value of ΔH_{iso} can be measured directly or indirectly; the indirect method uses calorimetric techniques, instead the indirect uses the isotherms. In fact, the adsorption is an equilibrium, as seen in Par. 2.2, and the isotherm is the equilibrium curve, so it is possible to use on it the thermodynamic equations that correlate an equilibrium process with the enthalpy, in particular the Van't Hoff equation that follows:

$$\frac{\partial \ln K}{\partial T} = \frac{\Delta H}{RT^2} \qquad \text{Eq. 2.15}$$

this relation contains the equilibrium constant, but this can be replaced by the pressure by modifying the Langmuir equation, indeed the Langmuir equation can be rewritten in the following form [7]:

$$\ln K + \ln p = \ln\left(\frac{\theta}{1-\theta}\right) \qquad \text{Eq. 2.16}$$

that differentiating respect T and rearranging becomes:

$$\left[\frac{\partial}{\partial T}\ln K\right]_\theta = -\left[\frac{\partial}{\partial T}\ln p\right]_\theta \text{ [7]} \qquad \text{Eq. 2.17}$$

which replaced in the Eq. 2.15:

$$\left[\frac{\partial}{\partial T}\ln p\right]_\theta = -\frac{\Delta H_{iso}}{RT^2} \qquad \text{Eq. 2.18}$$

then through two or more isotherms between the same substrate and the same gas at different temperature, it is possible to derive the value of the interaction energy between adsorbent and adsorbate.

On a practical level the curves at different temperature must be fitting with an equation, in order to determine the pressure value at different temperatures with the same quantity adsorbed, then, through the calculated pressure values, the curve $\ln p$ as a function of $1/T$ is constructed and from the angular coefficient, is obtained the value of isosteric heat of adsorption.

2.6| Selectivity

The industrial processes where the porous materials can be used need that the adsorption occurs in the presence of a mixture of gases, for which is necessary that the porous materials have a preferentially adsorption for a gas respect at another, i.e. that porous materials are selective. Pure-component adsorption isotherms are routinely measured with high accuracy, instead accurate measurements of adsorption isotherms in the presence of a mixture of gases are complicated. Over the past several decades, a variety of models has been proposed for predicting multicomponent adsorption data using only pure-component adsorption isotherms. However, none of these theories has matched the influence and applicability of the Ideal Adsorbed Solution Theory (IAST) by Myers and Prausnitz in 1965 [8]. The theory was developed using three major assumption:

- adsorbate molecules in the mixture have equal access to the entire surface area of adsorbent,

- the adsorbent is homogeneous,
- the adsorbed phase is an ideal solution in which interaction between molecules are equivalent in strength.

IAST is a thermodynamic approach that assumes an ideal solution is formed by the adsorbed phase. It is essentially an adsorption similar to Raoult's law for vapour-liquid equilibrium. To meet the ideal requirement, there must be no interactions between the adsorbate molecules in the adsorbed phase mixture, and the spreading pressure of the component must be equal at constant temperature. The spreading pressure can be calculated for the pure component using the following equation:

$$\pi = \frac{RT}{A}\int_0^{p_i^0} \frac{n_i(p)}{p_i}\,dp \qquad \text{Eq. 2.19}$$

where π is the spreading pressure; the partial pressure is calculated using a similar Raoult's law and $n_i(p)$ is the pure-component adsorption isotherm. Spreading pressure is two-dimensional and can be thought of as the negative of surface tension. The total adsorbed amount is calculated using standard state loadings from the pure component isotherm:

$$\frac{1}{n_T} = \sum_{i=1}^{N} \frac{x_i}{n_i^0} \qquad \text{Eq. 2.20}$$

where N is the number of species in the mixture, x_i is the mole fraction of component i in the adsorbed phase and n_i^0 is the amount of component i adsorbed at constant temperature and spreading pressure in the absence of the other components. The Eq. 2.19 and 2.20 allow calculating the selectivity starting from of the pure-component isotherm, the adsorption selectivity, indicated with S, for a binary mixture is defined as:

$$S = \frac{q_1/q_2}{p_1/p_2} \qquad \text{Eq. 2.21}$$

where q_1 and q_2 are the loadings of the two components and p_1 an p_2 are the partial pressure of the two components.

2.7| High-pressure adsorption

High-pressure experiment introduce several complexities, both in terms of collecting isotherm data and interpreting results, that are not as significant at lower pressures. For this is necessary introduce a new terms related at describing high-pressure adsorption capacity as excess, total and absolute adsorptions.

In principle, a gas is considered adsorbed when the attractive forces of a surface determine a greater density of gas molecules than those normally present at the same pressure and temperature. In two-dimensional surface adsorption, the strength of the interaction between the gas and surface decrease with increasing distance until the attractive forces of the surface become negligible and only bulk or free gas are present. This distance is called Gibbs dividing surface that is an imaginary line parallel to the interface, can be used to divide the total free volume into adsorbed and bulk regions [9].

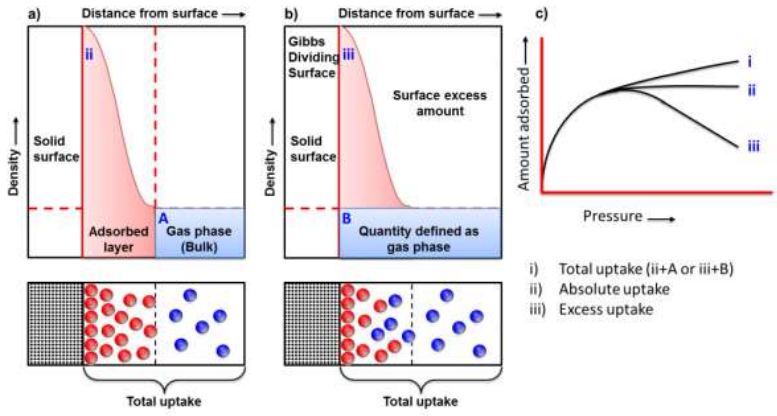

Figure 2.3. Schematic representation of the relation between the a) absolute, total and b) excess adsorbed amount. c) Typical isotherms for total, absolute and excess adsorption.

The absolute amount adsorbed (n_{abs}) is defined simply as the total number of molecules that are in the adsorbed region. Unfortunately, absolute adsorption cannot be directly measured since it is not possible to determine the location of the Gibbs surface experimentally. For which, all adsorption measurements give the excess adsorption (n_{exc}), that is the difference between the absolute

adsorption amount and the bulk amount that would have been present in the adsorbed region (V_a) without surface (Fig. 2.3), and this definition is related at the following equation:

$$n_{exc} = n_{abs} - V_a \cdot \rho_{bulk}(p,T) \qquad \text{Eq. 2.22}$$

where $\rho_{bulk}(p,T)$ is the density of bulk gas. Is not possible to determine experimentally V_a, there is no straightforward method for calculating absolute amount from the measured of excess adsorption. Instead, the total adsorption (n_{tot}), which includes all gas molecule inside the pores, is often used as an approximation for absolute adsorption. Total adsorption can be calculated from the excess using the following equation:

$$n_{tot} = n_{exc} - V_p \cdot \rho_{bulk}(p,T) \qquad \text{Eq. 2.23}$$

where the V_p is the experimental measured total pore volume determined from an N_2 adsorption isotherm at 77 K.

For gas storage applications, the total adsorption is most relevant for comparing the capacities of different adsorbent, as it is an intrinsic property of a material and represents the total amount of gas that can be stored within porous materials. Moreover, the total adsorption considers the density of gas in bulk phase; this one is significant at high pressures. Usually, the difference between the excess and the total amount is relevant in the conditions to natural gas storage.

Below, my contribution in the field of porous materials will be explained and their interaction with gases will be explored.

.

2.8| Porous materials for methane storage

In recent years, our society has started a search for the use of alternative fuels to oil in order to decrease the carbon emission. Methane or natural gas, it is a quick choice to lower carbon

emissions, waiting for the development of more eco-sustainable solutions. However, technologies for the transport of natural gas, such as pipeline and liquid natural gas (LNG) may prove unsatisfactory for political and economic reasons [10]. Therefore, Compressed Natural Gas (CNG) technology has become the most widely used for methane transport [11]. The CNG is a technology where the natural gas is compressed up to high pressures for storage and transportation inside appropriate containment systems. This technology is also applied in other industrial areas including the automotive field.

The use of porous materials in storage of natural gas, also known as Adsorbed Natural Gas (ANG), has been proposed, as an innovative way to transport and store large amounts of natural gas. The most studied for this application include zeolites, activated carbons and MOFs [9] but in some cases, they have of limitations, as the thermal and chemical stability [12]. Moreover, since the absorption measurements are limited to moderate pressures, such as 35 or 65 bar, however, these pressures are suitable for vehicular applications. As a result, the need for high-pressure methane storage materials remains, which would improve their general-purpose performance.

POPs (Par. 1.5.2) offer a valid option because the carbon-carbon connectivity of these polymers gives high thermal and chemical stability, resistance to contaminants and low water affinity. In fact, some of them with high surface areas and pore volumes have been proposed in recent years for the capture and storage of gas [13]. For optimal high-pressure performance, the contribution of mesopores must be significant, and high deliverable capacity is achieved only if a moderate amount of gas is retained at low pressure during the discharge step [14]. POPs are endowed with a mesoporous component and can fulfill these requirements, and therefore, are promising candidates for efficient storage and delivery. For this family of materials methane capture has been investigated only in a limited number of papers, and methane storage at high pressure has not yet been explored.

This research focus on the synthesis and methane uptake/release over a wide range of pressures (180 bar), of porous materials with carbon-carbon covalent bonds connecting the aromatic rings. Two synthetic paths were pursued the Yamamoto coupling and the Friedel-Crafts alkylation

reactions. The monomers choice for this study possess a high number of aromatic rings and accordingly multiple reactive sites (Fig. 2.4) which connect with other monomers to form multiple links, resulting in a cross-linked framework in which each monomer is bound to more than two other monomers. A systematic variation of the connectivity and geometry of monomer units allowed the investigation of the influence of the polymer structure on gas adsorption properties up to high pressures. A number of new monomers and synthetic conditions were explored to compare methane adsorption for an extensive collection of aromatic porous networks, thus providing efficiency and convenience parameters for these materials.

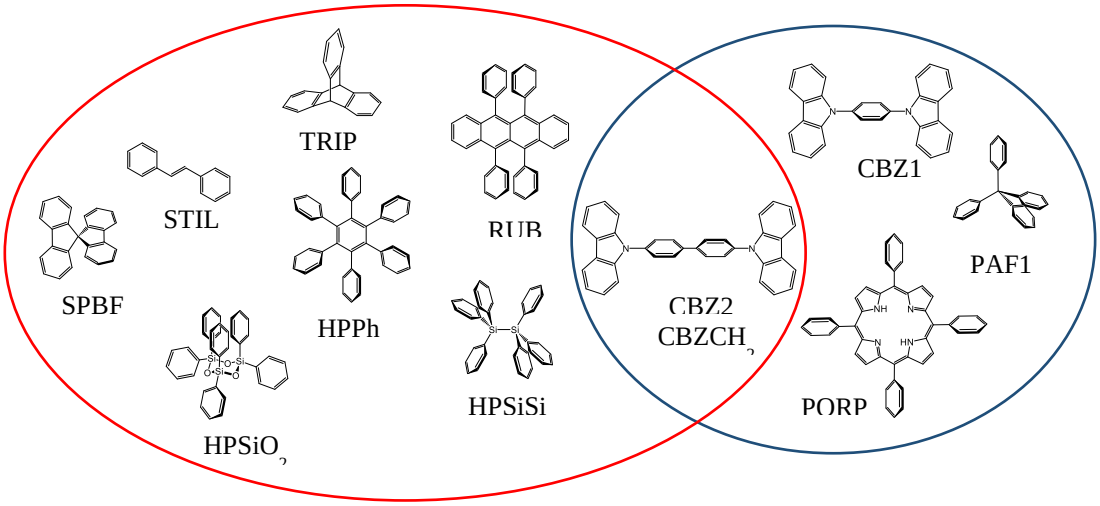

Figure 2.4. Monomer structures used for the synthesis of porous materials. In the red circle the monomers used for the Friedel-Crafts reaction and in the blue circle the monomers for the Yamamoto coupling.

2.8.1| Experimental

For the Friedel-Crafts alkylation, the solvent and reagents for synthesis were commercially available and used without further treatment. Instead, for the Yamamoto coupling it is necessary to carry out a bromination reaction on the monomers, except the 5,10,15,20-tetrakis(4-bromophenyl)porphyrin that was bought, and the solvents were used freshly distilled.

2.8.1.1| Synthesis of tetrakis-(4-bromophenyl)methane [15]

In a round-bottom flask containing bromine (20 ml, 390 mmol), tetraphenylmethane (6 g, 18.7 mmol) was added in small portion under vigorous stirring at room temperature. After the addition was completed, the resulting solution was stirred for 20 min and then cooled to 0 °C. At this temperature, ethanol (45 ml) was added slowly and the reaction mixture was allowed to warm to room temperature overnight. After this, the precipitate was filtered and washed with saturated aqueous sodium hydrogensulfite solution (50 ml). After drying in vacuo, the yellow crude product was recrystallized by chloroform/ethanol solution (1:1) to give a white solid (8.4 g, 13.2 mmol, yield 96%). ^{1}H NMR (300 MHz, $CDCl_3$) δ: 7.39 (d, *J* = 8.7 Hz, 8H), 7.01 (d, *J* = 8.7 Hz, 8H) (Fig. 2.5).

2.8.1.2| Synthesis of 1,4-bis(3,6-dibromo-9*H*-carbazol-9-yl)benzene [16]

In a round bottom flask were dissolved 1,4-di(9*H*-carbazol-9-yl)benzene (0.5 g, 1.23 mmol) and *N*-bromosucccinimide (0.961 g, 5.39 mmol) in anhydrous *N*,*N*'-dimethylformamide (4 ml). The mixture was refluxed under nitrogen atmosphere for 4 h. After that time, the crude was poured into water (30 ml) and light brown solid was filtered and washed with water. Subsequently, the obtained solid was washed with dichloromethane-ethanol solution and recrystallized from THF to give a white solid (0.7 g, 0.97 mmol, yield 78%). ^{1}H NMR (300 MHz, DMSO-d_6) δ: 8.44 (d, *J* = 2.0 Hz, 4H), 7.92 (s, 4H), 7.60 (dd, *J* = 9.0, 2.0 Hz, 4H), 7.51 (d, *J* = 9.0 Hz, 4H) (Fig. 2.6).

2.8.1.3| Synthesis of 4,4'-bis(3,6-dibromo-9*H*-carbazo-9-yl)1,1'-biphenyl [17]

In a round-bottom flask 4,4'-bis(9*H*-carbazo-9-yl)1,1'-biphenyl (1 g, 2.06 mmol) was dissolved in THF (20 ml). The temperature of the solution was adjusted to 40 °C. After the addition of *N*-bromosuccinimide (1.58 g, 8.87 mmol) the temperature was maintained for 16 h, during which a white precipitate is formed. The reaction mixture was filtered and the white precipitate was washed thoroughly with dichloromethane and ethanol. ^{1}H NMR (300 MHz, $CDCl_3$) δ: 8.23 (d, *J* = 1.88 Hz, 2H), 7.36 (d, *J* = 8.7 Hz, 2H), 7.55 (dd, *J* = 8.89, 1.88, 2H), 7.65 (d, *J* = 8.33 Hz, 2H), 7.91 (d, *J* = 8.70 Hz, 2H) (Fig. 2.7).

2.8.1.4| General procedure for the Friedel-Crafts reactions [18]

Formaldehyde dimethyl acetal (FDA) and anhydrous $FeCl_3$ were added to a solution of monomer in 1,2-dichloromethane, under an inert atmosphere. The mixture was then stirred at 80 °C for 24 h in a round-bottom flask equipped with a cooling vapour condenser. After the reaction, the resulting powder was collected by filtration and then washed with methanol several times, until the filtrating liquor was colourless. The product was purified by Soxhlet extraction using methanol for 48 h and subsequently dried under vacuum at 130 °C for 15 h. The monomer:FDA:$FeCl_3$ molar ratios are writing in the following (Tab. 2.1):

Table 2.1. Stoichiometric ratio of the reagents for the Friedel-Crafts alkylation reaction for distinct monomers.

Sample	Monomer	FDA	$FeCl_3$	Stoichiometric ratios Mon:FDA:$FeCl_3$	1,2-dichloroethane
TRIP	1 g	2.1 ml	3.83 g	1:6:6	20 ml
$CBZCH_2$	1 g	1.5 ml	2.68 g	1:8:8	20 ml
$HPSiO_2$	1 g	1.8 ml	3.27 g	1:12:12	20 ml
HPPh	1 g	2.0 ml	3.64 g	1:12:12	20 ml
RUB	1 g	1.3 ml	2.44 g	1:8:8	20 ml
STIL	1 g	2.0 ml	3.60 g	1:4:4	20 ml
HPSiSi	1 g	2.0 ml	3.75 g	1:12:12	20 ml
SPBF	1 g	2.2 ml	4.10 g	1:8:8	20 ml

2.8.1.5| General procedure for the Yamamoto coupling [19]

The catalytic complex was prepared by adding bis(1,5-cycloocatdiene)nickel(0) ($Ni(COD)_2$) to 2,2'-bipyridil and cis,cis-1,5-cyclooctadiene (COD) in dry DMF and THF solution. The porous polymers were obtained by adding dropwise the brominated monomers, dissolved in THF, to the catalytic mixture was stirred at 0 °C for 4 h and at room temperature for 44 h. The reaction was then quenched by adding concentrated HCl (30 ml), until the solution turned green with a white suspension. The filtered product was washed with THF (3 × 100 ml), water (3 × 100 ml) and chloroform (3 × 100 ml) and dried in a vacuum at 200 °C. Moreover, with this procedure was also synthetized a copolymer between tetrakis(4-bromophenyl)methane and 5,10,15,20-tetrakis(4-bromophenyl)porphyrin with a 80:20 ratio, called PAFPORP. The molar ratios of single reactions are writing in the following (Tab. 2.2):

Table 2.2. Stoichiometric ratio of the reagents for the Yamamoto coupling for distinct monomers.

Sample	Monomer	$Ni(COD)_2$	COD	2,2'-bipyridyl	THF	DMF
CBZ1	760 mg	1.2 g	1 ml	1 g	300 ml	200 ml
CBZ2	670 mg	2.0 g	1 ml	1 g	200 ml	200 ml
PORP	800 mg	1.2 g	1 ml	1 g	300 ml	200 ml
PAF1	700 mg	2.0 g	1 ml	1 g	160 ml	180 ml
PAFPORP	370 mg TFM 135 mg PORF	1.0 g	0.5 ml	0.5 g	120 ml	180 ml

2.8.2| Results and discussion

The multiple reaction sites on the aromatic rings provide a tendency for cross-linking. Moreover, the three-dimensional geometry of the monomers, combined with the formation of carbon-carbon crosslinks, not permitted the packing of the framework. Indeed, the molecular shape of the monomers, which is generally maintained within the individual monomeric units in the framework, contributes to the formation of low-density structures. The Friedel-Crafts alkylation allow connecting the monomeric units through the formation of methylene linker between aromatic rings. Instead, with Yamamoto coupling, the monomers are bound by direct C-C covalent bonds between aromatic groups [20]. In the case of the Friedel-Crafts alkylation, the maintenance of a constant stoichiometry of both FDA and $FeCl_3$ with respect to each aromatic ring in the monomer unit were applied, in particularly for one phenyl ring two FDA moles and two $FeCl_3$ moles, resulted in an advantage for a systematic comparison of the results.

The structural investigation at the molecular level was performed by ^{13}C and 2D ^{1}H-^{13}C NMR spectroscopy. The spectra of the porous materials obtain by both synthetic routes show resonances between 110 and 150 ppm assigned to the aromatic ring of monomeric units (Fig 2.8) [21]. The aliphatic region not present peaks for the frameworks obtained by the Yamamoto coupling reaction, except in the case of PAF1 sample (Fig 2.8), related at the quaternary carbon at the core of the monomeric unit.

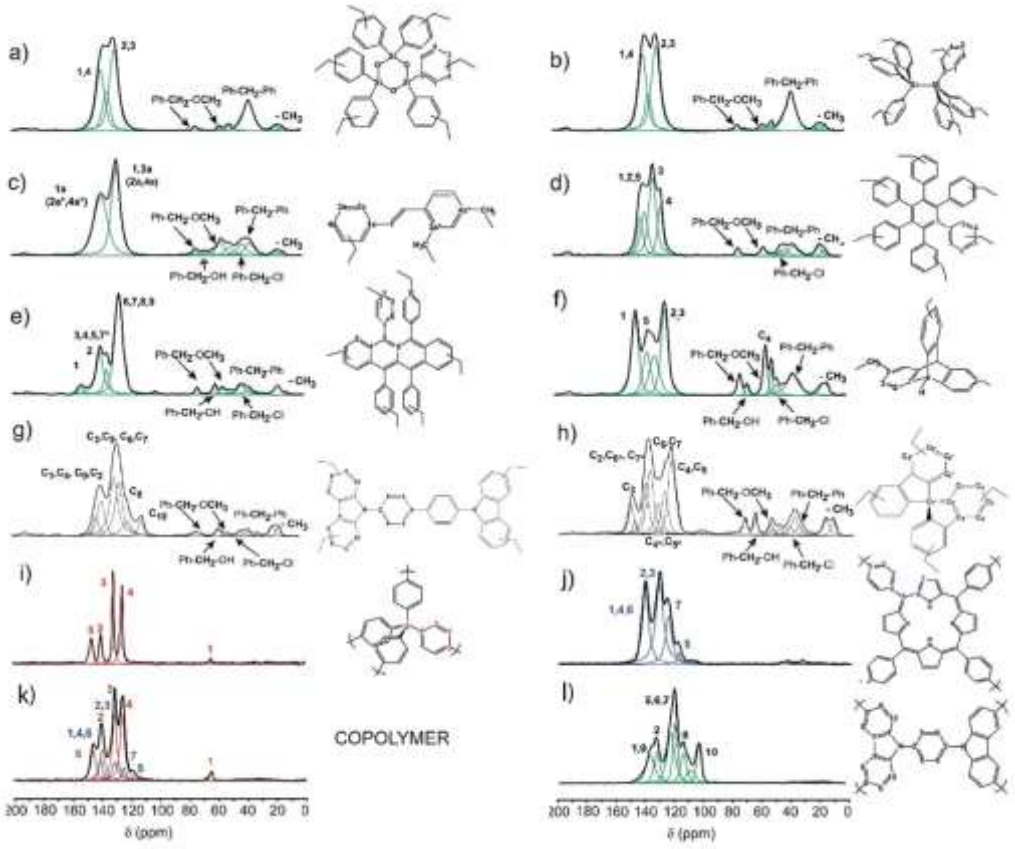

Figure 2.8. ^{13}C MAS NMR spectra of a) $HPSiO_2$, b) HPSiSi, c) STIL, d) HPPh, e) RUB, f) TRIP, g) $CBZCH_2$, h) SPBF, i) PAF1, j) PORP, k) PAFPORP, l) CBZ1.

On the opposite, additional signals appear in the aliphatic region for the Friedel-Craft reaction frameworks, independent of the monomer (Fig 2.8). The pattern is complex, because of multiple alkylation reactions of the aromatic rings, incomplete reactions of the FDA and secondary reactions that with the solvent generate a series of pendant in the frameworks, including pendants as CH_2—O—CH_3, CH_2—OH, CH_2—Cl. The connectivity in the frameworks was deduced by 2D NMR spectra, which through nuclear dipole-dipole interactions, highlighted the correlation between carbon and hydrogen nuclei in close spatial proximity, providing evidence of the insertion of connecting bridges and pendant groups [22]. The 2D MAS spectrum of the triptycene-based porous polymer (TRIP) shows the aromatic hydrogens of the main architecture δ_H = 6.6 ppm are in correlation with the carbon of the methylene groups at δ_C = 36.3 ppm [23] that bridge the aromatic paddles of connected monomer units and, vice versa, the benzylic hydrogens of methylene bridge at δ_H = 4.9

ppm communicate with the aromatic substituted carbons, unambiguously showing the phenylene groups to be covalently bonded to the CH_2 linkers (Fig 2.9). In addition, the CH_2—O carbons of the pendant groups reside at a short distance with respect to the aromatic hydrogens, in fact is present the cross peak between the aromatic hydrogens at $\delta_H = 6.6$ and the carbon at $\delta_C = 72.8$ ppm, demonstrating that they are directly substituted in the aromatic rings through a carbon-carbon bond.

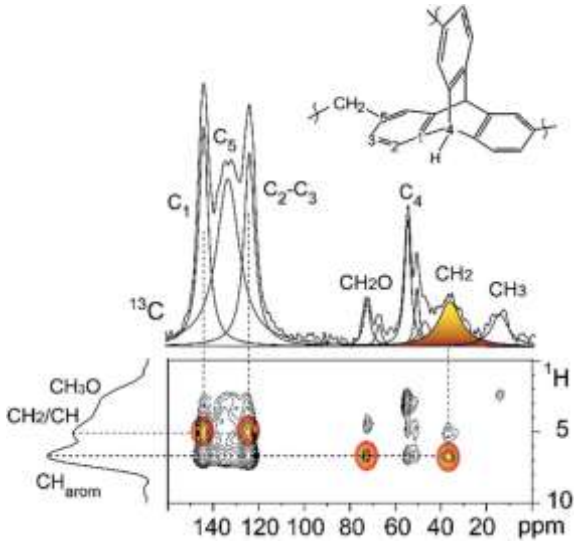

Figure 2.9. 2D ^{1}H - ^{13}C HETCOR NMR spectra with Lee-Goldburg decoupling of TRIP. The cross-peaks between hydrogens and carbons are highlighted in orange.

FTIR spectra confirmed the presence of the methylenic bridge in the frameworks synthetized by Friedel-Crafts alkylation. In particularly, the peak between 2800-3000 cm^{-1}, characteristic of asymmetric and symmetric C—H stretching, revealing that the networks are linked by CH_2 groups, confirmed also that the peaks around 1500 cm^{-1} related at the bending vibration by CH_2 (Fig 2.10). The spectra show a band at about 1700 cm^{-1}, typical of hyper-crosslinked aromatic systems. The spectra of frameworks synthetized by Yamamoto coupling show the disappeared of the peaks around 520 cm^{-1} (Fig 2.10), this peaks are related at the C—Br bond stretching, thus demonstrating the success of the phenyl-phenyl coupling.

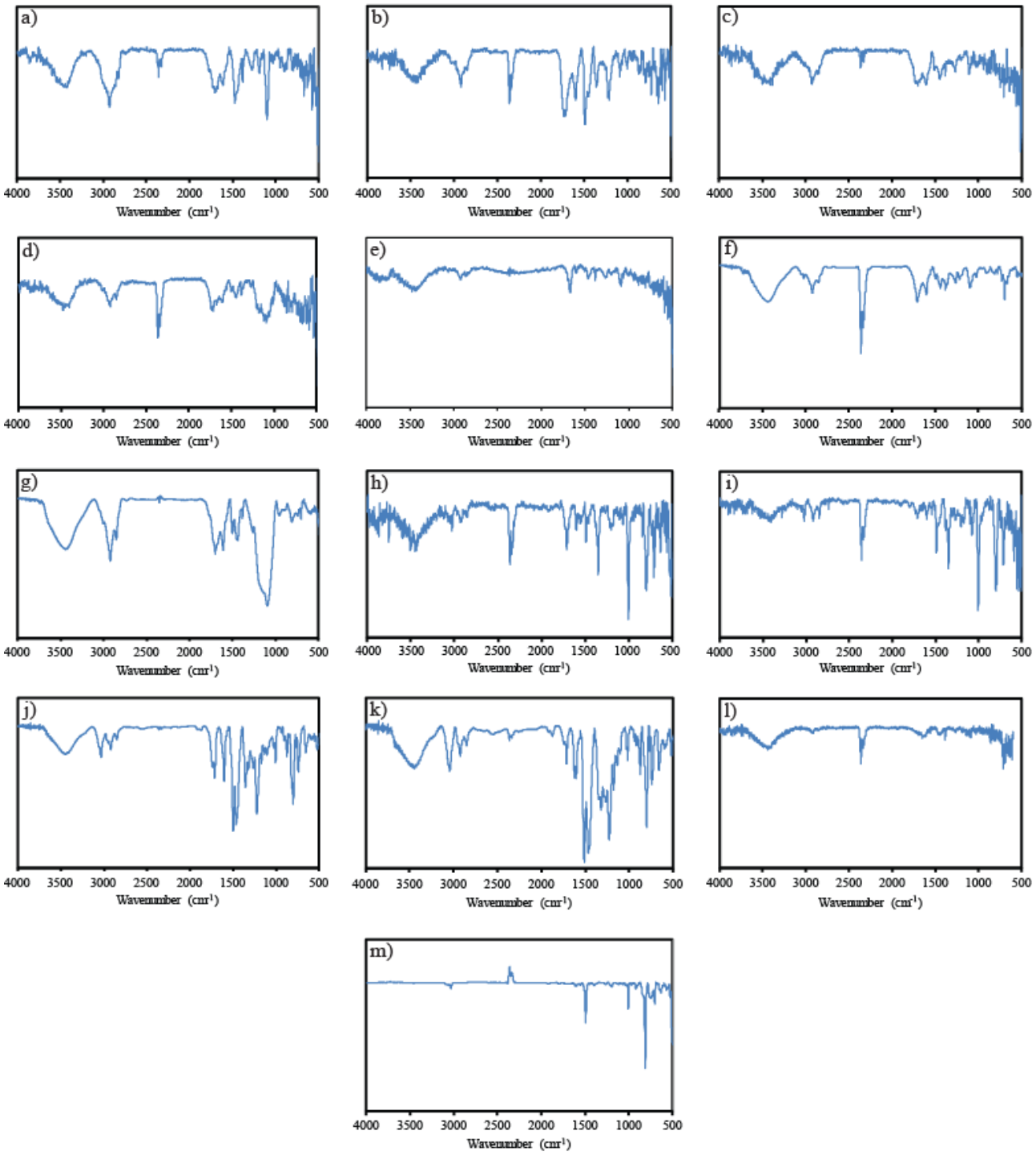

Figure 2.10. FT-IR analysis of the samples a) TRIP, b) CBZCH2, c) STIL, d) HPSiO2, e) RUB, f) HPPh, g) HPSiSi, h) PORP, i) PAFPORP, j) CBZ1, k) CBZ2, l)SPBF, m) PAF1.

The absence of residual bromine in the porous polymers by the Yamamoto coupling is also indicated by the elemental analysis (Tab. 2.3). In the case of copolymer (PAFPORP), the analysis allowed to determine the stoichiometric of the resulting polymer, accordingly of the results the copolymers is formed by a molar ratio to 23/77 mol/mol of porphyrin/tetraphenylmethane. Moreover,

the concentration of Fe and Ni inside the samples was analysed by X-ray fluorescence, all samples have a concentration of metal below the 0.3% of the sample (Tab. 2.4). Thermogravimetric analysis (TGA) conducted in air demonstrated the stability of these materials up to or more than 500 °C (Fig. 2.11), in the case, of the materials HPSiSi and $HPSiO_2$ the TGA shows a residual around 20% related at the formation of SiO_2 during the thermal treatment. While the powder X-ray diffraction patterns show no defined peak, suggesting the structural disorder of the networks (Fig. 2.12), this is because the formation reaction of the framework is fast and irreversible, so during the synthesis the polymer does not have time to self-assemble to form crystalline domains.

Table 2.3. Elemental analysis of the polymers synthetized by Yamamoto coupling reaction.

Sample	C %	H %	N %	Residue %
CBZ1	84.84	5.20	6.57	3.39
CBZ2	86.51	4.42	6.06	3.01
PAF1	88.72	6.55	-	4.73
PORP	76.85	3.82	8.13	11.2
PAFPORP	74.55	3.63	7.01	14.81

Table 2.4. X-ray fluorescence analysis for the polymers.

Sample	Ni (%)	Fe (%)
PAF1	0.027	-
CBZ2	0.045	-
CBZ1	0.260	-
SPBF	-	0.126
STIL	-	0.252
RUB	-	0.077
HPPh	-	0.115
$CBZCH_2$	-	0.164
$HPSiO_2$	-	0.130
HPSiSi	-	0.062
TRIP	-	0.116

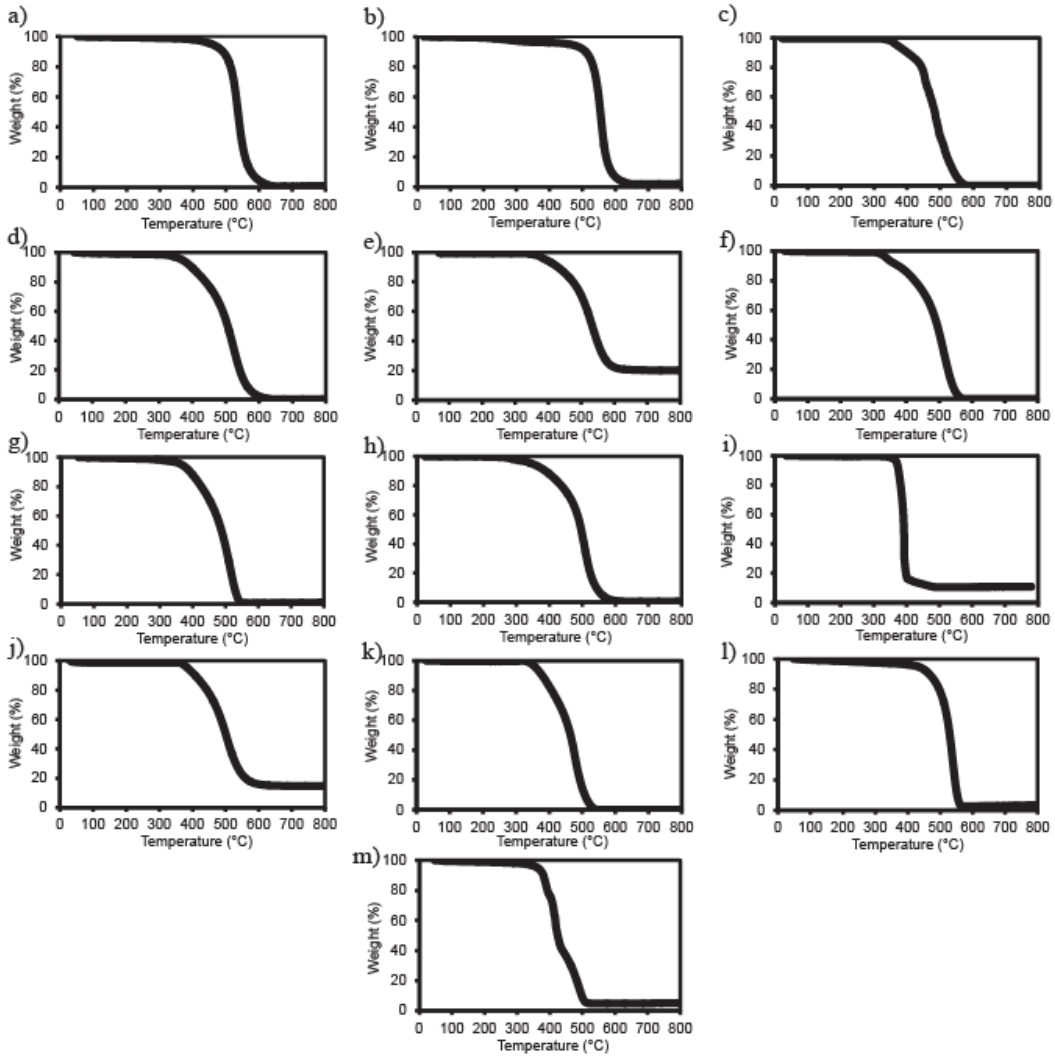

Figure 2.11. Thermogravimetric analysis of a) CBZ1, b) CBZ2, c) TRIP, d) $CBZCH_2$, e) $HPSiO_2$, f) HPPh, g) RUB, h) STIL, i) PORP, j) HPSiSi, k) SPBF, l) PAF1, m) PAFPORP performed in air.

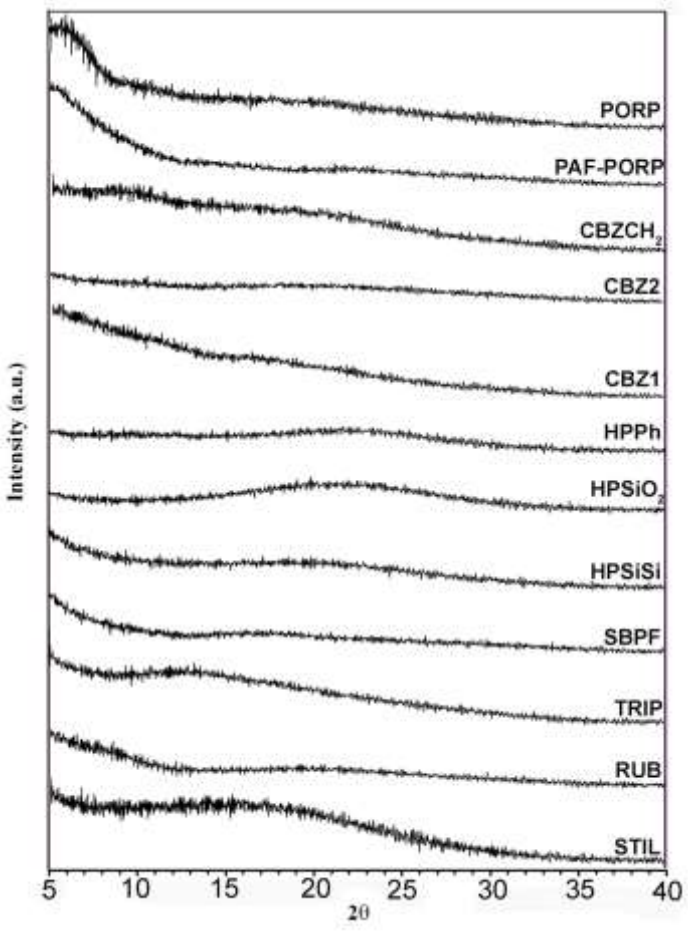

Figure 2.12. Powder X-ray diffraction patterns of the porous polymers.

The porosity of the frameworks was tested by N_2 adsorption isotherms at 77 K, which exhibited BET surface areas, evaluated to linearize of the isotherm in the range 0.05-0.1 p/p°, ranging typically from 1000 to 1700 m^2/g and up to 4800 m^2/g (Tab. 2.5) for the structures containing tetraphenylmethane as the monomer unit. The N_2 adsorption isotherms exhibit a steeply sloping gas uptake at relatively low pressures and continuous rise at higher relative pressures (Fig. 2.13), reflecting the presence of micro/mesopores distribution. Pore size distribution was calculated by the NLDFT method using carbon slit pore model (Fig. 2.14), through the NLDFT was also evaluated the total pore volume of all materials (Tab. 2.5); all materials show a predominance microporosity with the presence of a mesoporosity part.

Table 2.5. BET and Langmuir surface areas, total pore volume (T.P.V.) for the samples.

Sample	BET (m^2/g)	Langmuir (m^2/g)	T.P.V. (cm^3/g)
PAF1	4784	5485	2.70
PAFPORP	2194	2492	2.02
CBZ1	1622	1834	1.40
CBZ2	1698	1942	1.42
PORP	1494	1703	1.13
TRIP	1592	1895	1.20
SPBF	1418	1612	0.93
STIL	1254	1525	0.92
RUB	1258	1428	0.85
HPPh	1082	1284	0.72
$CBZCH_2$	1090	1250	0.53
$HPSiO_2$	1054	1256	0.69
HPSiSi	872	1004	1.15

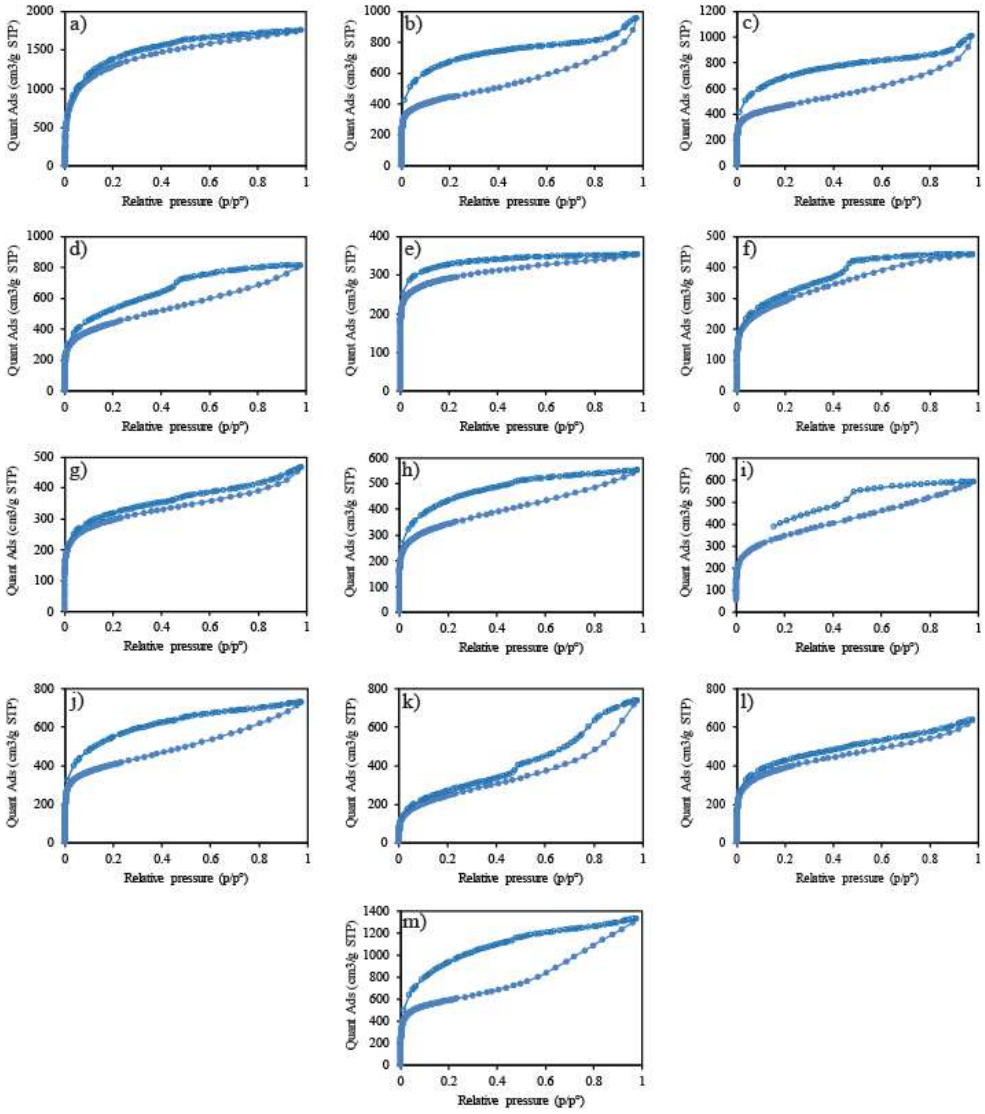

Figure 2.13. N_2 isotherms collected at 77 K of a) PAF1, b) CBZ1, c) CBZ2, d) TRIP, e) $CBZCH_2$, f) $HPSiO_2$, g) HPPh, h) RUB, i) STIL, j) PORP, k) HPSiSi, l) SPBF, m) PAFPORP.

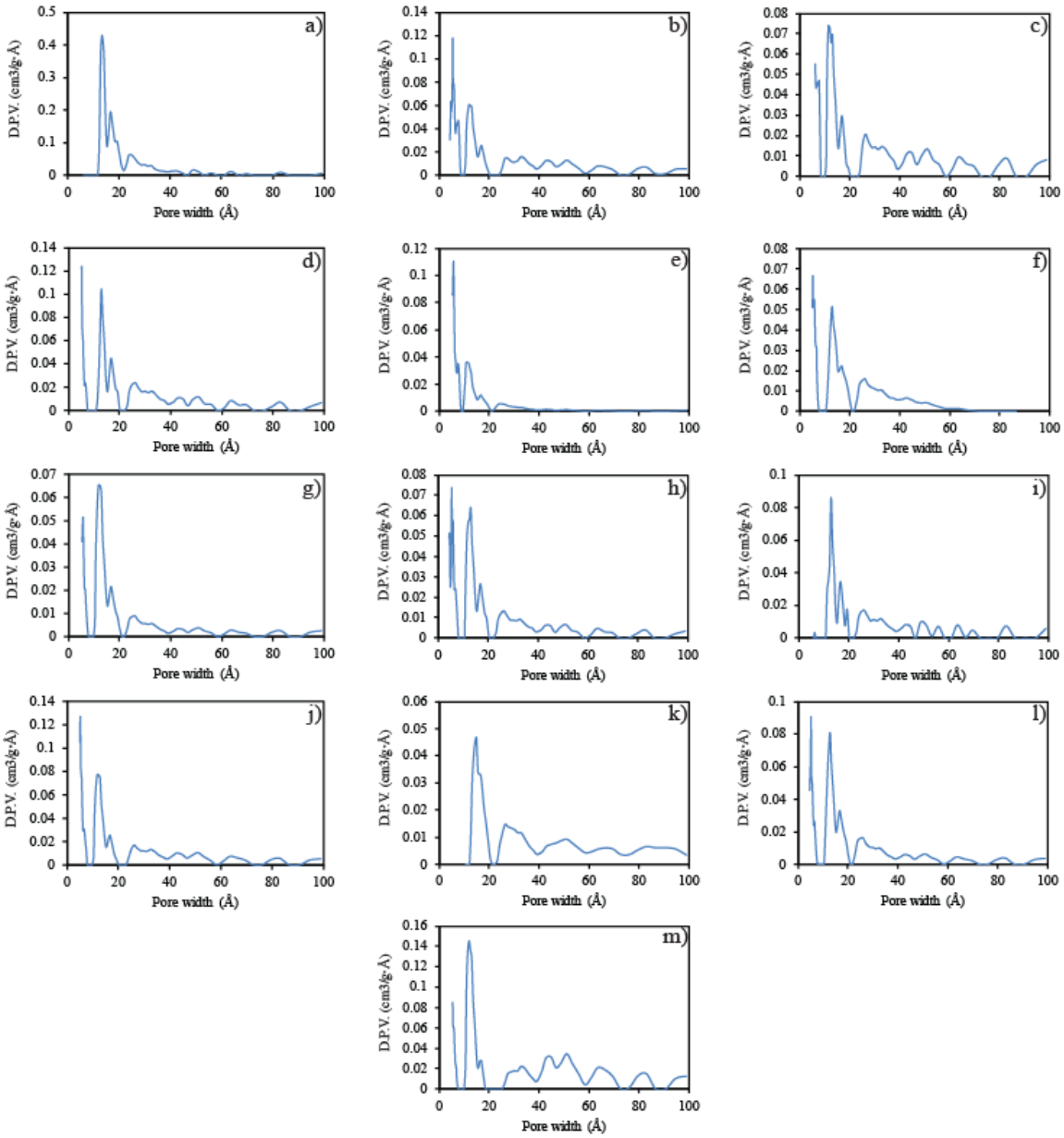

Figure 2.14. Differential pore size distribution of the samples: a) PAF1, b) CBZ1, c) CBZ2, d) TRIP, e) $CBZCH_2$, f) $HPSiO_2$, g) PPh, h) RUB, i) STIL, j) PORP, k) HPSiSi, l) SPBF, m) PAFPORP.

A large hysteresis is observed in many cases between the adsorption and desorption branches, as is mostly evident in the samples CBZ1, CBZ2, TRIP, RUB, STIL, HPSiSi and PAFPORP. Desorption curve closes only at low partial pressures. The hysteresis loop in the isotherm is consistent with the swelling of the network during sorption, because capillary condensation in the mesopores causes some strain in the network, as systematically observe in soft polymeric materials [24].

It can be observe that the best performance, as surface area, were obtained by rigid structures in which 3 or 4 aromatic rings connected to a node protrude at different angles, such as trypticene, spirobifluorene and tetraphenylmethane, because these structures are favourable to ensure expansion of the framework in all directions. In contrast, a number of aromatic rings higher than four did not provide an advantage in both the surface area and pore volume owing to the overcrowded arrangement on the same monomer.

The polymer were tested under a wide range of high pressure conditions up to 180 bar, with all measurements being taken two times to check the reproducibility of the data. In CH_4 excess isotherms, it is possible to observe an increasing uptake at low pressures, followed by a decrease in the quantity adsorbed starting from about 100 bar (Fig. 2.15). This is because the excess sorption is relative to what would have been in the pore volume. At high pressures, the bulk phase can still be compressed, but eventually, the pores are filled up and the adsorbed phase density levels off. Once the bulk phase density is higher than the adsorbed phased density, the excess sorption turns negative, as described in the Eq. 2.22. Applying the Eq. 2.23 it is possible to derive form the excess the total adsorption, which as described above takes into account the structural parameters of the framework and the variation of the density of the gas as a function of the pressure. The latter is derived from NIST data.

In total adsorption, it is possible to observe an increasing uptake over the whole range of pressures (Fig. 2.16), although the slope diminishes at high pressures. At 180 bar, adsorption values up to 445 cm^3/g were measured for porous organic polymers endowed with pore volume range of 1.20—1.40 cm^3/g, such as CBZ1, CBZ2 and TRIP materials. Such an uptake is far above the HKUST-1 performance at the same pressure, which reaches a quantity adsorption of 321 cm^3/g at 180 bar.

Since these high-pressure conditions above 100 bar are not frequently reported in the literature, the materials were compared to lower pressure than those published. Under the conditions of 65 bar and 298 K the porous polymers CBZ1, CBZ2 and TRIP adsorb a CH_4 amount of 255.4,

252.8 and 240.4 cm^3/g, respectively. Such high values are comparable with the CH_4 uptake of COF-5 (156 cm^3/g), COF-8 (156 cm^3/g), PPN-2 (198 cm^3/g), PPN-3 (269 cm^3/g), PPN-13 (255 cm^3/g) and NiMOF-74 (212 cm^3/g) [25] [26] [27] [28]. For which these materials are competitive whit those present in the literature for the storage of large quantities of methane.

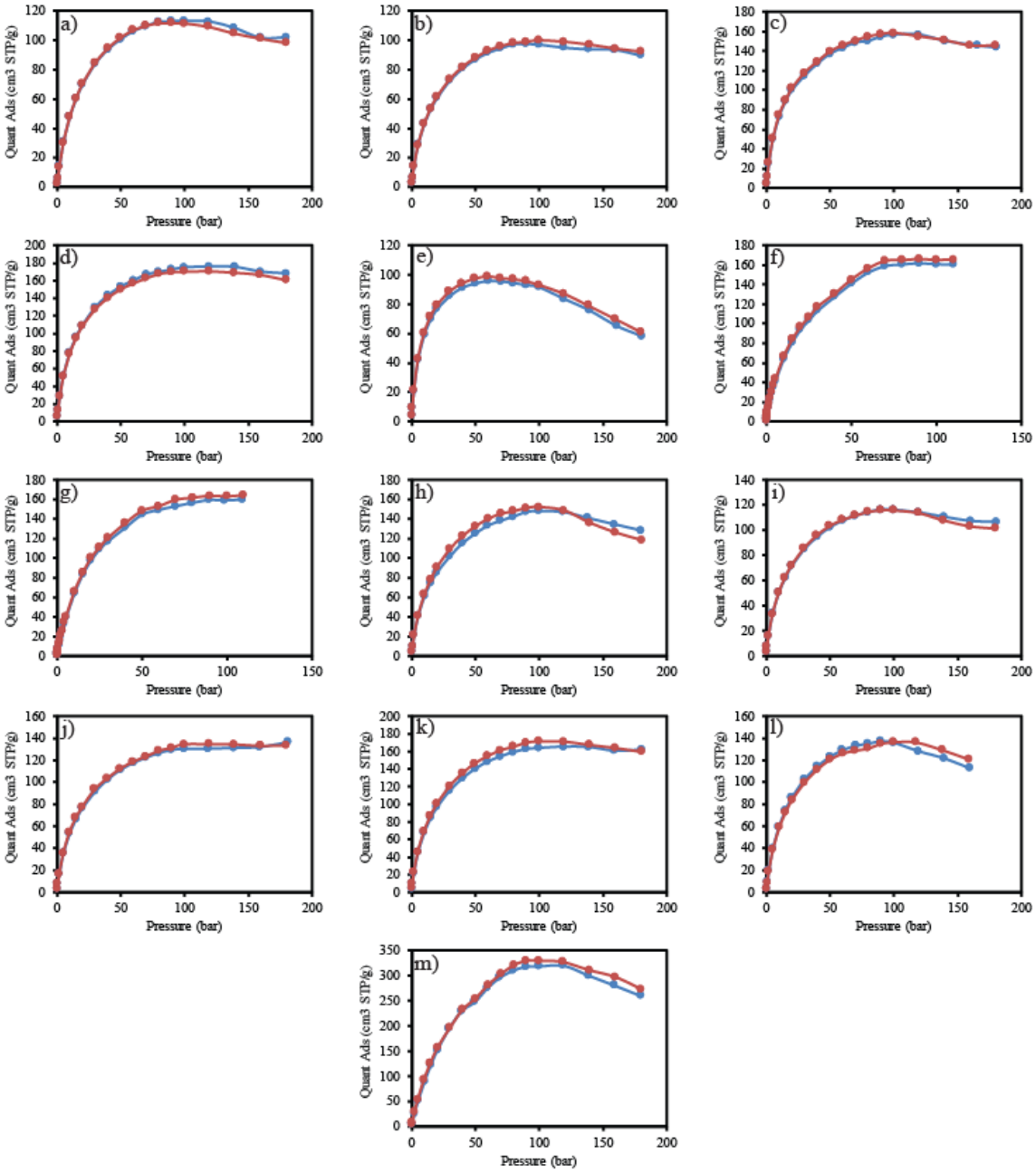

Figure 2.15. CH_4 excess isotherms adsorption at 298 K up to 180 bar for the samples: a) HPPh, b) $HPSiO_2$, c) CBZ1, d) CBZ2, e) $CBZCH_2$, f) PORP, g) PAFPORP, h) RUB, i) HPSiSi, j) STIL, k) TRIP, l) SPBF, m) PAF1. The blue curve is the first run and the red curve is the second run.

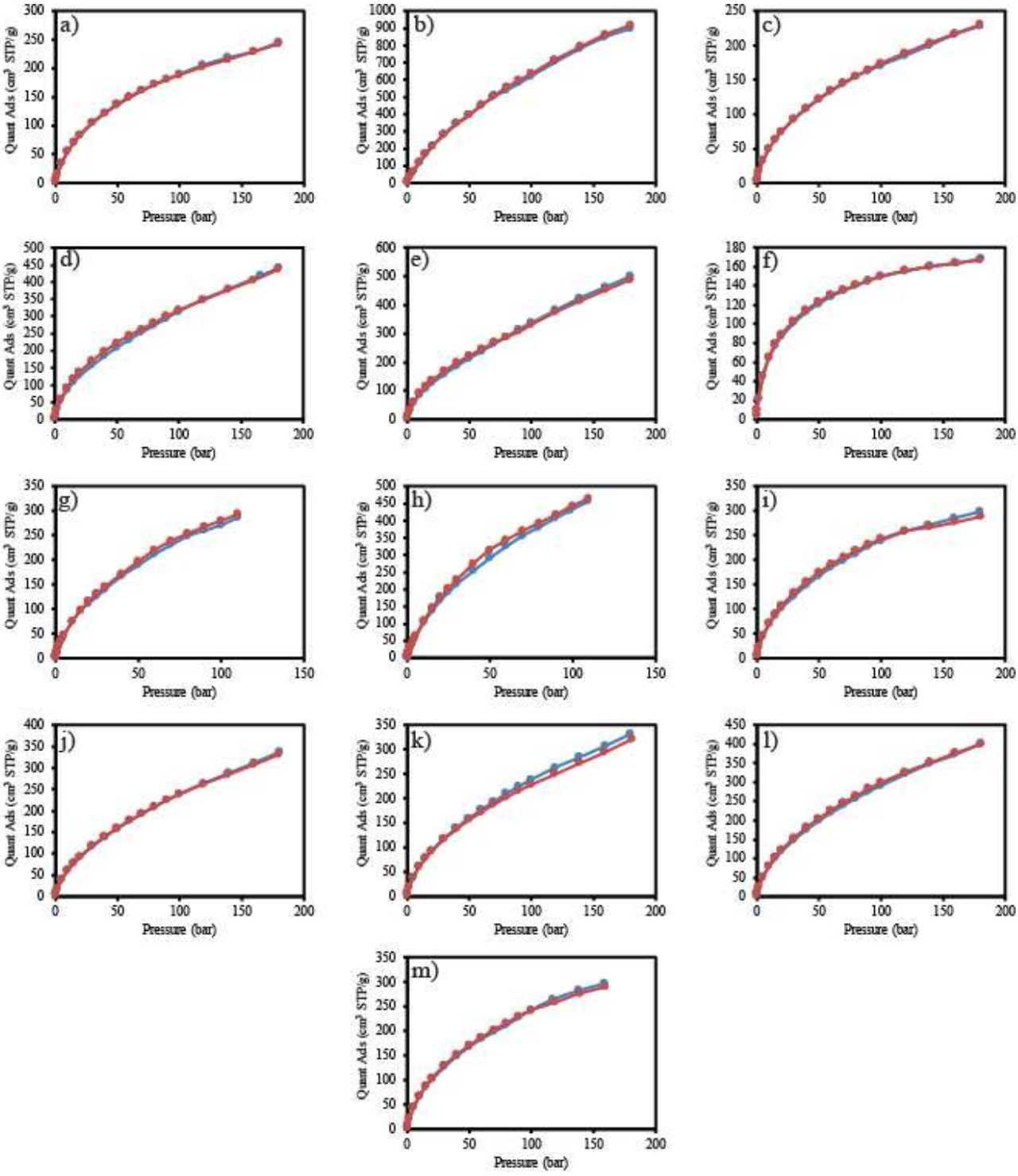

Figure 2.16. CH_4 total isotherms adsorption at 298 K up to 180 bar for the samples: a) HPPh, b) PAF1, c) $HPSiO_2$, d) CBZ1, e) CBZ2, f) $CBZCH_2$, g) PORP, h) PAFPORP, i) RUB, j) HPSiSi, k) STIL, l) TRIP, m) SPBF. The blue curve is the first run and the red curve is the second run.

In general, the maximum CH_4 adsorption amount are related to the pore capacity obtained by N_2 adsorption at 77 K, in fact, the HPSiSi compound which, despite the lowest surface area of 872 m^2/g, adsorb up to 332 cm^3/g owing to the large mesoporosity and the relatively large total pore

capacity of 1.15 cm^3/g. This is mainly derived from the geometry of the monomer in which six p-phenyl groups protrude from the Si—Si moiety, producing three-dimensional nodes that form a complex branching system.

The benchmark of these materials PAF1 reaches the value of 916 cm^3/g of adsorbed CH_4 at 180 bar, owing to its high pore volume (2.7 cm^3/g). The extremely high methane uptake, corresponding to 65% by weight, represents one of the top values in gravimetric adsorptive materials at room temperature. The comparison with HKUST-1 allowed showing that HKUST-1 saturates at 30-40 bar: at such pressure, it shows comparable performances, but a much more absolute amount of methane is stored in PAF1 at high pressures, proving the enormous relevance to explore high-pressure range. Already at 100 bar, PAF1 adsorbs 643 cm^3/g exceeding those of most best performing MOFs, COFs and carbon.

There is also a general desire to store or transport the largest amount of gas per tank available volume. Obviously, medium–high pressures help increase storage, but there has been little experimental testing of the practical gain obtained with an efficient adsorbent at high pressures. These desiderata are valid for any to-be-stored or transported gas, from the automotive area to CNG. The volumetric uptake allowed us to compare the results directly with compressed natural gas technology for naval transportation where volume, and not weight, is the critical issue.

The density of porous polymers plays a key role in the determination of volumetric gas uptake. Since the porous polymers presented here do not show crystalline order, a valuable method to determine the specific volume occupied by the material is based on the pore volume (known by N_2 adsorption at 77 K), combined with direct density measurements of the framework walls by He pycnometer, according to the following formula:

$$n_{tot}\left(\frac{V}{V}\right) = n_{tot}\left(\frac{V}{g}\right) \cdot \left[\frac{1}{\left(V_p + \frac{1}{\rho_{He}}\right)}\right] \qquad \text{Eq. 2.24}$$

where $n_{tot}(V/V)$ is the total adsorption in cm^3/cm^3, $n_{tot}(V/g)$ is the total adsorption in cm^3/g and ρ_{He} is the density by He pycnometer (Tab. 2.6). In Eq. 2.24, the part between square brackets calculates the density of the material, in fact, the pore volume is the reciprocal of the density given by the pores of the material, and however, the density of the He pycnometer is nothing else the density of the walls of the materials.

Table 2.6. He pycnometer density of the samples.

Sample	Density (g/cm^3)
CBZ1	1.26
CBZ2	1.25
TRIP	1.39
$CBZCH_2$	1.38
$HPSiO_2$	2.03
HPPh	1.25
RUB	1.15
STIL	1.38
PORP	1.45
HPSiSi	1.48
PAFPORP	1.24
SPBF	1.35
PAF1	0.98

Most of the MOFs exhibit a large adsorption capacity up to about 80 bar, after which saturation occurs. Instead, the CH_4 isotherms of the studied porous polymers reveal that on increasing the pressure to values higher than 100 bar there is a continuous gain in the adsorbed amounts (Fig. 2.17). This feature results in a high total volumetric uptake capacity, due to the remarkable contribution of mesoporosity. Furthermore, in such porous polymers, the slope of CH_4 adsorption isotherms is moderate at low pressure, which is a great advantage for a high working capacity, e.g. the amount of deliverable methane taking into account the practical discharge pressure, which can be of several atmospheres to feed the pipelines.

The total volumetric uptake of PAF1 measured at 110 bar is of 198 cm^3/cm^3 (Fig. 2.17). On comparing, the total volumetric uptake of CH_4 in the presence of PAF1 there is, with respect to pure

compressed methane, a maximum gain of an extra 110% at 70 bar. Collectively, most compounds of the family showed considerable volumetric uptake, although less capacitive than PAF1, consistent with their density, which is a critical parameter for volumetric uptake (Tab. 2.7).

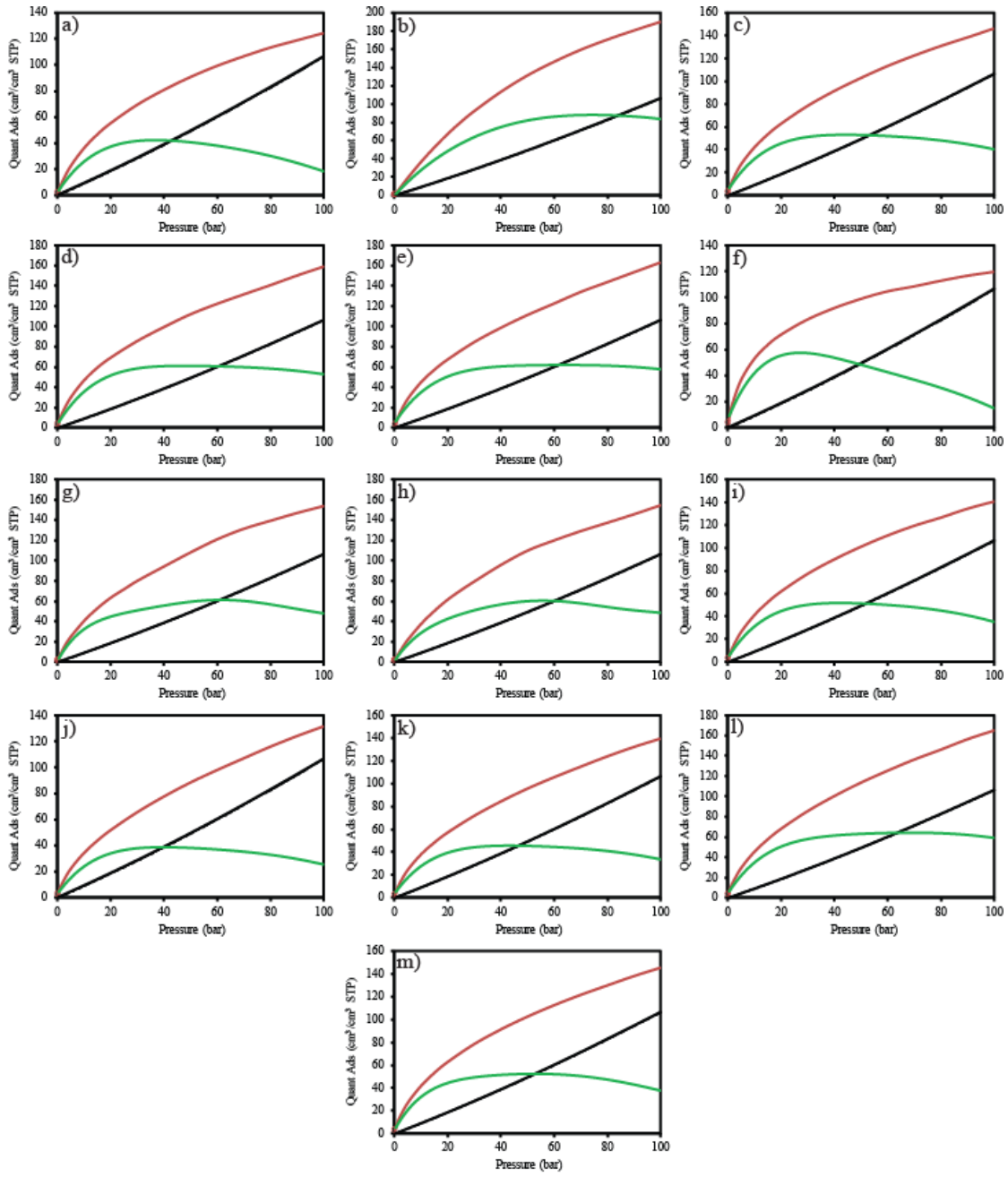

Figure 2.17. Work capacity of the sample a) HPPh, b) PAF1, c) $HPSiO_2$, d) CBZ1, e) CBZ2, f) $CBZCH_2$, g) PORP, h) PAFPORP, i) RUB, j) HPSiSi, k) STIL, l) TRIP, m) SPBF. The red curve is the CH_4 isotherms, the red curve the pressured methane and the green curve the work capacity.

Table 2.7. Work capacity value for samples at 35, 65 and 100 bar.

Sample	Work capacity at 35 bar (cm^3/cm^3)	Work capacity at 65 bar (cm^3/cm^3)	Work capacity at 100 bar (cm^3/cm^3)
CBZ1	60	60	53
CBZ2	59	62	58
TRIP	60	63	59
$CBZCH_2$	54	40	13
$HPSiO_2$	52	51	40
HPPh	47	37	19
SPBF	52	52	39
RUB	51	49	35
STIL	45	44	34
PORP	53	61	48
HPSiSi	38	36	25
PAFPORP	54	60	49
PAF1	70	87	84

The materials are promising for the storage of larger amounts of methane than CNG technology, but unfortunately these materials are very voluminous, so in case of implementation of the technology with these polymers it is necessary to reduce the volume, so it has been tested the mechanical stability. The materials were subjected to a mechanical pressure of about 600 bar and subsequently the capacity of adsorption of CH_4 to 180 bar was recorded again. The reduction of storage capacity was less than 8% (Fig. 2.18), consistent with the reduction of pore capacity measured by the N_2 adsorption isotherm at 77 K (Fig. 2.19). This result demonstrates the scarce tendency to close packing, owing to the intrinsic shape factor of the monomeric units that, had they been able to close-pack, would have resulted in reduced efficiency. The bridges realized to link the monomers through C—C or C—CH_2—C covalent bonds contributed to the creation of cross-linked polymeric frameworks that preserve their porosity after releasing compression. The compression allows the loading of large quantities of material inside the transport containers of methane, increasing the amount of methane that can be stored and then transported by reducing transport costs.

The materials have also been tested for CO_2 capture; they exhibit a high adsorption CO_2 capacity, as shown by the CO_2 isotherms at room temperature up to 10 bar (Fig. 2.20). The CO_2 uptake values found for the materials exceeding the performances of zeolite 13X (150 cm^3/g), ZIF-8

(78.4 cm^3/g) [28] and the active carbon (46 cm^3/g) [29]. The amount of CO_2 captured is proportional to the surface and to the pore volume. At 10 bar, the slope of the isotherms is still positive, indicating that the porous materials are not yet saturated. The samples PAF1 and copolymer are far more efficient than the other matrices. However, PAF1 shows a convex isotherm with respect to the abscissa axis at low pressures with subsequent change of slope at high pressures, this derives from the low affinity between the matrix and the gas. Despite this, PAF1 shows the highest value due to its high pore capacity. Moreover, reducing the temperature by only 25 °C, the uptake increases by 50% for the majority of the samples.

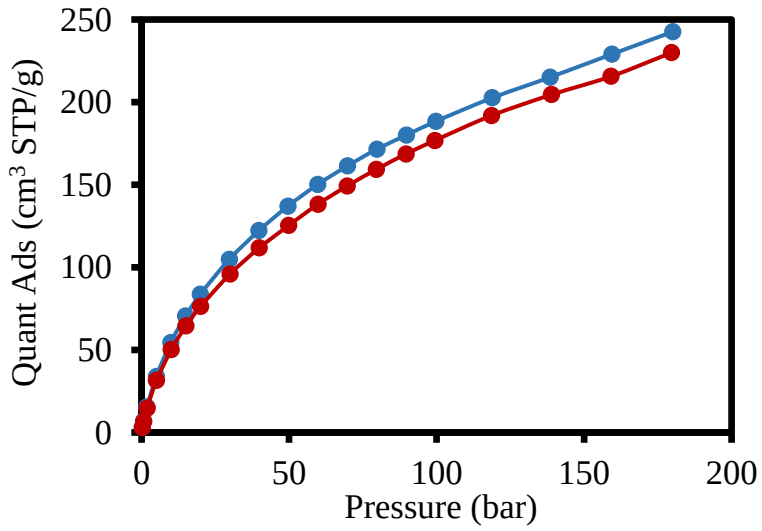

Figure 2.18. CH_4 adsorption isotherms before (blue curve) and after (red curve) mechanical pressure at 600 bar of HPPh sample.0

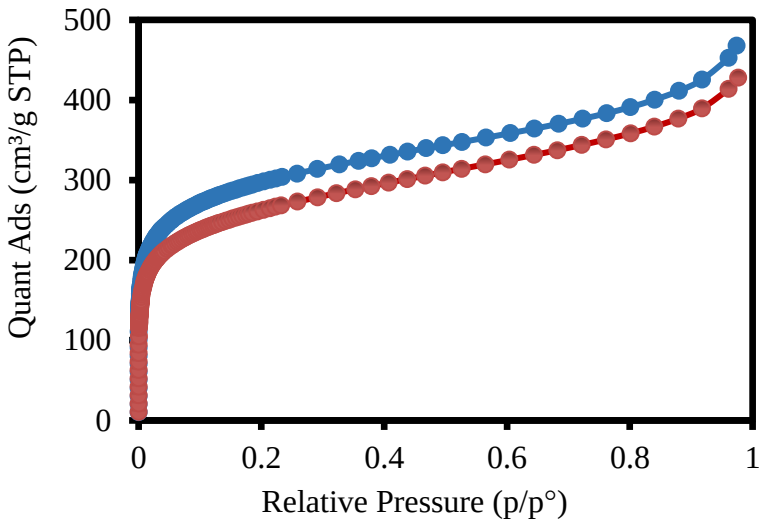

Figure 2.19. N_2 adsorption isotherms before (blue curve) and after (red curve) mechanical pressure at 600 bar of HPPh sample.

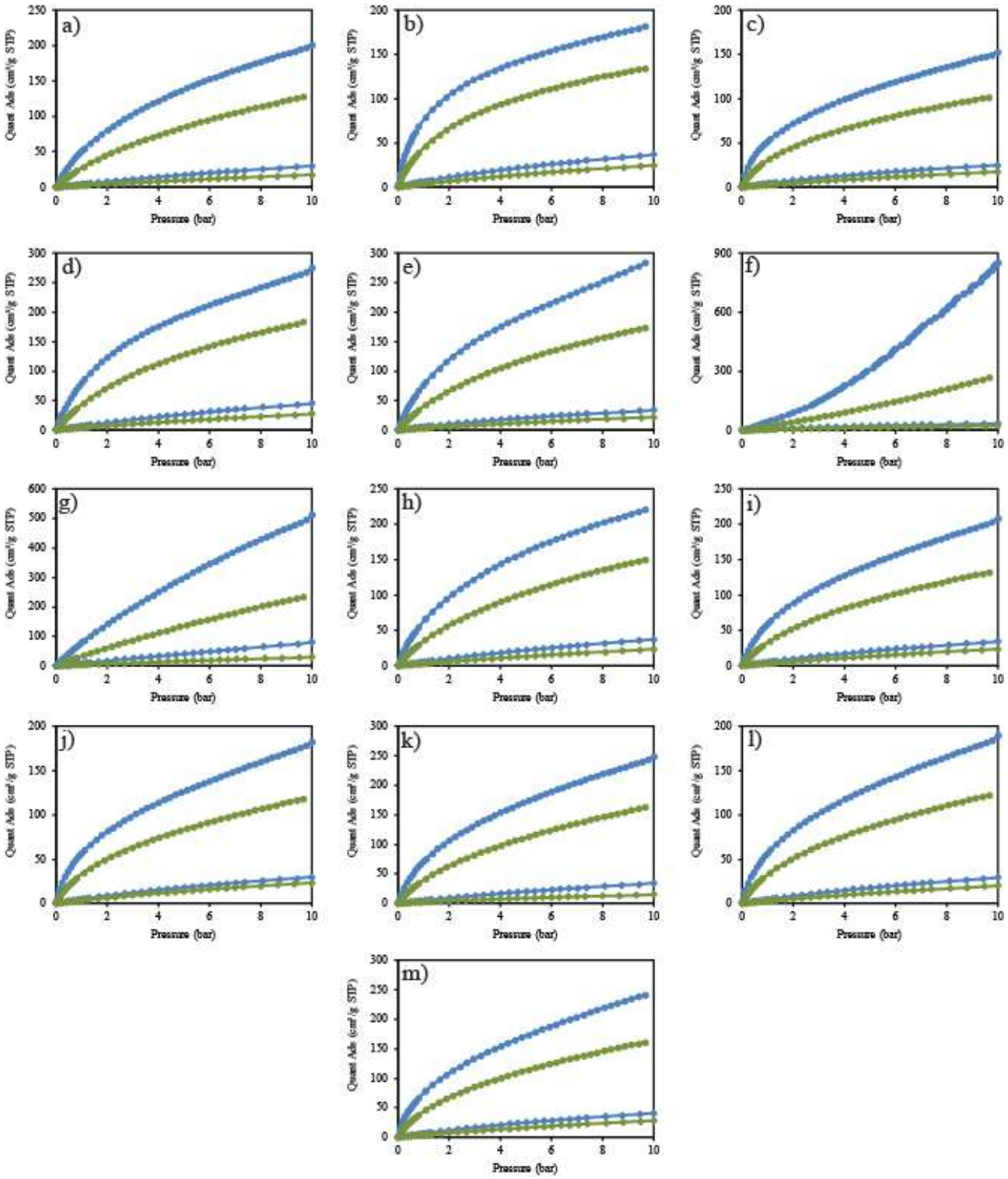

Figure 2.20. CO_2 (circle) and N_2 (diamond) adsorption isotherms of a) HPPh, b) $CBZCH_2$, c) $HPSiO_2$, d) CBZ1, e) CBZ2, f) PAF1, g) PAFPORP, h) PORP, i) RUB, j) HPSiSi, k) SPBF, l) STIL, m) TRIP collected at 273 K (blue) and 298 K (green) up to 10 bar.

The isosteric heat of adsorption at low coverage, determined by Van't Hoff equation, is quite high, ranging from 24.8 to 29.6 kJ/mol. Interestingly, the $CBZCH_2$ sample, obtained by Friedel-Crafts alkylation, exhibits a higher heat of adsorption of 29.0 kJ/mol, than that of compound CBZ2, which

was derived from condensation of the same monomer with the Yamamoto reaction (25.2 kJ/mol) (Fig. 2.21). This was due to the relevant presence of small microporosity in $CBZCH_2$ [30]. The interaction between CO_2 and the surface could be increased by the chains created by the oxygen-containing side rats, such as the CH_2—OH and CH_2—O—CH_3 groups originating from the FDA reagent and detected by MAS NMR.

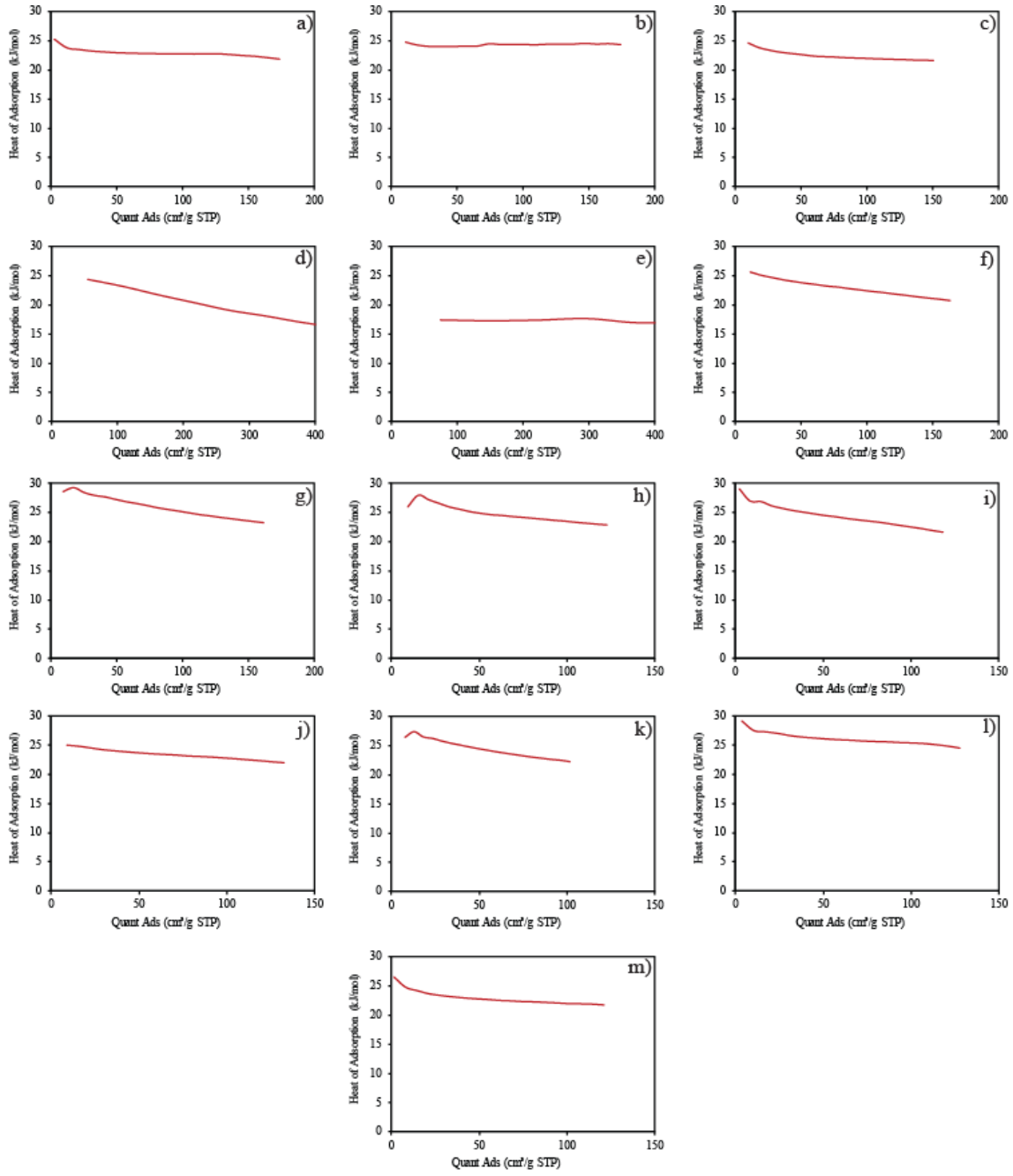

Figure 2.21. Heat of adsorption of a) CBZ1, b) CBZ2, c) PORP, d) PAF1, e) PAFPORP, f) SPBF, g) TRIP, h) STIL, i) HPSiSi, j) RUB, k) $HPSiO_2$, l) $CBZCH_2$, m) HPPh.

Consistently, the TRIP sample containing the highest number of pendant groups shows the highest isosteric heat of adsorption (29.6 kJ/mol). A value of about 30 kJ/mol is considered an optimal balance between an effective uptake and a convenient release by a porous framework.

The porous materials exhibit excellent CO_2/N_2 selectivity at low pressure ranging from 15 to 25 at room temperature with a 15:85 CO_2/N_2 mixture. The Selectivity value are weakly dependent of the pressure. Such values are higher as those reported for active carbon BLP AC (20-26 at 1 bar), zeolite 13X (18 at 1 bar) and ZIF-8 (7.6-8.4 at 1 bar) [29] [31] [32] (Tab. 2.8), opening perspectives for applications to post-combustion treatment of industrial polluting emission.

Table 2.8. Selectivity value at 1 bar at 273 and 298 K evaluated by IAST method.

Sample	Selectivity at 1 bar 273 K	Selectivity at 1 bar 298 K
CBZ1	19	15
CBZ2	23	18
PAF1	7	7
PAFPORP	11	11
PORP	19	16
HPPh	18	16
$HPSiO_2$	28	22
HPSiSi	25	16
RUB	20	15
SPBF	26	18
STIL	25	19
TRIP	26	18
$CBZCH_2$	30	21

2.9| Porous materials for gas adsorption

Gas capture and storage is a prominent issue for our society, since it enables solutions for environmental and energy problems, especially for the target gases carbon dioxide and methane, both massively present in the atmosphere and in the lithosphere, and their connection to power and heat generation [33]. Porous materials can efficiently store a considerable amount of such gases with a

moderate energy consumption for gas release, thus ensuring a sound energy balance in sorption/release cycles [34].

In recent years, there have been an increasing number of porous materials obtained by exploiting the formation of a variety of interactions and chemical bonds, which range from soft interactions to metal–organic and covalent bonds [35]. Among these families, porous organic polymers (POPs) boast some prerogatives derived from the stability of their 3D network of covalent bonds. These prerogatives include the absence of potentially toxic metal ions, high thermal robustness, resistance to solvents, especially water, and remarkable volumetric and gravimetric pore capacities [36].

2.9.1| Experimental

The monomers are been synthetized following the procedure present in literature, all reagents using for the synthesis are been used without purification. The solvents were used fresh distillates. The three monomers were obtained by the same starting reagent (Fig. 2.22).

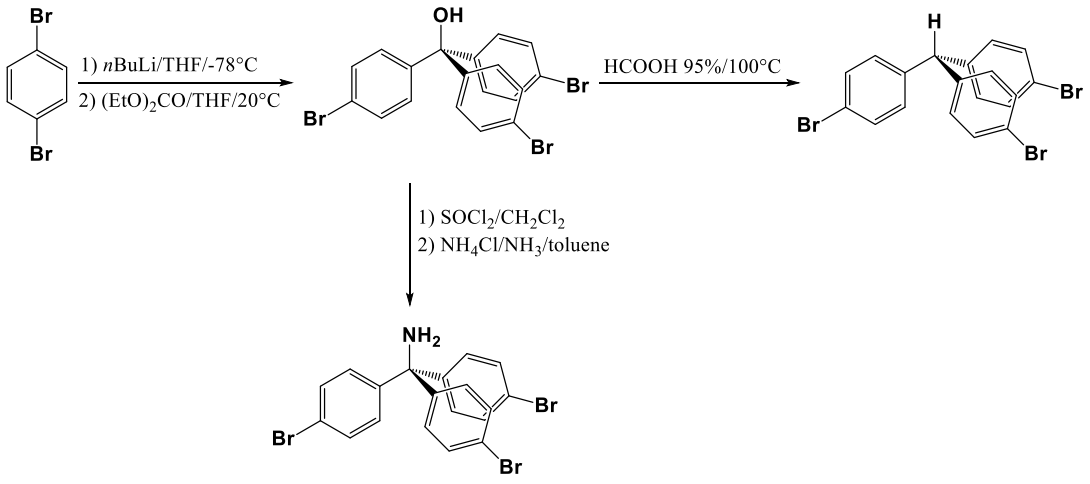

Figure 2.22. Scheme of monomer synthesis.

2.9.1.1| Synthesis of tris(4-bromophenyl)methanol [37]

p-dibromobenzene (8.7 g, 37.2 mmol) and fresh distilled THF (135 ml) were added to a 2-neck round-bottom flask equipped with a stirrer. The solution was cooled to -78 °C and n-BuLi (13.5 ml, 2.5 M in hexane 33.8 ml) was added dropwise. After 3 h, the solution was transferred in a 2-neck round-bottom flask containing diethyl carbonate (1.02 ml, 8.5 mmol) dissolved in THF (3ml). The solution was subsequently allowed to warm to room temperature. After 6 h, the reaction was quenched with saturated aqueous NH_4Cl (50 ml). The crude product was extracted with EtOAc (3x50 ml). The organic fractions were collected, washed with brine and evaporated with vacuum line. At the crude oil, was added hexane (60 ml) gently heated and sonicated to given a white solid, collected with filtration to yield 3.38 g (80%). ^{1}H NMR (300 MHz, $CDCl_3$): δ 7.45 (dd, 6H), 7.12 (dd, 6H), 2.70 (s, 1H) (Fig. 2.23).

2.9.1.2| Synthesis of tris(4-bromophenyl)methane [37]

Tris(4-bromophenyl)methanol (1.25 g, 2.52 mmol) was added to a 50 ml round-bottom flask equipped with a stirrer. Formic acid (95% in H_2O, 25 ml) was added slowly. A condenser was attached and the solution was heated to 100 °C for 19 h to give a yellow suspension. The reaction was quenched with saturated Na_2CO_3 (100 ml). The aqueous suspension was washed with Et_2O (3x40 ml) and the combined organic phases were washed with brine and evaporated. The resulting solid was run through a plug of SiO_2 in pentane, to isolate the product (0.897 g, 74% yield) as a white crystalline solid. ^{1}H NMR (300 MHz, $CDCl_3$): δ 7.42 (dd, 6H), 6.93 (dd, 6H), 5.40 (s, 1H) (Fig. 2.24).

2.9.1.3| Synthesis of tris(4-bromophenyl)methylamine [38]

Tris(4-bromophenyl)methanol (2 g, 4.03 mmol) and anhydrous CH_2Cl_2 (20 ml) were added to a 2-neck round-bottom flask. The solution was cooled to 0 °C and fresh distilled $SOCl_2$ (2 ml) was added dropwise. After 5 h, the solvent was evaporated; the resulting solid was diluted in anhydrous toluene (25 ml) and added dropwise to a saturated solution of NH_4Cl in 25% of aqueous ammonia (25 ml) at 0 °C. Then, the reaction was stirred for 24 h at 20 °C; organic phase was separated, dried and evaporated. At the crude solid was added hexane (20 ml) and sonicated for 30 minutes. The white solid was collected with filtration and dried. Pure product (1.046 g, 52.6% yield) could be obtained by precipitation of its hydrochloride. ^{1}H NMR (300 MHz, $CDCl_3$): δ 7.42 (dd, 6H), 6.93 (dd, 6H), 4.5 (s, 2H) (Fig. 2.25).

2.9.1.4| General procedure for frameworks synthesis [19]

The catalytic mixture was prepared by adding *cis*,*cis*-1,5-cyclooctadiene (1 ml), 2,2'bypiridyl (1g) and $Ni(COD)_2$ (2 g) in fresh distilled DMF (180 ml) and THF (60 ml) and stirred at 0 °C for 10 minutes. The porous polymers were obtained by adding dropwise the monomer (0.800 g), dissolved in THF (60 ml), to the catalytic mixture and the resulting mixture was stirred at room temperature for 48 h. The reaction was then quenched by adding concentrated HCl (30 ml), until the solution turned green with a white suspension. The product was filtered and washed with THF (3x30 ml), water (3x30 ml) and chloroform (3x30 ml) and dried in a vacuum at 170°C.

2.9.2| Result and discussion

Important properties of selective gas absorption are given by the post-synthetic insertion of organic functional groups, each promoting specific interactions with target gases [36]. The post-functionalization of the porous material is the most used methodology to modify its properties, but this way has some problems. Since the simple organic reactions of addition of functional groups carried out in solution, are more complex because they are carried out in a heterogeneous system, leading to not having a control over the number and in some cases on the position of the functional group. Thus, in the search for enhanced interactions by innovative solutions, new porous organic frameworks were prepared, starting from simple three-dimensional synthons bearing organic functions. The monomers consisting of tetrahedral nuclei carry both branches and functional groups; will be retained in the skeleton of the resulting structure. Therefore, the permanent motif of the structures consists of three *p*-phenylene rings protruding from a central core, with the fourth substituent being the organic function chosen, directly linked to the same nucleus, producing low-density architectures called triphenylmethane aromatic frameworks (TAFs). Using this synthetic strategy, the branches sustain the porous network and the functions protrude towards the empty spaces of the pores. The functions are regularly bound onto the central aliphatic carbon and do not modify the reactivity of the aromatic groups during the condensation reaction.

The organic functions are exposed to the gases that diffused into the framework. As a result, the behaviour of the three-dimensional frameworks with hydroxyl and aliphatic amine groups (TAF–OH and TAF–NH_2) is quite distinct from that of the fully hydrocarburic network (TAF). Monomers to be polymerized by the Yamamoto coupling reaction require bromine atoms substituted on the aromatic rings in the para-position. The presence of three such sacrificial functions on each monomer ensures a large number of cross-links.

Solid state MAS NMR spectra of the powders recorded on ^{13}C and ^{1}H nuclei indicate the formation of carbon-carbon bonds between the aromatic rings and highlight the dramatic change in

tetrahedral carbon chemical shift due to the presence of hydrogen, hydroxyl or amine substitution (Fig. 2.26). The ^{13}C and ^{1}H quantitative spectral evaluation confirms the full retention of the –OH and $–NH_2$ substituents upon polymerization, as expected by Yamamoto coupling (Fig. 2.26 and Fig. 2.27). This is an indication for optimal regularity in terms of constant stoichiometry and controlled insertion of functional groups into the overall frameworks.

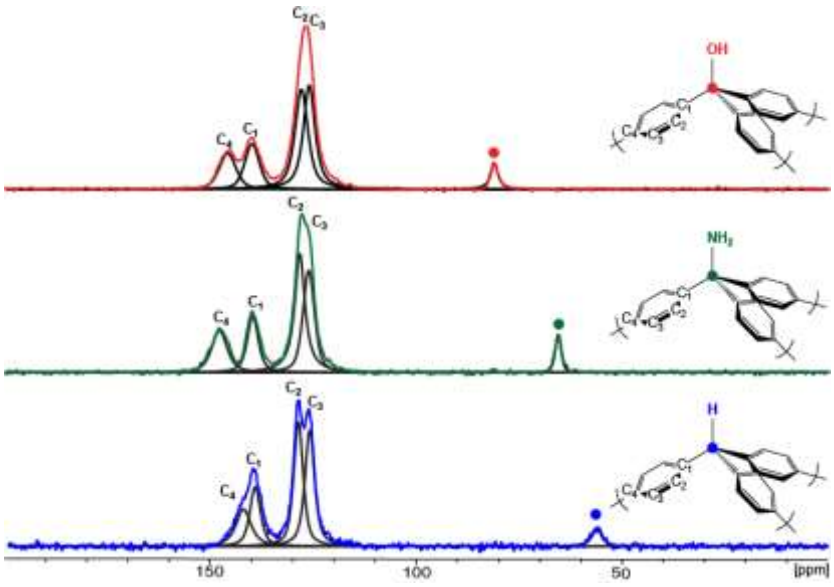

Figure 2.26. ^{13}C MAS NMR spectra with deconvolution of TAF (blue), TAF-NH_2 (green) and TAF-OH (red).

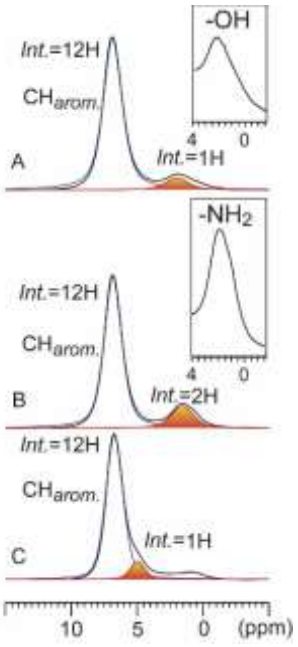

Figure 2.27. ^{1}H solid state NMR with deconvolution. A) TAF-OH, B) TAF-NH_2 and C) TAF.

Infrared spectra confirms the presence of the respective functional groups attached to the quaternary carbon atoms at the core of the monomer units. Distinctive bands related to the functionality on the ternary carbon appear in the regions 1000-1600 cm^{-1} and 3000-3600 cm^{-1}. In TAF—OH the C—O stretching gives rise to a sharp peak at 1158 cm^{-1} and an additional peak at 920 cm^{-1} usually observed for tertiary alcohols. In the region above 3000 cm^{-1} a broad band at 3580 cm^{-1} is associated to the presence of O—H groups. No such stretching bands are present in the TAF. TAF—NH_2 shows peculiar absorption bands at 3320 and 3380 cm^{-1} due to symmetric and asymmetric stretching of N—H bond (Fig. 2.28). Moreover, the maintenance of the stoichiometric ratio is further confirmed by the elementary analysis, which shows the percentage ratios of C, N, H and O that correspond to the expected values (Tab. 2.9). Powder XRD revealed no short-range periodicity, as typically occurs in covalent frameworks obtained by irreversible bond formation (Fig. 2.29). The presence of the functional groups does not affect the thermal stability of the frameworks, as confirmed by the TGA, which shows a thermal stability up to 400 ° C (Fig. 2.30).

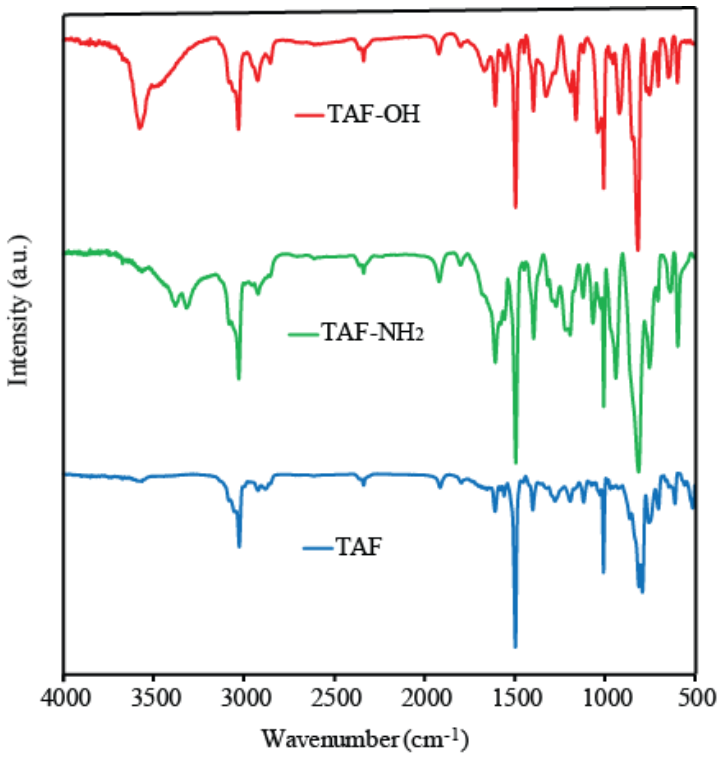

Figure 2.28. Infrared spectra of TAF (blue), TAF-OH (red) and TAF-NH_2 (green).

Table 2.9. Elemental analysis of the frameworks.

Sample	C		H		N		O	
	Calc	Exp	Calc	Exp	Calc	Exp	Calc	Exp
TPAF	94.57%	91.63%	5.43%	5.52%	0%	0.38%	0%	-
TPAFOH	88.69%	86.26%	5.09%	5.31%	0%	0.48%	6.22%	6.00%
$TPAFNH_2$	89.03%	85.71%	5.51%	5.59%	5.46%	5.09%	0%	-

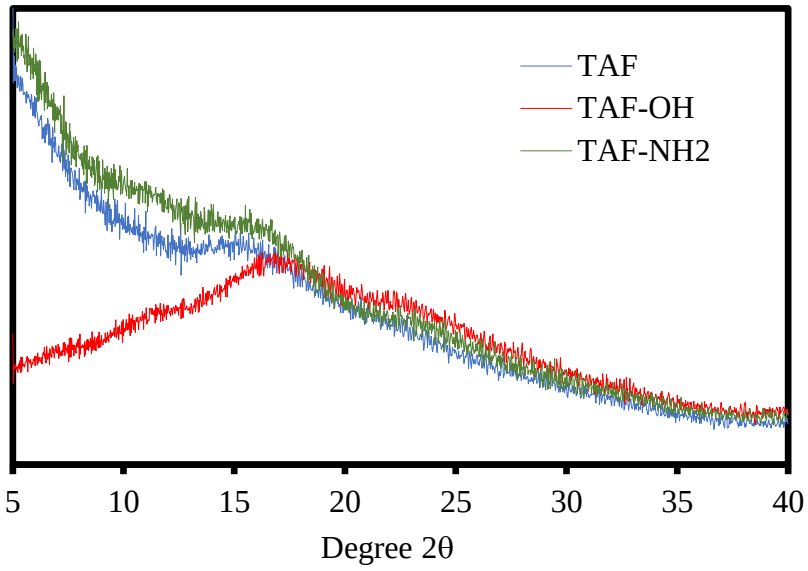

Figure 2.29. Powder XRD analysis of the TAF (blue), TAF-OH (red) and TAF-NH_2 (green).

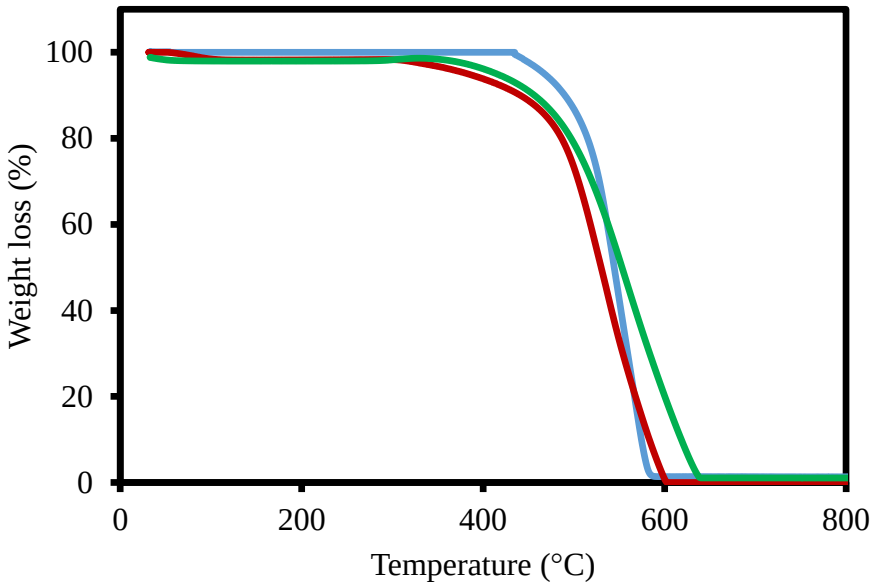

Figure 2.30. TGA runs of TAF (blue), TAF-OH (red) and TAF-NH_2 (green) compounds in air.

Particle size distribution, as determined by dynamic light scattering (DLS) in dilute suspension, follow Gaussian profiles centred at 40 nm, with 96% of the particles restricted to the 10—100 nm range (Fig. 2.31), irrespective of the 3 compounds, consistently with the preservation of a constant and homogeneous reaction course even in the presence of diversified functions in the monomer. The SEM images confirmed the particle size dimension, showing the tendency of these particles to aggregate in agglomerates of some hundreds of nanometers (Fig. 2.32).

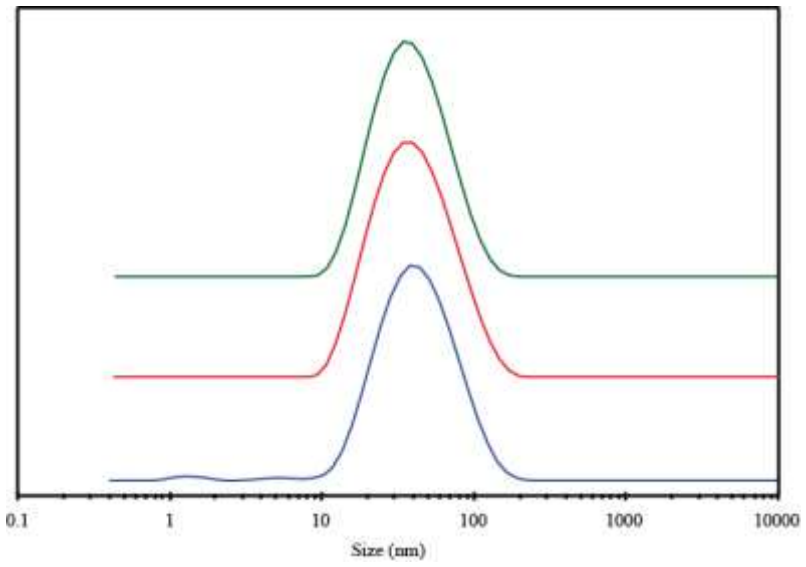

Figure 2.31. Particle size distribution of TAF (blue), TAF-OH (red) and $TAFNH_2$ (green).

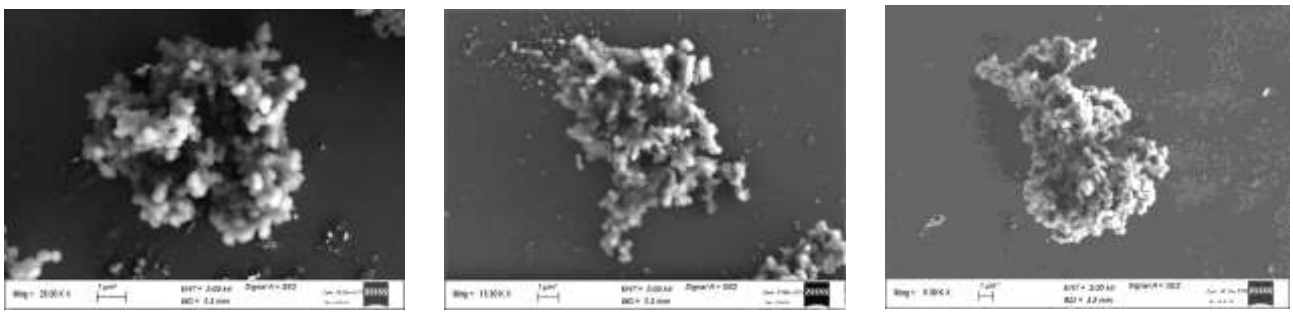

Figure 2.32. SEM imagines of TAF (left), TAFOH (middle) and TAFNH2 (right).

N_2 adsorption isotherms, collected at 77 K (Fig. 2.33) provided BET surface areas of 1383, 1190 and 984 m^2/g for TAF, $TAFNH_2$ and TAFOH, respectively. The surface area and pore-volume (Tab. 2.10) despite the space occupied by the organic functions in the pores are outstanding and comparable to many of the best performing functionalized POPs [39]. Indeed, there was a

considerable contribution of mesoporosity (Fig. 2.24 and Tab. 2.10) to the total pore volume. N_2 desorption branches run distinctly above the adsorption curves, especially for TAF, forming large hysteresis loops indicative of the framework swellability and capillary condensation effect. The micro/mesoporosity ratio increase with the increment of the substituent's basicity, probably this is an effect related at the hydrogen bonds that can created during the synthesis, which can coordinate the growth of particle leading to the formation of microporosity.

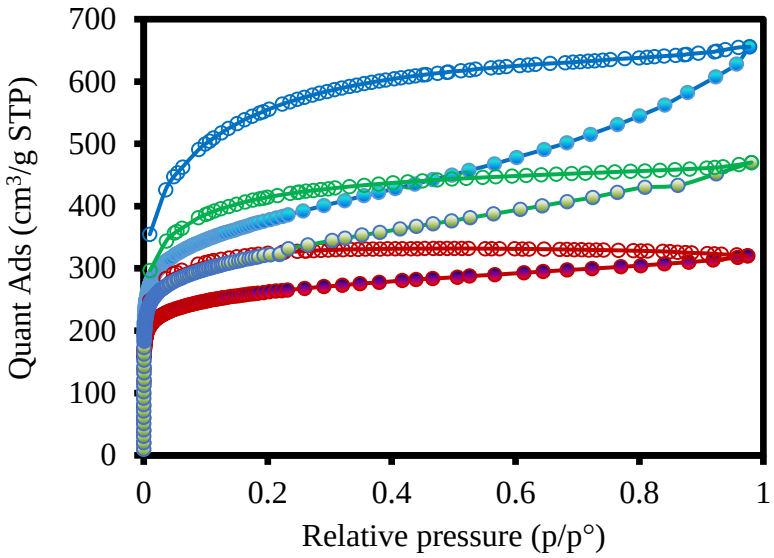

Figure 2.23. N_2 adsorption isotherms at 77 K of TAF (blue), TAF-NH_2 (green) and TAF-OH (red).

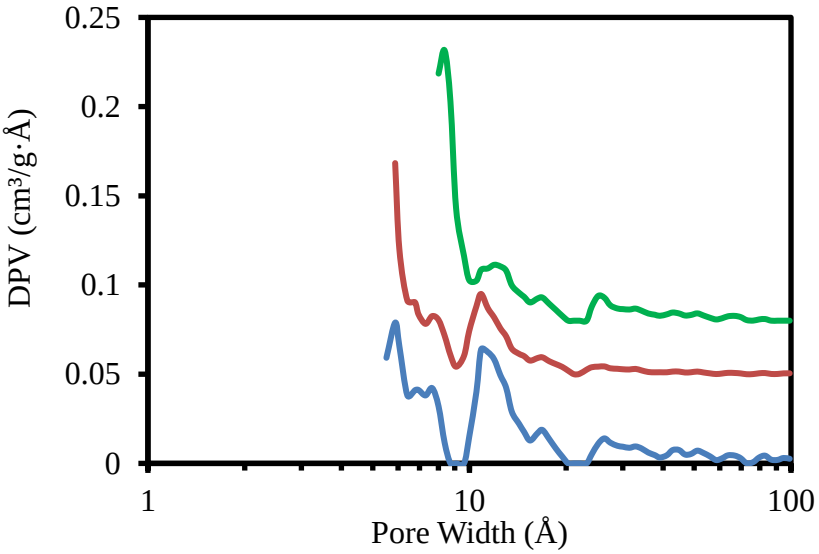

Figure 2.24. Differential pore volume distribution of TAF (blue), TAF-NH_2 (green) and TAF-OH (red).

Table 2.10. Surface areas with BET and Langmuir model, total pore volume (T.P.V.) and micropore total pore ratios (M./T. Ratio) of the samples.

Sample	BET (m^2/g)	Langmuir (m^2/g)	T.V.P. (cm^3/g)	M./T. ratio (%)
TAF	1383	1565	0.95	47
TAF-OH	984	1108	0.45	78
TAF-NH_2	1190	1343	0.68	60

CO_2 adsorption isotherms recorder at three distinct temperatures (273 K, 283 K and 298 K) revealed excellent uptakes already at low pressure (Fig. 2.25-2.26-2.27). The uptake up to 1 bar is relevant, reaching 42 cm^3/g at ambient temperature and 71 cm^3/g at 273 K in TAF-NH_2; these values appear attractive for applications also considering the relatively low cost of triphenylmethane and its derivatives and the high thermal stability of the frameworks. These frameworks are competitive with the best performing porous materials of similar pore capacity, irrespective of the family they belong to: covalent, metal-organic or molecular crystals [34] [40] [41].

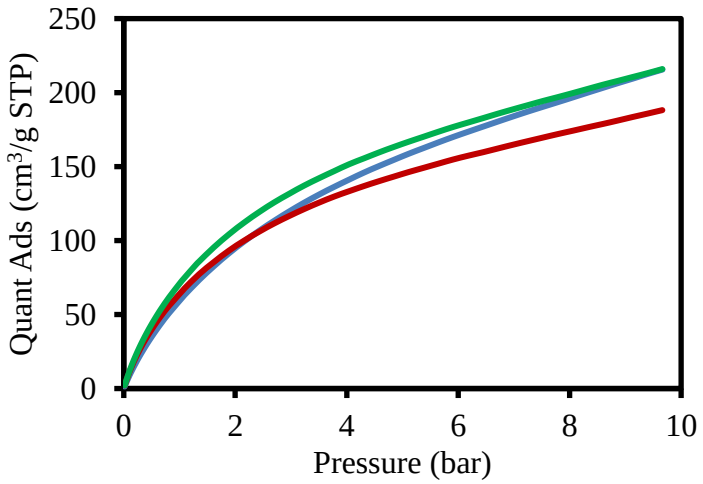

Figure 2.25. CO_2 adsorption isotherms of TAF (blue), TAF-OH (red) and TAF-NH_2 (green) collected at 273 K up to 10 bar.

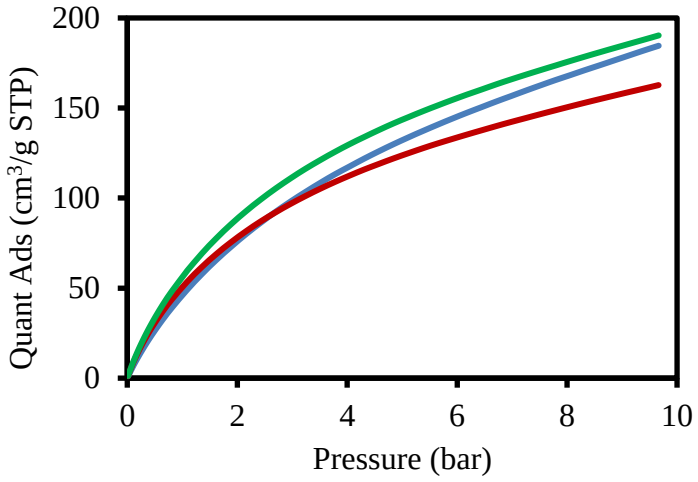

Figure 2.26. CO_2 adsorption isotherms of TAF (blue), TAF-OH (red) and TAF-NH_2 (green) collected at 283 K up to 10 bar.

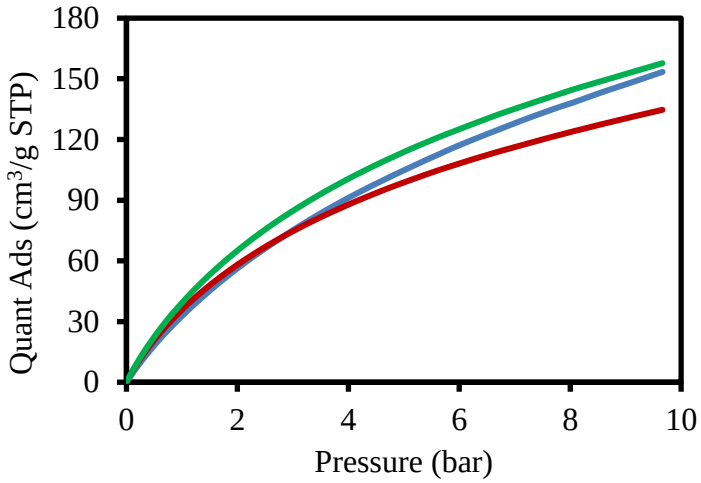

Figure 2.27. CO_2 adsorption isotherms of TAF (blue), TAF-OH (red) and TAF-NH_2 (green) collected at 298 K up to 10 bar.

The adsorption isotherms recorded at three distinct temperature and elaborated by the Van't Hoff equation yielded adsorption energy at low coverage as high as 54 kJ/mol for the TAF-NH_2, which outperforms the other two 26 kJ/mol and 30 kJ/mol for TAF and TAF-OH respectively (Fig. 2.28), and is comparable to the highest values of amine-containing POPs [41]. This trend of isosteric heat is attributable to the polarizing effect of the functional groups used. In fact, it is known that the moment of quadrupole of CO_2 interacts with the aromatic rings and that any polarization undergoes CO_2 increases the interaction with the aromatic rings, it is also known that CO_2 is very similar to the amines substantially raising the isosteric heat.

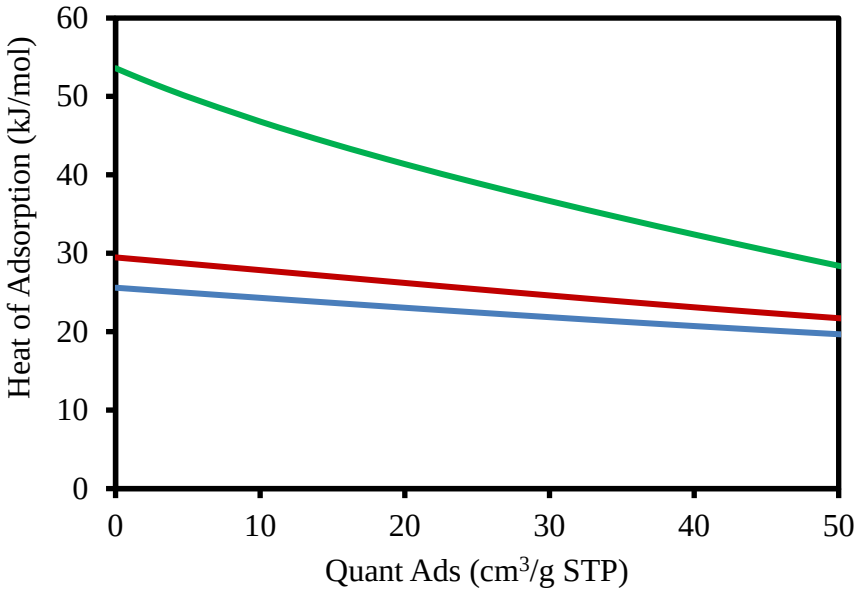

Figure 2.28. CO_2 isosteric heat of adsorption of TAF (blue), TAF-OH (red) and TAF-NH_2 (green).

The direct spectroscopic observation of the intimate spatial relationship between the CO_2 gas and the NH_2 group was provided by 2D ^{1}H—^{13}C HETCOR MAS NMR (Fig. 2.29). The spectrum recorded at 215 K shows through space cross-correlations between the hydrogen of the matrix and ^{13}C-enriched CO_2 carbons. In the 2D NMR, NH_2 hydrogens correlate with CO_2 carbons, indicating that the CO_2 molecules sit in close contact with the amine group. In addition, the NH_2 interaction site is surrounded by aromatic hydrogens that correlate with CO_2. These results are rare spectroscopic observations, supporting the highly energetic binding of CO_2 in porous materials.

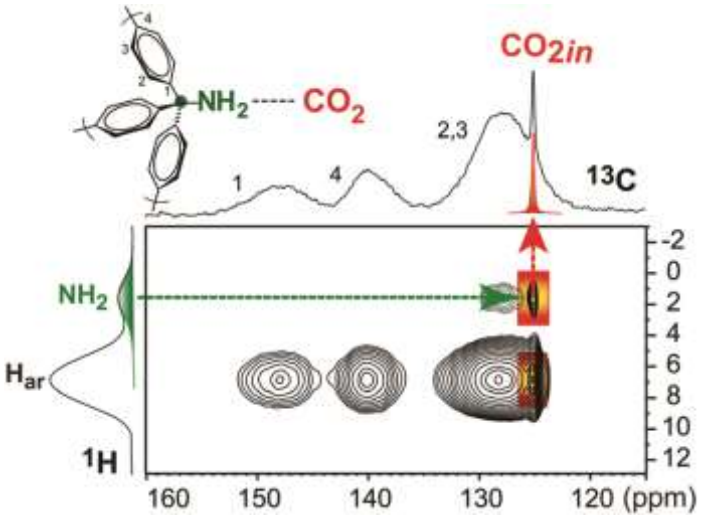

Figure 2.29. 2D ^{1}H—^{13}C HETCOR MAS NMR spectrum of TAF-NH_2 loaded with $^{13}CO_2$ at 215 K, contact time of 5 ms.

The CH_4 adsorption measurements collected up to 10 bar and at various temperatures (273, 283 and 298 K) (Fig. 2.30-2.31-2.32) indicate a stimulating sorption values reaching 92 cm^3/g for the TAF-NH_2 at 273 K and 70 cm^3/g at room temperature. The binding energies at low coverage exhibit values of 18 and 19 kJ/mol for TAF and TAF-NH_2, respectively and up to 21 kJ/mol for TAF-OH (Fig. 2.33). This value approaches the more performing MOFs in order of interaction with CH_4, reaching the record values attributed to the Ni-MOF-74 (21.4 kJ/mol) [25]. The great interaction between TAF-OH and CH_4 is to be attributed at the high amount of micropores in the sample that trap CH_4.

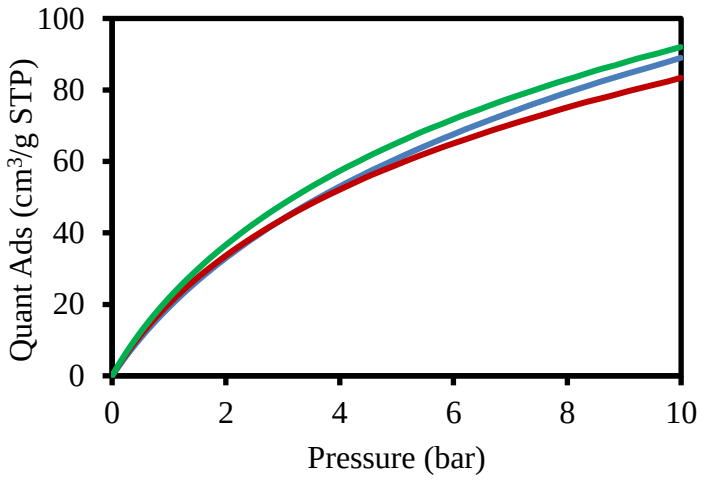

Figure 2.30. CH_4 adsorption isotherms of TAF (blue), TAF-NH_2 (green) and TAF-OH (red) collected at 273 K up to 10 bar.

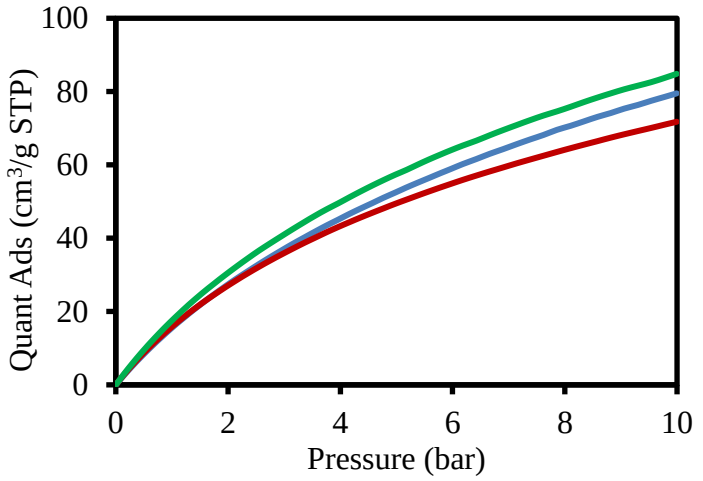

Figure 2.31. CH_4 adsorption isotherms of TAF (blue), TAF-NH_2 (green) and TAF-OH (red) collected at 273 K up to 10 bar.

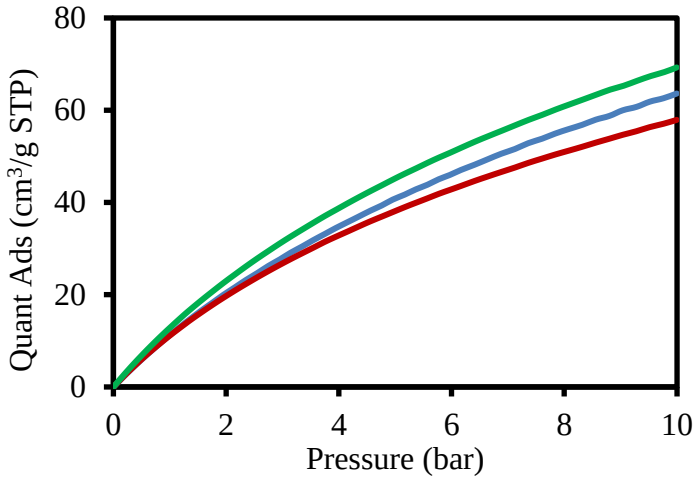

Figure 2.32. CH_4 adsorption isotherms of TAF (blue), TAF-NH_2 (green) and TAF-OH (red) collected at 273 K up to 10 bar.

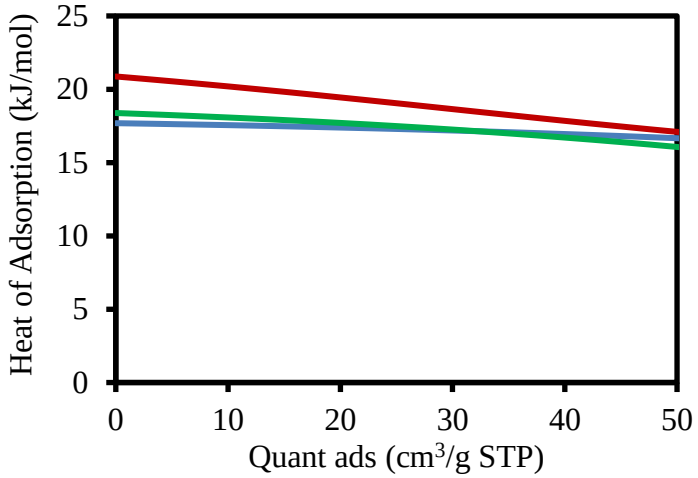

Figure 2.33. CH_4 isosteric heat of adsorption of TAF (blue), TAF-OH (red) and TAF-NH_2 (green).

The interest in the delivery of large amounts of natural gas has led to the exploration of high-pressure solutions in the presence of adsorbent materials; thus, methane isotherms of TAF, TAF-OH and TAF-NH_2 have been recorded up to 100 bar at room temperature (Fig. 2.34). As mentioned in the Par. 2.8.2 the volumetric uptake is important for ANG technology, in order to compare the high-pressure adsorption data with the compressed methane. The results are encouraging since a total adsorption value of 100 cm^3/cm^3 is achieved at 38 bar with a gain of 55 cm^3/cm^3 with respect to compressed methane (Tab. 2.11). This gain is reduced significantly only under extreme conditions. The adsorption value for TAF at 35 and 65 bar are 88 and 119 cm^3/cm^3 respectively, comparable to those POPs. The TAF resulted the best in order to high-pressure storage methane, this one, for the

higher capacity of pores than TAF-OH and TAF-NH_2, confirming the data in the Par. 2.8.2. The higher value of work capacity at 35 bar of TAF-OH is attributed at the higher heat of adsorption, but the small amount of mesoporosity in this sample reduce the pressure thus the pore of sample are completely full of gas.

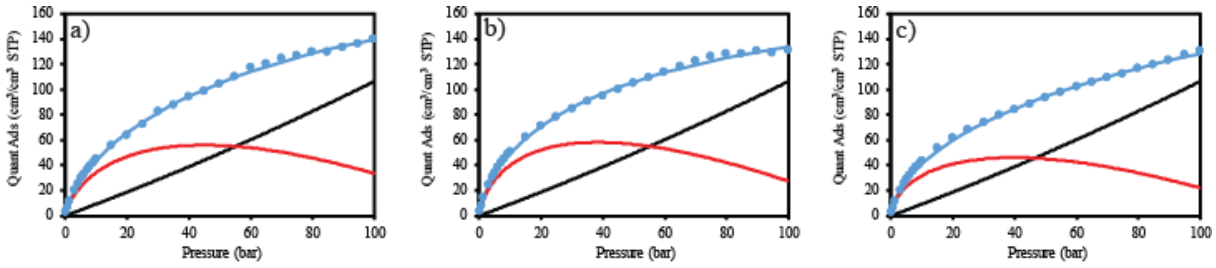

Figure 2.34. High-pressure CH_4 isotherms a) TAF, b) TAF-OH and c) TAF-NH_2. The blue circle is the experimental data, the blue line the data fit, the black line the compressed CH4 value by NIST and the red line the work capacity of materials.

Table 2.11. Work capacity of the samples at 35, 65 and 100 bar.

Sample	Work capacity at 35 bar (cm^3/cm^3)	Work capacity at 65 bar (cm^3/cm^3)	Work capacity at 100 bar (cm^3/cm^3)
TAF	55	52	33
TAF-OH	58	50	27
TAF-NH_2	46	41	22

2.10| Conclusion

In the first part of my work on porous materials for adsorption and storage, an experimental screening was carried out including the gravimetric and volumetric absorption of gas by the structures obtained by 3D polymerization or condensation of various monomers with an increasing number of phenyl, phenylene rings, carbazole and acenes in a single unitary framework. Indeed, a large variety of highly adsorptive polymers and copolymers were produced and in the case of the Friedel-Crafts alkylation, using possibly commercially available low-cost monomers to obtain a potentially scalable

synthesis as an industrial process. These materials provide a suitable surface wall-to-pore volume balance and adsorption energies for optimizing high-pressure methane storage, paving the way to future developments in gas storage. The present results demonstrate that virtually all aromatic precursors with multiple connected aromatic groups can be condensed, and a few of them are suitable as precursors to form benchmark materials in the competition for efficiently loading methane and carbon dioxide.

In the second part, the investigation of porous frameworks generated by branched monomers moved us to the design of three-dimensional aromatic frameworks, starting from monomers with three rigid aromatic branches and a functional group connected to the same tetrahedral core. This arrangement ensures the generation of a robust covalent scaffold, resistant to structural collapse, and with well-anchored organic functions, regularly spaced all over the framework. The newly designed strategy satisfies the requirements for creating a framework that supports hydroxyl and amine groups, which are constantly exposed to the pores. In particular, the presence of different functional groups has contributed to change the interaction with different gases. In fact, with the same rigid structure, the presence of the amine has increased the interaction of the framework for CO_2; instead, the hydroxyl has contributed to the formation of a framework that interacts better with CH_4, all through the use of a low cost material such as triphenylmethane.

References

[1] K. S. W. Sing, D. H. Everett, R. A. W. Haul, L. Moscou, J. R. R. A. Pierotti e T. Siemieniewska, *Pure & Appl. Chem.*, vol. 57, p. 603, **1985**.

[2] R. I. Masel, in *Principles of Adsorption and Reaction on Solid Surfaces*, New York, Wiley, **1996**, p. 240.

[3] H. J. Butt, K. Graf e M. Kappl, Physics and Chemistry of Interfaces, Weinheim: Wiley, **2006**.

[4] I. Langmuir, *J. Am. Chem. Soc.*, vol. 38, p. 2221, **1916**.

[5] S. Brunauer, P. H. Hemmett e E. Teller, *J. Am. Chem. Soc.*, vol. 60, p. 309, **1938**.

[6] J. Landers, G. Y. Gor e A. V. Neimark, *Colloids and Surface A: Physicochem. Eng. Aspects*, vol. 437, p. 3, **2013**.

[7] J. A. Mason, K. Sumida, Z. R. Herm, R. Krishna e J. R. Long, *Energy Environ. Sci.*, vol. 4, p. 3030, **2011**.

[8] A. L. Myers e J. M. Peausnitz, *A. I. Ch. E. Journal*, vol. 11, p. 121, **1965**.

[9] J. A. Mason, M. Veenstra e J. R. Long, *Chem. Sci.*, vol. 5, p. 32, **2014**.

[10] S. Thomas e R. A. Dawe, *Energy*, vol. 28, p. 1461, **2003**.

[11] M. J. Economides e D. A. Wood, *J. Nat. Gas Sci. Eng.*, vol. 1, p. 1, **2009**.

[12] H.-M. W. B. Li, W. Zhou, J. Q. Xu e B. Chen, *Chem*, vol. 1, p. 557, **2016**.

[13] D. Zhou, Y. Han, B. W. Laursen, C.-G. Yan e B.-H. Han, *J. Am. Chem. Soc.*, vol. 134, p. 6084, **2012**.

[14] J. A. Mason, J. Oktawiec, M. K. Hudson, j. Rodriguez, J. E. Bachman, M. I. Gonzalez, A. Cervellino, A. Guagliardi, C. M. Brown, P. L. Llewellyn, N. Masciocchi e J. R. Long, *Nature*, vol. 527, p. 357, **2015**.

[15] W. Lu, D. Yuan, D. Zhao, C. I. Schilling, O. Plietzsch, T. Muller, S. Brase, J. Guenther, J. Blunmel, R. Krishna, Z. Li e H.-C. Zhou, *Chem. Mater.*, vol. 22, p. 5964, **2010**.

[16] A. Coli-Molina, S. Pérez-Estrada, A. E. Roa, A. Villagrana-Garcia, S. Hernàndez-Ortega, M. Rodriguez, S. E. Brown e B. Rodriguez-Molina, *Chem. Commun.*, vol. 52, p. 12833, **2016**.

[17] U. Stoeck, S. Krause, V. Bon, I. Senkovska e S. Kaskle, *Chem. Commun.*, vol. 48, p. 10841, **2012**.

[18] B. Li, R. Gong, W. Wang, X. Huang, W. Zhang, H. Li, C. Hu e B. Tan, *Macromolecules*, vol. 44, p. 2410, **2011**.

[19] T. Ben, H. Ren, S. Ma, D. Cao, J. Lan, X. Jing, W. Wang, J. Xu, F. Deng, J. M. Simmons, S. Qiu e G. Zhu, *Angew. Chem. Int. Ed.*, vol. 48, p. 9457, **2009**.

[20] T. Yamamoto, S. Wakabayashi e K. Osakada, *J. Organomet. Chem.*, vol. 428, p. 223, **1992**.

[21] R. V. Law, D. C. Sherrington, C. E. Snape, I. Ando e H. Kurosu, *Macromolecules*, vol. 29, p. 6284, **1996**.

[22] P. Sozzani, A. Comotti, S. Bracco e R. Simonutti, *Angew. Chem. Int. Ed.*, vol. 43, p. 2792, **2004**.

[23] J. Schmidt, M. Werner e A. Thomas, *Macromolecules*, vol. 42, p. 4426, **2009**.

[24] J. Weber, M. Antonietti e A. Thomas, *Macromolecules*, vol. 41, p. 2880, **2008**.

[25] Y. Penag, V. Krungleviciute, I. Eryazici, J. T. Hupp, O. K. Farha e T. Yildirim, *J. Am. Chem. Soc.*, vol. 135, p. 11887, **2013**.

[26] Z. Hulvey, B. Vlaisavljevich, J. A. Mason, E. Tsivion, T. P. Dougherty, E. D. Bloch, M. Head-Gordon, B. Smit e J. R. L. C. M. Brown, *J. Am. Chem. Soc.*, vol. 137, p. 10816, **2015**.

[27] H. Furukawa e O. Yaghi, *J. Am. Chem. Soc.*, vol. 131, p. 8875, **2009**.

[28] W. G. Lu, D. Q. Yuan, D. Zhao, C. I. Schilling, O. Ploetzsch, T. Muller, S. Brase, J. Guenther, J. Blumel, R. Krishna, Z. Li e H.-C. Zhou, *Chem. Mater.*, vol. 22, p. 5964, **2010**.

[29] S. Cavenati, C. A. Grande e A. E. Rodriguez, *J. Chem. Eng. Data*, vol. 49, p. 1095, **2004**.

[30] I. Bassanetti, A. Comotti, P. Sozzani, S. Bracco, G. Calestani, L. Mezzadri e L. MArchiò, *J. Am. Chem. Soc.*, vol. 136, p. 14883, **2014**.

[31] D. Liu, Y. Wu, Q. Xia, Z. Li e H. Xi, *Adsorption*, vol. 19, p. 25, **2013**.

[32] J. McEwen, J.-D. Hayman e A. O. Yazaydin, *Chem. Phys.*, vol. 412, p. 72, **2013**.

[33] E. S. Sanz-Pérez, C. R. Murdock, S. A. Didas e C. W. Jones, *Chem. Rev.*, vol. 116, p. 11840, **2016**.

[34] A. Schoedel, Z. Li e O. Yaghi, *Nat. Energy*, vol. 1, p. 1, **2016**.

[35] J. R. Holst, A. Trewin e A. J. Cooper, *Nat. Chem.*, vol. 2, p. 915, **2010**.

[36] W. Lu, D. Yuan, J. Sculley, D. Zhao, R. Krishna e H.-C. Zhou, *J. Am. Chem. Soc.*, vol. 133, p. 18126, **2011**.

[37] D. N. Bunck e W. R. Dichtel, *Angew. Chem. Int. Ed.*, vol. 51, p. 1885, **2012**.

[38] M. Soroka e W. Goldeman, *ARKIVOC*, vol. 2010, p. 360, **2010**.

[39] M. H. Weston, O. K. Fahra, B. G. Hauser, J. T. Hupp e S. T. Nguyen, *Chem. Mater.*, vol. 24, p. 1292, **2012**.

[40] J. R. Holst, A. Trrewin e A. J. Cooper, *Nat. Chem.*, vol. 2, p. 915, **2010**.

[41] L. Zou, Y. Sun, S. Che, X. Yang, X. Wang, M. Bosch, Q. Wang, H. Li, M. Smith, S. Yaun, Z. Perry e H.-C. Zhou, *Adv. Mater.*, vol. 29, p. 1700229, **2017**.

3| Porous Materials for confined polymerization

In recent decades, there has been a growing interest in the development of synthetic techniques and types of materials capable of reproducing what is normally done on a biological level, called biomimetic. Biomimetic is the research for materials that can control the chemical reactions that occur near it or inside them, which is what commonly happens in nature by enzymes. In nature, controls on chemical reactions by enzymes allow living organisms to produce, in the case of enantiomer molecules, only the active enantiomer in biological processes. This control is one of the challenges that scientists try to achieve by developing materials that are able to induce stereoselectivity and specificity to chemical reactions without the use of catalysts. Among the materials most used for this purpose there are the microporous materials, this feature allows to obtain artificial reactors of sizes comparable to the molecular dimensions, obtaining materials that can be stereoselective. In recent years, this synthetic approach has also extended the development of polymers inside these pores. In fact, in some works it has been seen that such microporous structures can influence the growth of the polymer, leading to polymer chains with a very distinct tactics, which would only be possible with the use of expensive catalysts, such as those of Ziegler-Natta.

The second part of my work was based on the synthesis of polymers in microporous materials, in particular within the PAFs and MOFs, with different end purposes. Therefore, the following chapter will be divided into two parts, in the first part the synthesis of new types of completely organic

composites and the second the use of crystalline systems for the development of new technologies. Before focusing on my work, an introduction will be made to the state of the art of polymerizations confined within porous materials.

3.1| An overview to confined polymerization

Over the years, researchers have carried out polymerizations confined within various porous materials in order to control the growing structure or to obtain certain properties of the final polymer. Next, a description will be followed of how the researchers developed this field by dividing it by type of porous matrix used.

3.1.1| Confined polymerization in porous organic molecules

The seminal works of Brown and White [1] [2] is the first reported polymerization in confined state. In these works, they reported the γ-rays initiated polymerization inside the urea clathrate of different kind of vinyl and diene monomers. In particular, the polymerization of 1,3-butadiene is of some importance. In fact, the size of pores affects the reaction kinetics and the finally structure of polymer. The polymerization inside the urea of 1,3-butadiene led to the formation of a microstructure of the entirely 1,4-*trans* polymer, consequently a high crystallinity of the polymers and therefore a higher melting point than the polymer synthesized in solution. This control of the microstructure of polymers is due to the interaction between guest and channel walls. Unfortunately, this work has

limitation, indeed, just a limited number of monomers could co-crystallize to generate clathrate and not all could polymerize. Despite these limitations, even more controlled reactions could be obtained: for example, pro-chiral monomers could be stereospecifically polymerized within the channels of a chiral host. In the 1967 Natta et co-worker [3] demonstrated that is possible obtain a optically active *trans*-1,4-polypentadiene through a confined polymerization of monomer inside the channels of –(R)-perhydrotriphenylene.

The radical polymerization of vinyl monomers is difficult to achieve due to the higher reorientation of the monomeric units during the polymerization and the chain transfer that generate a crosslink in the polymer chain. However, the polymerization of acrylic and vinylic monomers could be performed in compound having channels, like cyclotriphosphazene. For example, polymethacrylonitrile synthetized inside the cyclotriphosphazene channels showed an enrichment of isotactic units and the polymers is soluble respect at the bulk radical polymerization that give a crosslink materials [4].

The development of new porous materials has consequently increased the number of porous materials that can be used as reactors. In the last years, a new class of porous materials was discovered, the organic cages, and a recent paper reported the first polymerization inside at these porous materials. The organic cages possesses permanent porosity after removal of the guests. When a small amount of styrene is accommodates the physical separation between single monomers prevents the polymerization. Instead, at higher styrene loadings the monomers also locate in the interparticle space, with structure amorphization and leading to efficient polymerization. The polymerization process is organised by the dynamic comportment of the host material that imposes strong selectivity on the polymerizable monomers [5].

The biologic systems were also used to nanoreactors for in-situ polymerization. In particular dipeptides generate a porous crystals in which is present an aliphatic and mono-dimensional channels. These channels were used to polymerization reactions of acrylonitrile. A considerable advantage in

the use of dipeptides consists in the fact that in their zwitterionic form they dissolve rapidly in water at room temperature; with this way it is possible to obtain, once the matrix is removed, the precise morphological replication of the crystal as a polymer. Moreover, the dipeptide crystals allow the intramolecular cyclization of PAN. The PAN chains confined inside the channel are assisted by the dipeptide during the transformation process. The dipeptide is easily removed in the heating, in fact, the sublimation temperature is around 270-320°C; The resulting ladder polymer showed a reduce conformational flexibility, and after thermic treatment at 1100°C, was obtained graphitic carbon in which the morphology is similar at the dipeptide (Fig. 3.1) [6].

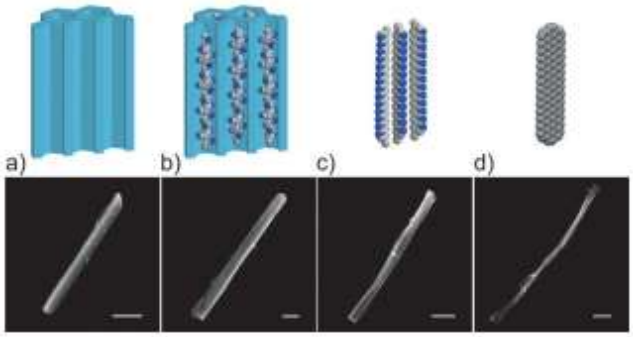

Figure 3.1. Schematic representation of the process at the molecular level and SEM images of various steps.

3.1.2| Polymerization in mesoporous silica

The first confined polymerization in mesoporous silicas was reported in the 1997 by Aida and co-workers [7]; they described the radical polymerization in MCM-41. In this porous materials, the microstructure could not controlled due to larger pore size, but the polymeric chains showed an increase in the molecular weight compared to bulk polymerization and a lower polydispersity index. Through the EPR experiment, they observed that the radical species are protected inside the pore of

the matrix, with 25% of living radicals still present after one month. This effect is ascribed to a suppression of bimolecular termination [7].

The mesoporous materials not allowed the microstructure of polymers control, but they could lead to precise control of mesoscopic structure. For example, the gaseous ethylene is polymerized through the channels of mesoporous silica and the polymerization give a polyethylene (PE) with an ultra-high molecular weight. The mesoporous confinement not allowed the chain folding and leaded to novel polymer mesostructure. This mechanism, which mimics biological formation of natural fibres, has been called “extrusion polymerization” [8].

Polymerization inside mesoporous materials has been studied as a tool for fabrication of polymeric carbonaceous replicas [9]. Ozin et co-worker performed a polycondensation reaction within MCM-41 and they obtained poly(phenolformaldehyde) that after the extraction showed a fibre-like morphology with diameter comparable that of the host matrix [10]. The radical polymerization of divinylbenzene inside a three-dimensional network, as MCM-48 and SBA-15, leads to the formation of porous polymeric replica that maintains porosity and ordered structure. This strategy consent to produce organic replicas from silica micro-objects. The shape and dimension of the silica could be modify (Par. 1.3.2) allowed the formation of different kind of organic micro-objects. The polymerization of styrene and methyl methacrylate and subsequent removal of the silica creates polymer replicas that shows permanent porosity (Fig. 3.2) [9].

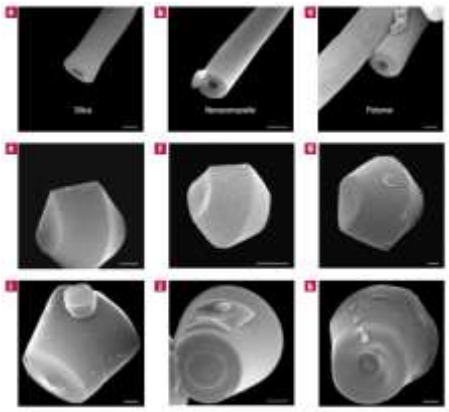

Figure 3.2. Replication of single shapes for tubes (a,b,c) truncated bicones (e,f,g) and muffin-shaped objects (i,j,k).

3.1.3| Confined polymerization in Zeolites

The zeolites are widely used for in-situ polymerization reactions. The uniform and finely tunable pore size consents the design of specific environment for polymeric growth, instead, the type and number of the cations permits the fine of the chemical surrounding. This last feature is widely used to study the encapsulation of conductive polymers in nanometer-sized channels. In this sense, there is a double advantage in the use of porous materials: on the one hand, the encapsulation prevents oxidation of the conductive polymer and other degradations that would affect the conductive properties; on the other, the encapsulation of single chains allows the study of the processes of intrachain conduction, separating them from those that are interchain [11]. In this context in 1989, Bein and co-worker encapsulated the polypyrrole inside the three-dimensional and one-dimensional channels of zeolite Y and morderite, respectively [12]. The cations present in the structure play a fundamental role in the polymerization reaction, in fact they observed that the zeolites containing Cu(II) and Fe(III) cations assist the confined polymerization, while the matrix with Fe(II) or hydrogenated prevents it. Therefore, the oxidative polymerization is mediated by the cations, that being inside the pores ensure that the polymer chains grow only inside, as confirmed by the electron microscope measurement. Unfortunately, they observed that the nanocomposites not shows conductivity, because the counter-ions trapping polarons and bipolarons, confirmed by EPR analysis.

3.1.4| Polymerization in MOFs

Since the early nineties, a lot of work has been performed on MOFs leading to a gamut of hybrid materials obtained by self-assembling processes from metal ions and organic ligands. Due to their ease of variation and tuning, these materials are widely used in various fields including for

confined polymerizations [13]. As for the other porous matrices, also in these the polymerization allows the polymeric reproduction of the pore morphology and the study of the behaviour of isolated chains. Several studies have been dedicated at the polymerization of vinyl and acrylic monomers within MOFs aimed at the understanding of confinement effects on monomers reactivity, molecular weight and stereochemistry. A systematic study of a $[M_2(L)_2ted]_n$ (where M = Cu^{2+} or Zn^{2+}, L = dicarboxylate ligand and ted = triethylenediamine) pore size changing the organic ligand (L) and polymerization of methyl methacrylate and styrene have been performed [14]. This work showed that smaller pores leads to a decrease of monomer adsorption capacity and polymer yield, but the extracted polymers had a significant lower polydispersity. This effect, typical of living polymerization, is attributed by an efficient stabilization of the propagating radicals in the pores leading to a decrease in side reactions that restrict the molecular weight distribution. Moreover, smaller pores increase the percentage of isotactic content in the polymer. An interesting result in this work is the polymerization of vinyl acetate; instead, standard radical polymerization of this monomer produces a highly branched polymer and accordingly a large polydispersity. The confined polymerization of vinyl acetate in the MOFs gave a polymer with a polydispersity index of 1.7 with an almost linear structure difficult to obtain with a bulk polymerization [14]. This technique is also used to obtain a poly-*p*-divynilbenzene where only one of the two vinyl groups reacts leading to a linear polymer, impossible to obtain with normal polymerization [15].

The confined polymerization techniques are not limited to the examples previously described, but can also open a new approach to solve problems in polymer science. A recent work by Kitagawa and co-workers has demonstrated the possible application of in situ polymerization to the problem of polymer blend. The polymerization at different times of two different monomers was performed inside a MOF thus creating a three-component nanocomposite. The removal of the matrix under mild conditions has led to polymer mixtures, which are composed of sub-nanometric domains. These new polymer mixtures exhibit high thermal stability by effective suppression of the high temperature de-polymerization reaction that could not be achieved in physically mixed composites [16].

3.1.5| Confined polymerization in PAFs

The extraordinary chemical stability of these materials makes them promising candidates to host chemical reactions inside them without undergoing the destruction of the lattice or a decrease in the degree of porosity [17]. The chemical-physical stability that makes them unique is due to the presence of covalent bonds and the rigid phenyl reticulum; these characteristics are also responsible for the low density and large volume of the pores. Another interesting aspect of PAFs is the pores; these have an irregular shape but have about all the same dimensions.

In the 2012, Sozzani and co-workers used PAF1 as a reactor to perform the polymerization and thermal evolution of polyacrylonitrile. The low density and large volume of the pores allowed the encapsulation of a large amount of polyacrylonitrile in the PAF1. In the composite, the rigid structure of PAF1 and the polyacrylonitrile chains were in a very small distance, confirmed by bi-dimensional NMR that evidenced the cross-peaks interactions a short contact time, which is usually rare [18].

Recently Dai and co-workers used a functionalize PAF to synthetize, with an atom transfer radical polymerization (ATRP), polyacrylonitrile anchored at the porous structure; subsequently, the polymer has been converted in polyamidoxime, in order to allow the extraction of uranium ions to seawater [19].

3.2| Anionic polymerization in PAFs

As part of the development of new plastic materials, the research world has developed into the formation of new composites in which the charges added to a polymer could modify its chemical-physical and rheological properties. One of the major problems in this synthetic procedure is the physical incompatibility of the materials, which in the end leads to the de-mixing of the composite components. The most used fillers are based on silica and in order to overcome the problem of

incompatibility, these silicas are appropriately modified with organic chains on the surface to "camouflage" them in the organic polymeric matrix [20]. Obviously this process lengthens the production times of the plastics and consequently also the costs. The use of porous materials as reinforcing agents in polymers is a possible strategy to overcome this problem. In fact, the growth of the polymer from inside the pores of the material towards the outside produces a composite where the chains of the matrix result in some parts of the composite trapped in the charge with no possibility of separation. The use of porous organic frameworks for the development of this concept also ensures the affinity between the two parts of the composite.

As already seen previously, various frameworks of different kinds have been used for confined polymerizations, but the common point of each work is the use of radical polymerization. This is because the porous matrices used are chemically unstable to other types of polymerization. In this sense the use of chemically stable materials such as PAFs, allow the use of other synthetic techniques such as anionic polymerization. Anionic polymerization is a type of polymerization that brings some advantages, in fact, turns out to be faster than a radical [21]. Moreover, a characteristic of the anionic polymerizations is to be a living polymerization, i.e. if the system is free of impurities, the active sites do not switch off and this allows the creation of block copolymers, in case a second monomer is added.

The anionic polymerization within porous materials will be discussed for the first time. Previously, the polymerization within the benchmark of this class of materials will be described as PAF1 and then we will talk about an anchored polymerization, i.e. a polymerization where the porous matrix is not only the reactor but also the polymerization initiator leading to a composite where matrix and charge are chemically linked to each other.

3.2.1| No-anchored polymerization

The anionic polymerization within the PAF1 served as a starting point, to test the problems and the possibility of carrying out this new procedure within the porous materials. Not having the PAF1 sites in which anions can be created; the porous matrix turns out to be only a reactor, so the resulting composite will be defined as no-anchored.

Isoprene and Methyl methacrylate have been selected as monomers for polymerization due mainly to their different features of their relative polymers, rubbery and glassy respectively. Moreover, these two monomers, through the anionic polymerization, generate polymers with a well-defined tacticity that will be compared with that of the polymer grown inside.

3.2.1.1| Experimental part

The synthesis of the porous matrix precursor was described in the Par. 2.8.1.1. The anionic polymerization was performed in inert atmosphere, with minor differences between the polymerization of isoprene and methyl methacrylate.

The porous matrix is previously emptied through a vacuum treatment at 200 °C overnight. The fresh distilled monomers was added (5 ml) and the mixture was cooled in a liquid nitrogen bath (-196 °C). Then 0.2 ml of *n*-BuLi 1.6 M are added, twice freeze-pump-thaw are performed; during the defrosting phase the system is placed in a cold bath to prevent the polymerization from beginning, for isoprene the bath was at -131 °C (liquid N_2 and pentane) and for methyl methacrylate the bat was at -41 °C (dry ice and acetonitrile). During the second defrosting, the excess monomer was removed by cannula equipped with a filter. Subsequently the mixture is brought to room temperature and allowed to react for one day. After that, the polymerization is stopped with the addition of methanol and then filtered.

3.2.1.2| Result and discussion

N_2 adsorption isotherms collected on nanocomposites show a drastic decrease of gas uptake attributable to polymer chains growth along the pores (Fig. 3.3 and Tab. 3.1). The amount of the polymers has been evaluated with TGA analysis: for PAFPI and PAFPMMA, the polymer corresponds to 62% and 85% by weight of the nanocomposite respectively (Fig. 3.4). The multi-step mass loss in PMMA TGA were mostly observed, and in general, these three step was related at the depolymerisation beginning from head-to-head linkages, depolymerisation starting form unsaturated vinyl ends and the random scissions, respectively [22].

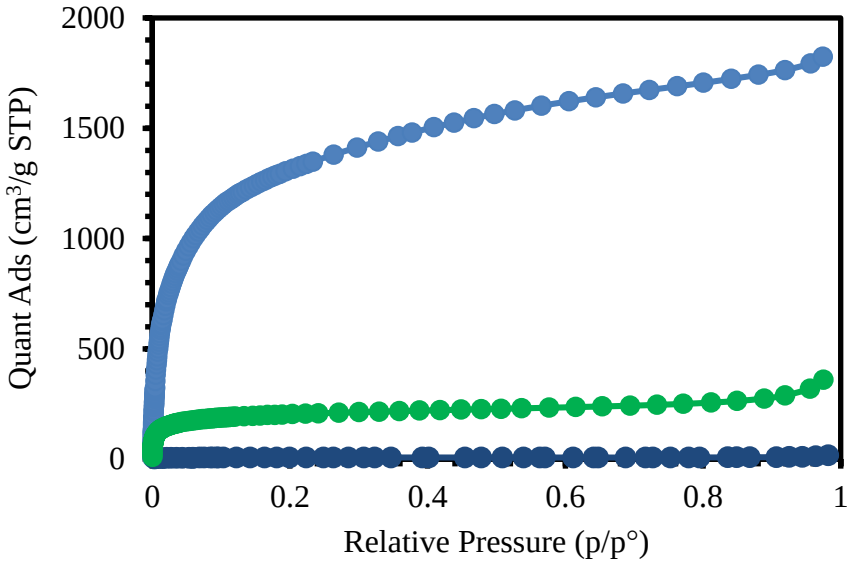

Figure 3.3. N_2 adsorption isotherms at 77 K of PAF1 (blue), PAFPI (dark blue) and PAFPMMA (green).

Table 3.1. Surface area value of the composts evaluated with the BET model.

Sample	BET (m^2/g)
PAF1	4784
PAFPI	22
PAFPMMA	716

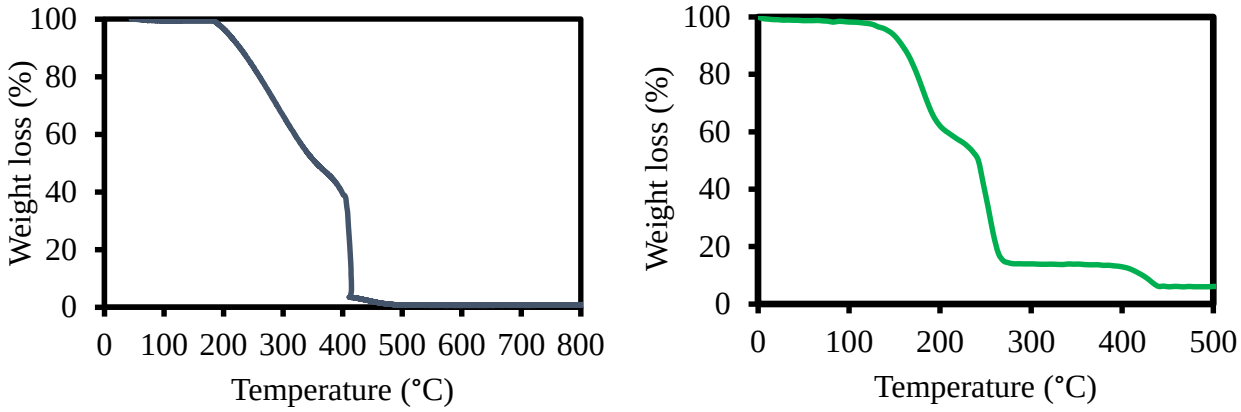

Figure 3.4. Thermogravimetric analysis of the PAFPI (left) and PAFPMMA (right) composts.

^{13}C CP-MAS SSNMR analysis shows clearly the presence of the polymers for both nanocomposites. The NMR analysis confirms that the porous carbon matrix has not undergone modifications by the anionic polymerization, confirming that such polymer synthesis is possible within these porous matrices. For PAFPMMA, all the PMMA signals are noticeable and the matrix signals result more disturbed due to a rigidity induced by the polymer. For PAFPI instead, from this analysis is possible to evaluate the nature of the PI (Fig. 3.5, 3.6). In fact, the signals attributable to 1,4-cis isomer are more pronounced respect to those of 1,4-trans, 1,2 and 3,4 isomers [23]. This is thanks to the Li^+ small counterions, which, coordinating the anionic growing chains, promotes the 1,4-cis chaining. The 1,4-cis conformation is typical of the anionic polymerizations of the isoprene [24], this shows that the porous matrix has no influence on the growth of the polymer, as regards the PMMA instead, the tacticity of the polymer is not easily identifiable from the solid state NMR. It is therefore necessary to extract the polymer from the porous matrix and analyse it by liquid NMR. The extraction process was carried out by washing the composite with reflux chloroform for a day, and then filtered to remove the porous matrix and the polymer precipitated with methanol. The liquid NMR of the extracted PMMA shows a predominance of isotacticity in the polymer (Fig. 3.7), typical of a PMMA grown by anionic route [24]. Therefore, it results that the porous matrix does not seem to influence the growth of the polymer with respect to bulk polymerization.

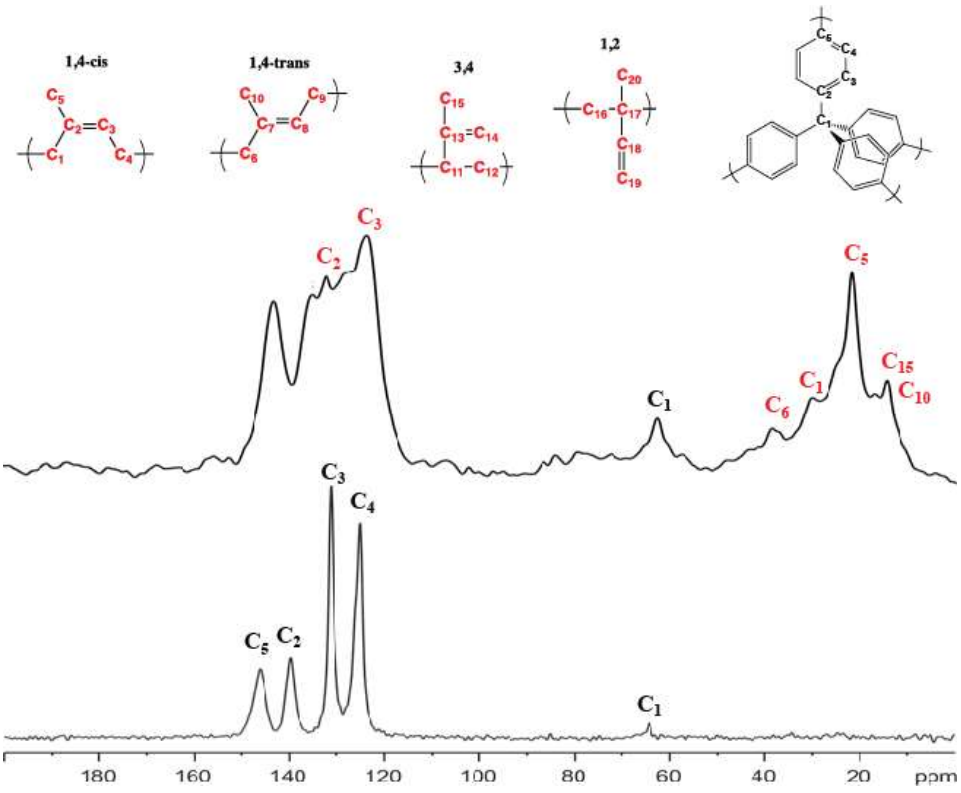

Figure 3.5. ^{13}C CPMAS NMR analysis of PAF1 (down) and PAFPI (up) with relative peaks assignation.

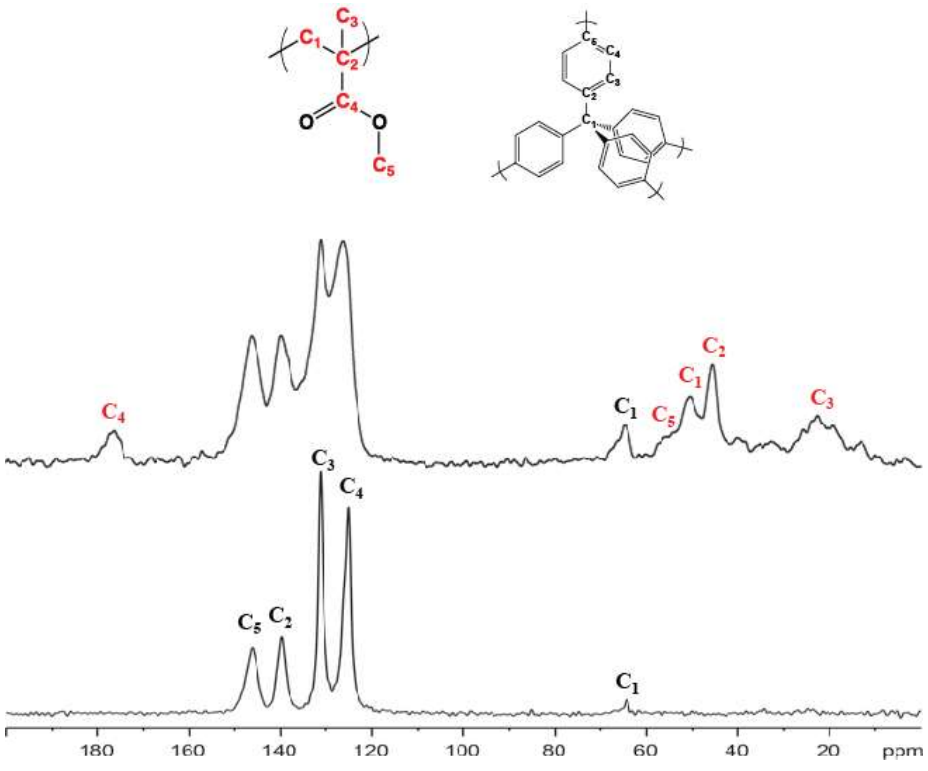

Figure 3.6. ^{13}C CPMAS NMR analysis of PAF1 (down) and PAFPMMA (up) with relative peaks assignation.

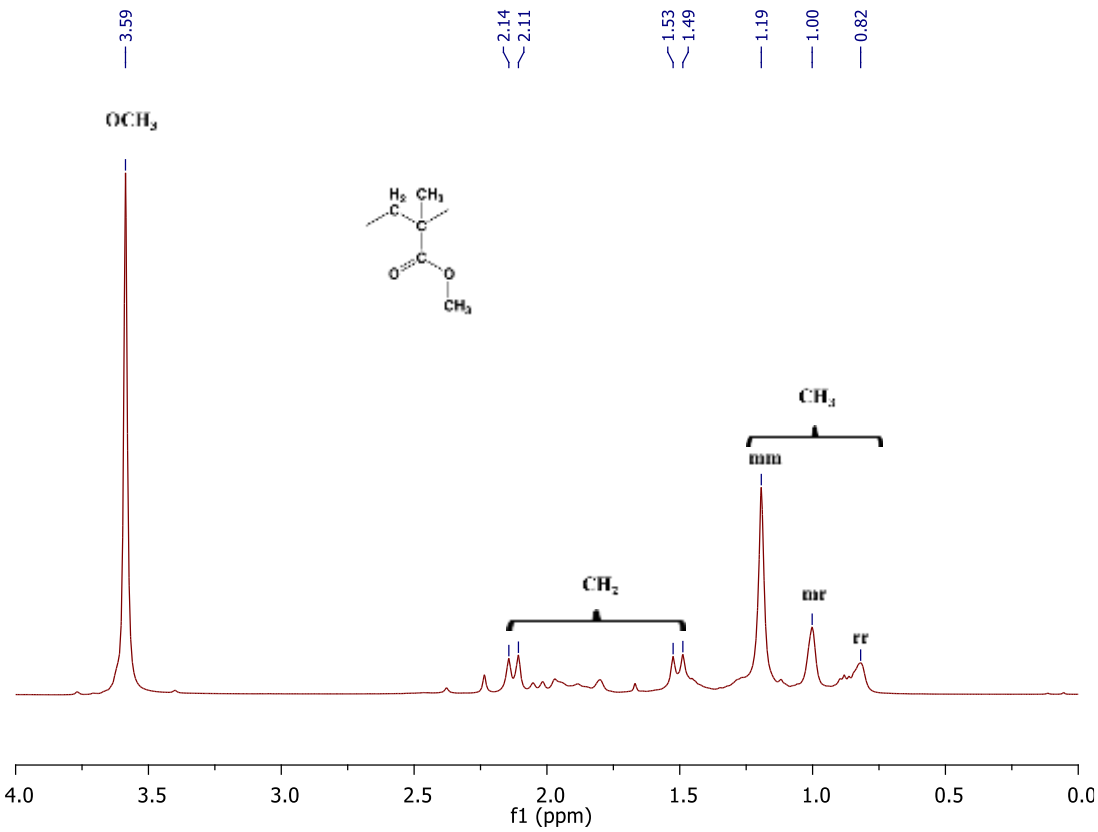

Figure 3.7. NMR analysis of PMMA extracted from PAFPMMA composite with related assignment.

For the nanocomposites PAFPI and PAFPMMA, DSC analyses show no visible transition glass temperature (Tg) (Fig.3.8). This means that the polymer chain is confined inside a channel with a size comparable to its dimension and it is not able to move [25]. In fact, since the glass transition is a massive process of the amorphous part of a polymer it is not possible to observe it in single chains, so that polymers confined in porous materials do not have this transition.

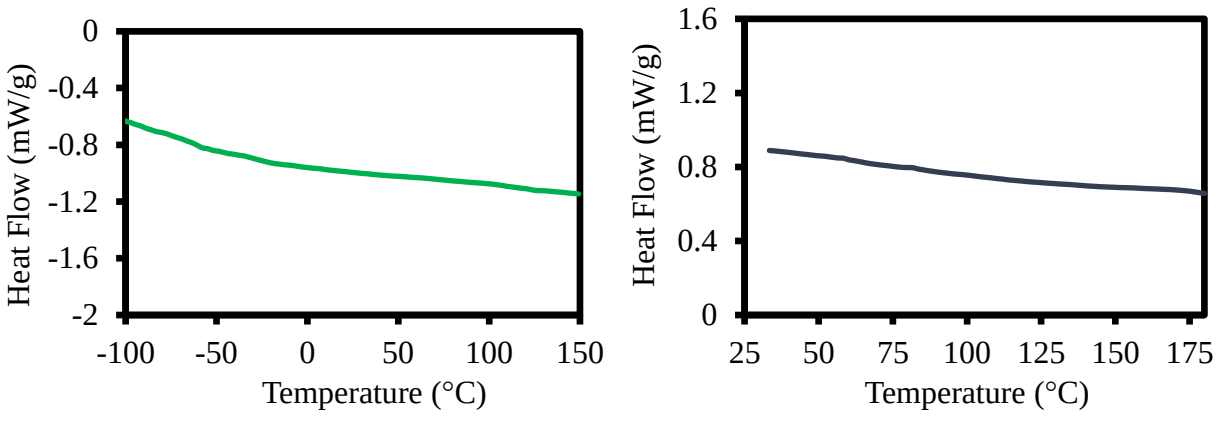

Figure 3.8. DSC analysis of the composites. In the left PAFPI and in the right PAFPMMA.

This result is confirmed by ^{1}H-^{13}C HETCOR SS-NMR collected on the two nanocomposites, a technique that checks through-space intramolecular host/guest correlations [26]. In particular, for the nanocomposite PAFPMMA (Fig. 3.9), a correlation between the hydrogens of the PMMA polymer and C nuclei of the matrix is plain visible also at very short contact time (0.5 ms). The extreme closeness at molecular level between PMMA chains and the aromatic part of the matrix is highlighted at longer contact time: in fact, at 5ms, a cross-peak between the carboxylic carbon (C=O) of polymer and the aromatic hydrogens of the PAF1 appears, demonstrating proximity with the pores matrix walls. Instead, the analysis for PAFPI (Fig. 3.10) show the presence of the cross-peaks between polymer and matrix at contact time of 2 ms. the difference in contact time with respect to PMMA can be attributed to the high mobility of the PI chains with respect to PMMA.

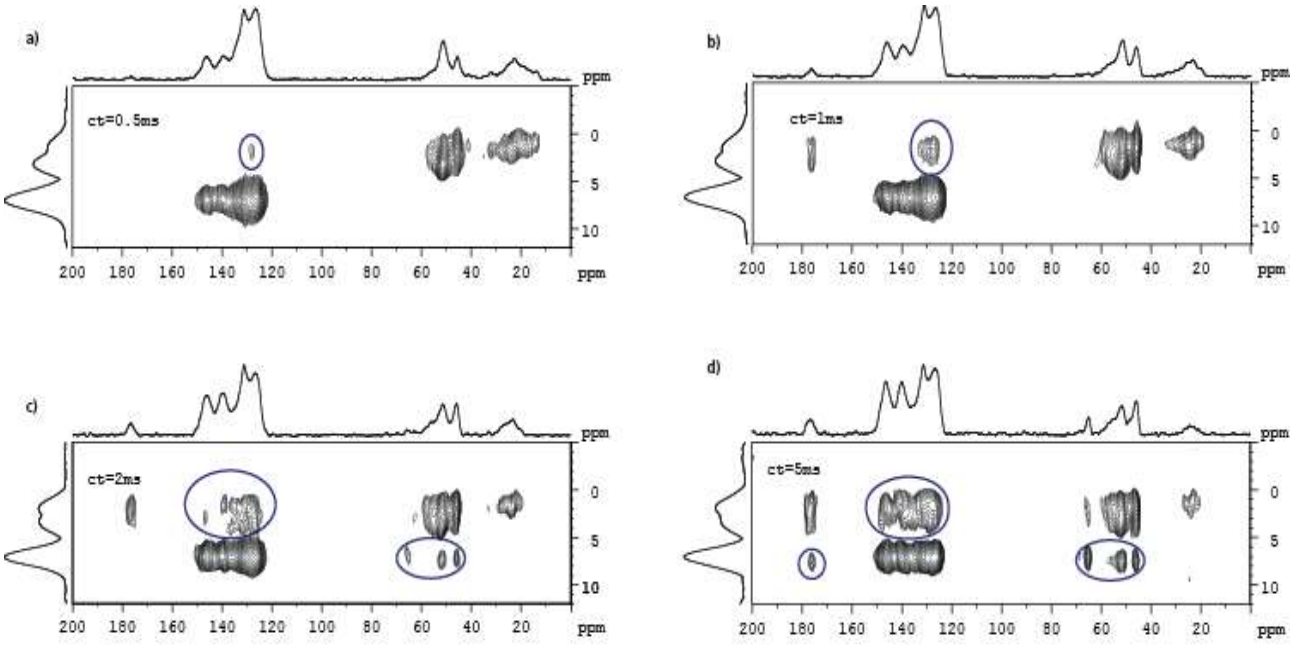

Figure 3.9. ^{1}H-^{13}C HETCOR SS-NMR analysis of PAFPMMA at contact time a) 0.5 s, b) 1 ms, c) 2 ms and d) 5 ms. In the blue circles are present the cross-peaks signal between PAF and PMMA.

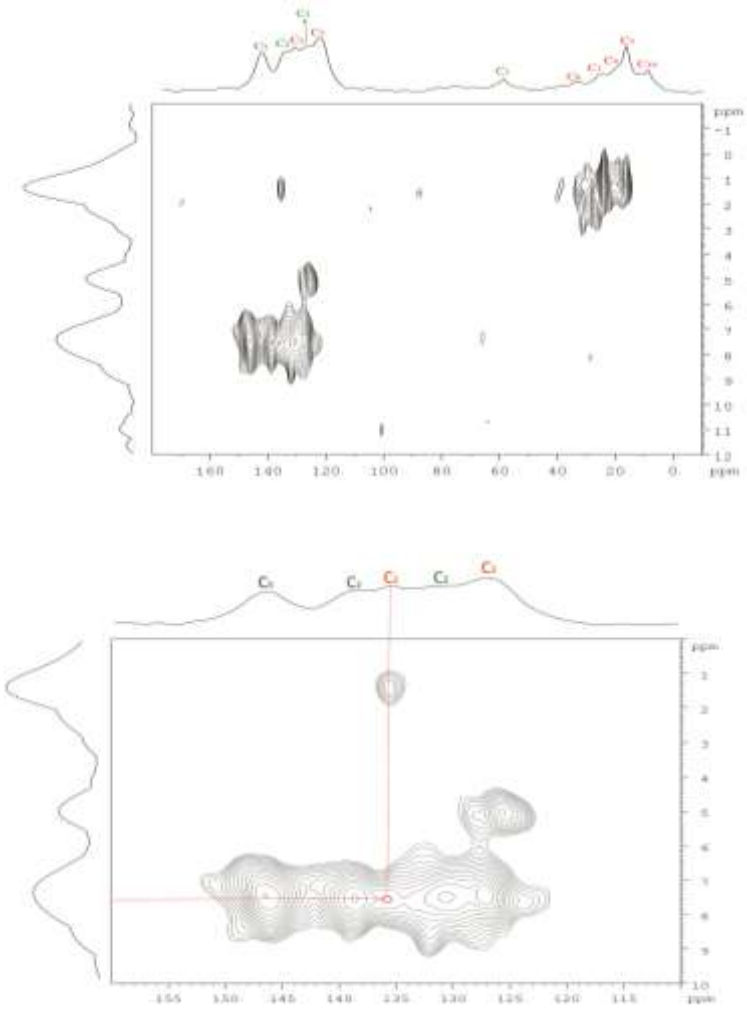

Figure 3.10. ^{1}H-^{13}C HETCOR SS-NMR analysis of PAFPI at contact time of 2 ms. In the up the complete spectrum and in the down the zoom in the unsatured area of the polymer.

These results confirm the possibility of using organic porous matrices as reactors for anionic polymerizations, never performed so far in a porous material.

3.2.2| Anchored polymerization

The fact that these matrix could withstand this aggressive process of polymerization, unsustainable by many other classes of porous materials, open the way to novel processes inside nanocavities and nanopores. Once proved the matrix stability, we introduce on the matrix skeleton a

pendant to anchor the polymer. Accordingly, the building blocks appropriately designed for the matrix, itself performs two different and fundamental functions: it serves as a rigid linker with three-dimensional structure to create voids inside the material and, at the same time, it has to be a precursor of an initiator for anionic polymerization. The chosen porous matrix is a modification of the tetraphenylmethane, to continue to have an adamantoid structure that guarantees a high surface area and pore capacity. The chosen modification is the addition of a methyl group on one of the four aromatic rings of the matrix.

3.2.2.1| Experimental part

The precursor was synthesized by the method described in the literature [27] and presented below (Fig. 3.11):

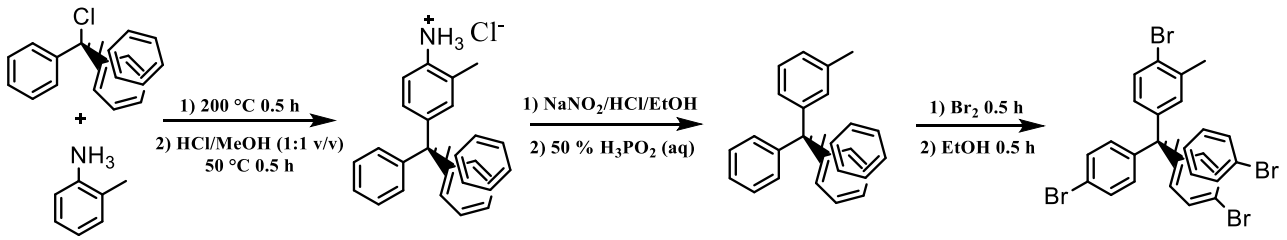

Figure 3.11. Synthetic scheme of (4-bromo-3metilfenil)*tris*(4-bromophenyl)methane.

Into a 250 mL round-bottom flask equipped with a water-cooled reflux condenser and a magnetic stir bar were added trityl chloride (9.2 g, 32.9 mmol) and o-toluidine (9.4 mL, 88.8 mmol). This mixture was stirred at reflux (200 ºC) for 0.5 h. The resulting purple slurry reaction mixture was allowed to cool to room temperature when it solidified. This solid was grounded and the resulting powder was combined with a mixture of 2M HCl and MeOH (25 mL : 60 mL) mixture. The reflux condenser was reattached and the mixture was then heated at 80 °C for 0.5 h. After cooling to room temperature, the reaction mixture was filtered and washed with H_2O (125 mL) to afford a light purple solid, which was briefly air-dried on a Büchner funnel. At the powder was added EtOH (65 ml) and

concentred H_2SO_4 (10 ml), the mixture was cooled at 0 °C, and a solution of $NaNO_2$ (2.44 g) in water (10 ml) was added dropwise, and then the solution was mixed for 1 h. Subsequently, was added a solution 50% of H_3PO_2 (15 ml) and was heated at 50 °C for 2 h. The resulting solid was filtered and washed with H_2O and EtOH and dried to give (3-Methylphenyl)triphenylmethane (8.8 g, yield 80%). ^{1}H NMR (300 MHz, CDCl3) δ: 7.3-6.9 (m, 15 H), 2.26 (s, 3 H).

A 150 mL round-bottom flask equipped with a magnetic stir bar was charged with compound (3-Methylphenyl)triphenylmethane (3.0 g, 8.96 mmol). Neat bromine (3.5 mL, 67.3 mmol) was slowly added dropwise through the septum via a syringe over a 5 min period before the resulting solution was allowed to stir at room temperature for 0.5 h. EtOH (60 mL) was then added to the reaction mixture and the reaction was allowed to stir for an additional 0.5 h. The resultant precipitate was collected by suction filtration and washed with a copious amount of EtOH (150 mL). The collected crude product was then combined with an equivolume mixture of EtOH : $CHCl_3$ (60 mL) in a 125 mL round-bottom flask and boiled at 80 ºC for 10 minutes. After cooling to room temperature, the solid was filtered, washed with a minimum amount of EtOH (10 mL) and dried under vacuum to afford (4-bromo-3metilfenil)*tris*(4-bromophenyl)methane (2.9 g, 4.46 mmol, 50%) as an off white solid. ^{1}H NMR (300 MHz, $CDCl_3$) δ: 7.42 (s, 1 H), 7.39 (d, *J* = 8.7 Hz, 6 H), 7.02 (d, *J* = 8.7 6 H), 6.99 (d, *J* = 8.5 Hz, 1 H), 6.80 (d, *J* = 8.5 Hz, 1 H), 2.30 (s, 3 H).

The procedure for the framework synthesis is already descripted in the Par. 2.8.1.1; the resulting matrix was called PAFMe. The formation of anion in the framework follow a procedure reported in a patent [28], with a small different: the procedure is the following:

The framework was degassed at 200 °C in vacuum overnight. At the framework was added fresh distilled hexane (20 ml) and tetramethylenediamine (TMEDA, 0.2 ml), then was added dropwise *n*-BuLi (2.5 ml, 1.6 M), the mixture was heated at 70 °C for 19 h. The activated framework was washed with hexane several times, in order to remove the excess of *n*-BuLi. Subsequently the activate matrix was cooled at -196 °C and the monomer was added. Then, twice freeze-pump-thaw are performed; during the

defrosting phase the system is placed in a cold bath to prevent the polymerization from beginning, for isoprene the bath was at -131 °C (liquid N_2 and pentane) and for methyl methacrylate the bat was at -41 °C (dry ice and acetonitrile). In the second defrosting, the monomer outside the pore was removed by cannula equipped with a filter. Subsequently, the mixture was heated at room temperature and the reaction was performed for 1 day. After that, the polymerization was stopped with the addition of methanol and then filtered.

Moreover, was also synthetized a block copolymer, with PI inside the pores and PMMA outside of the pores. The synthetic procedure is the same wrote previously for the PI without the final addition of methanol, instead, the second monomer was added in a second moment. Previously the PAFMePI was dispersed in fresh distilled THF and mixed in order to swell the PI and separate the particle, after the methyl methacrylate was added (5 ml) and the reaction was performed at room temperature for 1 day. After that, the polymerization was stopped with methanol and filtered.

3.2.2.2| Result and discussion

DSC of nanocomposites (Fig. 3.12) show a sharp glass transition at 8°C for the PAFMePI and at 109 °C for the PAFMePMMA, due to the polymers anchored on the particle surface while the inner polymer does not show any distinctive features. In fact, the anions for the polymerization also exist in the surface of the particle and during the defrosting process the first part of the system that thaw is the surface; this heat gradient generated the start of the polymerization outside of the pores. Glass transition temperature depends strongly on polymer microstructure. The glass transition temperature of PMMA is typical of a PMMA with a conformation atactic or syndiotactic, different of the microstructure that PMMA has in an anionic polymerization. This result is to attribute at the effect of the particle, in fact, the anionic polymerization of methyl methacrylate in presence of TMEDA do not influence the microstructure [29]. Natural 1,4-*cis* (natural rubber) or 1,4-*trans* (gutta-percha)

polyisoprenes show glass transition temperatures near -73 °C and -70 °C [30], respectively: The increment of the 3,4 and 1,2 monomeric units content in the polymer chain leads to an increase in glass transition temperature that goes up to 0 °C [31].

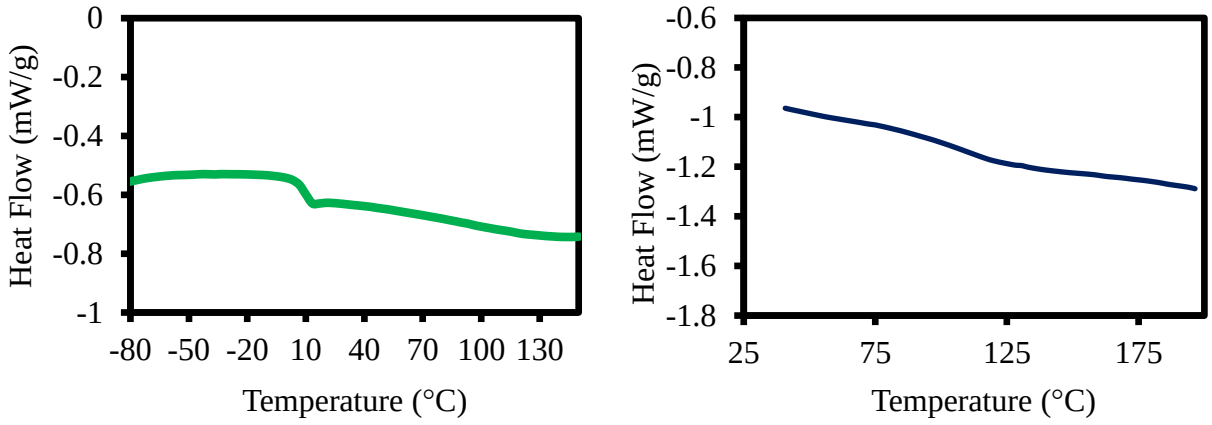

Figure 3.12. DSC analysis of the composite PAFMePI (left) and PAFMePMMA (right).

The atypical microstructure of PI is confirmed by solid state NMR. The ^{13}C CP MAS SSNMR of PAFMePI (Fig. 3.13) show a large amount of 3,4 and 1,2 addition products that produce the characteristic signals in the carbon spectrum at 111 and 148 ppm due to the olefinic carbon [23]. In the aliphatic region clear and sharp peaks could be assigned to specific atoms of 3,4 and 1,2 monomeric units. A 4:1 ratio is established between the amount of 3,4 and 1,2 units, moreover, 1,4-*trans* addition product could be detected giving a 1:1 ratio between 1,4 and 1,2 units. Instead, 1,4-*cis* monomeric units are just present as an impurity due to the very weak characteristic methyl signal at 23,5 ppm. The SSNMR of PAFMePMMA (Fig. 3.14) show the presence of a larger amount of polymer than the PAFMePI, this results is due to the more difficult control in the anionic polymerization of methyl methacrylate. Indeed, the highest melting temperature of methyl methacrylate monomers (-48 °C) respect to isoprene (-146 °C) allow the start of the polymerization at this temperature, in fact, the anions are already highly active; therefore, the complete removal of the monomer excess is impossible.

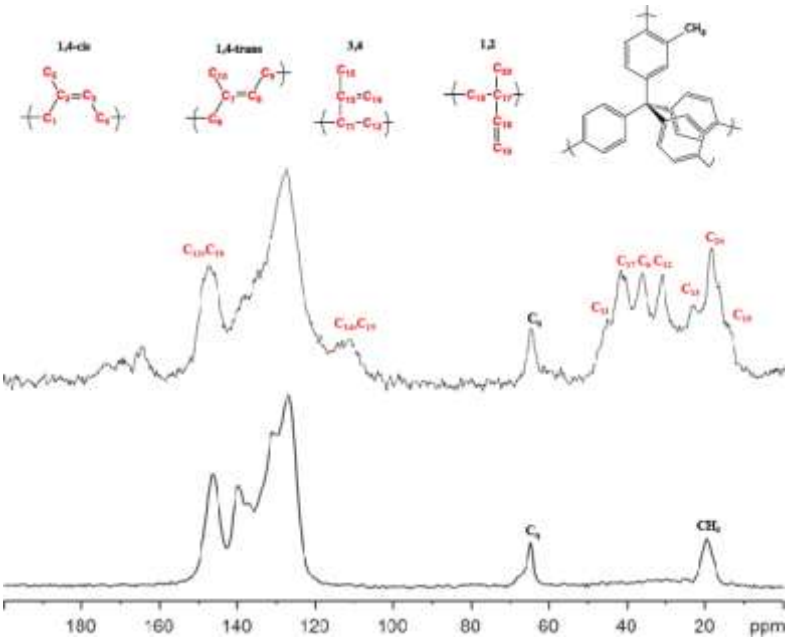

Figure 3.13. ^{13}C CPMAS NMR analysis of PAFMe (down) and PAFMePI (up) with relative peaks assignation.

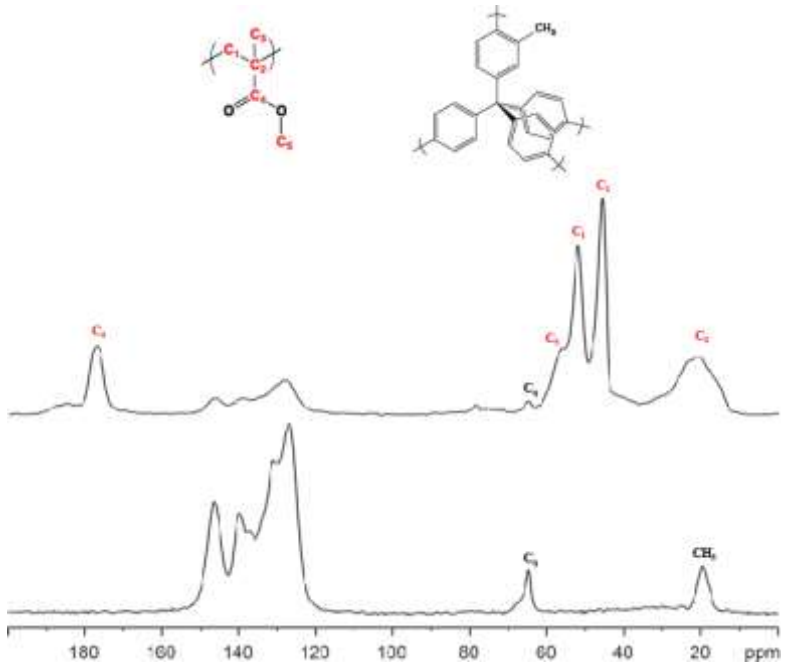

Figure 3.14. ^{13}C CPMAS NMR analysis of PAFMe (down) and PAFMePMMA (up) with relative peaks assignation.

The 2D ^{1}H–^{13}C NMR spectrum of the PAFMePI (Fig. 3.15) shows intense cross-peaks due to strong dipole–dipole interactions, occurring at short distances, between the polymer chains and the pore walls of the matrix. This is a clear demonstration of the proximity at the nanometer level between the polymer and matrix components. These strong through-space correlations at the hybrid interfaces are operative when the nuclei sit in close proximity, less than 1 nm. These cross-peaks are also evident

in the composite of PAFMePMMA and confirmed the effective presence of polymer inside the chains of the porous framework (Fig. 3.16).

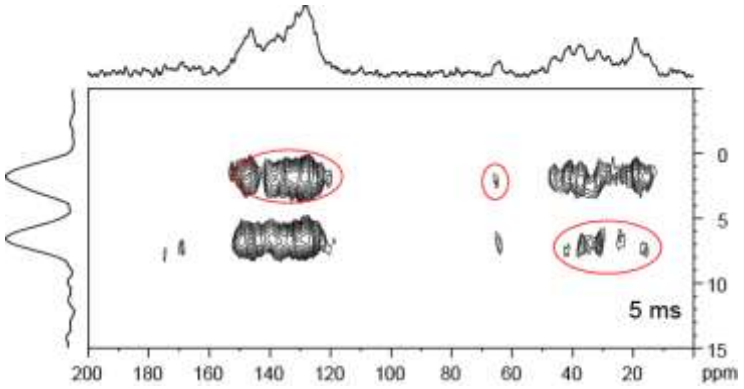

Figure 3.15. 2D ^{1}H-^{13}C NMR spectrum of PAFMePI at 5 ms of contact time. In the red circles are present the cross-peaks between the PAFMe and PI.

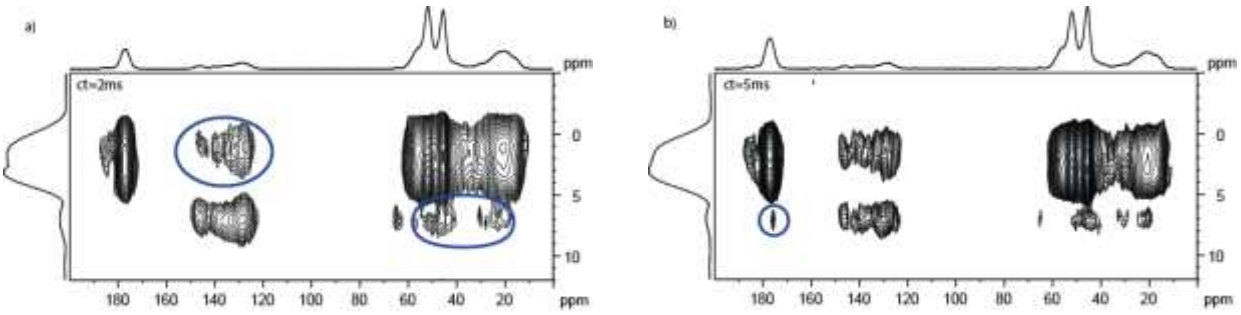

Figure 3.16. 2D ^{1}H-^{13}C NMR of the PAFMePMMA samples at contact time of a) 2 ms and b) 5 ms. In the blue circles are present the cross-peaks related at the interaction between PAFMe and PMMA.

The TGA shows a unique step for the PAFMePMMA degradation (Fig. 3.17) related at the change of the tacticity compared with the PAFPMMA [32]. The multi-step degradation of the PAFMePI is related at a partial vulcanization process and intra-cyclization reactions in the PI chains [33]. An interesting result is the increase in the degradation temperature of the porous matrix after polymerization (about 100 ° C); this is probably due to the polymer outside the matrix that degrades before and it protect the porous matrix.

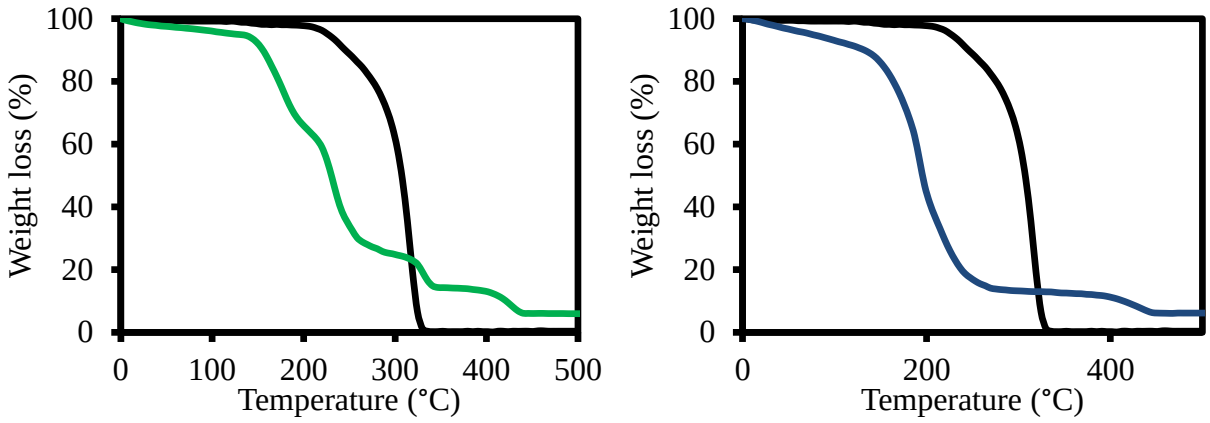

Figure 3.17. Thermogravimetric analysis of the samples. At left PAFMePI (green curve) and at right the PAFMePMMA (blue curve), the black curve is the analysis for the PAFMe.

Moreover, the addition of a second monomer at the living anions in the polymerization reaction produced a di-block copolymer covalently anchored to the porous matrix. This strong covalent interaction stabilizes the interfaces between the different components of the system and allows a uniform and homogeneous dispersion of matrix nanoparticles inside the composite (called PAFMePI-*b*-PMMA.

The DSC analysis of the copolymer nanocomposite show the same Tg of the homopolymers nanocomposite (Fig. 3.18). This result confirmed the effect of the matrix on the polymer growth; this effect not is related at the polymerization in the pores but at the presence in the polymerization reactions of the matrix, in fact the PMMA which growth outside the pores show a Tg typical of atactic or syndiotactic system.

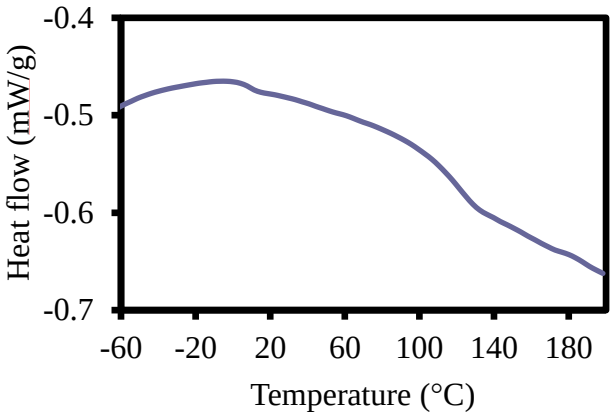

Figure 3.18. DSC analysis of PAFMePI-*b*-PMMA sample.

The tacticity of the PI is confirmed by SS NMR analysis. The peak related at the PI are less intensity than the PMMA, so for confirmed the structure a part of the sample was removed before the addition of methyl methacrylate and analysed. The SS NMR of the first step in copolymerization procedure confirmed the presence of 1,2 and 3,4 microstructure predominance (Fig. 3.20) [23]. The NMR of the nanocomposite show a typical profile that comprise three distinct region: the methyl group centred at 19 ppm and a large and poorly resolved signal; two strong peaks at 45 and 52 ppm with a shoulder at 55 ppm related to the quaternary carbon, the methylene and the methoxy carbon, respectively; the carboxylic carbon at 178 ppm. The peaks related at PMMA are more intensity than the peaks of porous material and PI, confirming the large amount added in the second step of polymerization process and leading to the desired structure in which the particle are dispersed in the polymeric matrix.

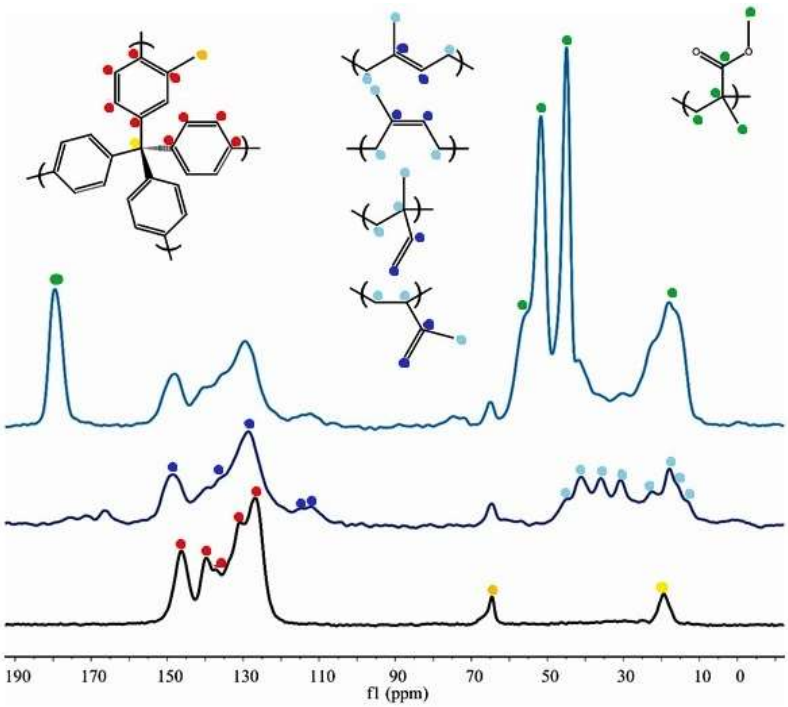

Figure 3.20. ^{13}C SS NMR spectrums of the PAFMe (down), PAFMePI (middle) and PAFMePI-b-PMMA (up) with respectively assignation.

Finally, 2D ^{1}H-^{13}C HETCOR NMR is applied to study the formation of the nanocomposite. Short contact time (0.05 ms) allows us to distinguish the different spots related to PI, PMMA and

aromatic matrix (Fig. 3.21). At longer contact time (2 ms), the interactions between different components are clearly visible (orange). Unexpectedly, we find out that also PMMA present through space interactions with the guest matrix proving that also this second polymer block has grown partially inside the host matrix and on its surface. The presence of the PMMA inside the pores was also confirmed by AFM analysis. The image of the modulus (Fig. 3.22) show a presence of a region in the sample like a volcano shape, in which in the internal part is present the polymer with the higher modulus (PMMA) and around the PMMA the polymer with the lower modulus (PI). The image of the adhesion instead, show this region with the lower adhesion in the middle of the "volcano" and around the higher adhesion. This can be explained by the presence of the polymer external to the particle. The polymerization of the PI was performed without solvent. This led to the formation of a barrier of the chains grown outside the particle, which without solvent aggregated obstructing the access to the pore to the monomer, preventing the growth of the internal chains to the pore. The addition of THF before methyl methacrylate has expanded the external chains making the anions inside the pores again accessible that reacted with methyl methacrylate.

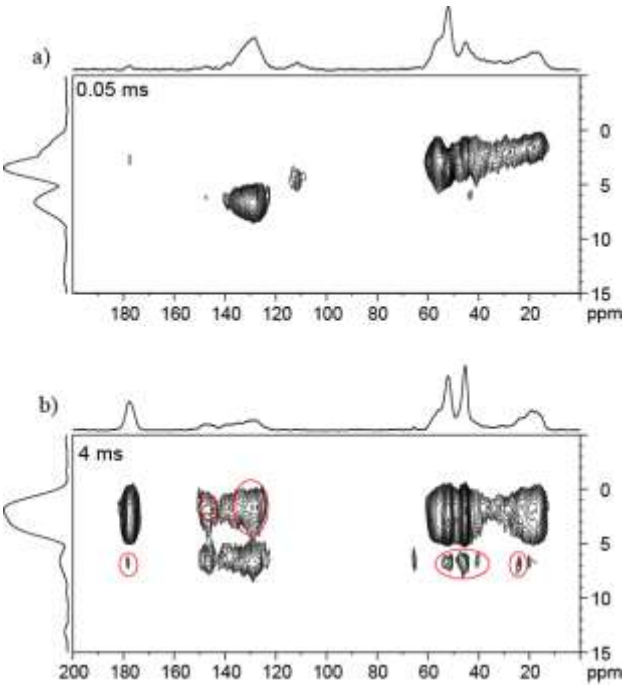

Figure 3.21. 2D ^{1}H-^{13}C SS NMR of the PAFMePI-*b*-PMMA at contact time of a) 0.05 ms and b) 4 ms. In the red circles are evidenced the cross-peaks by the interaction between porous matrix, PI and PMMA.

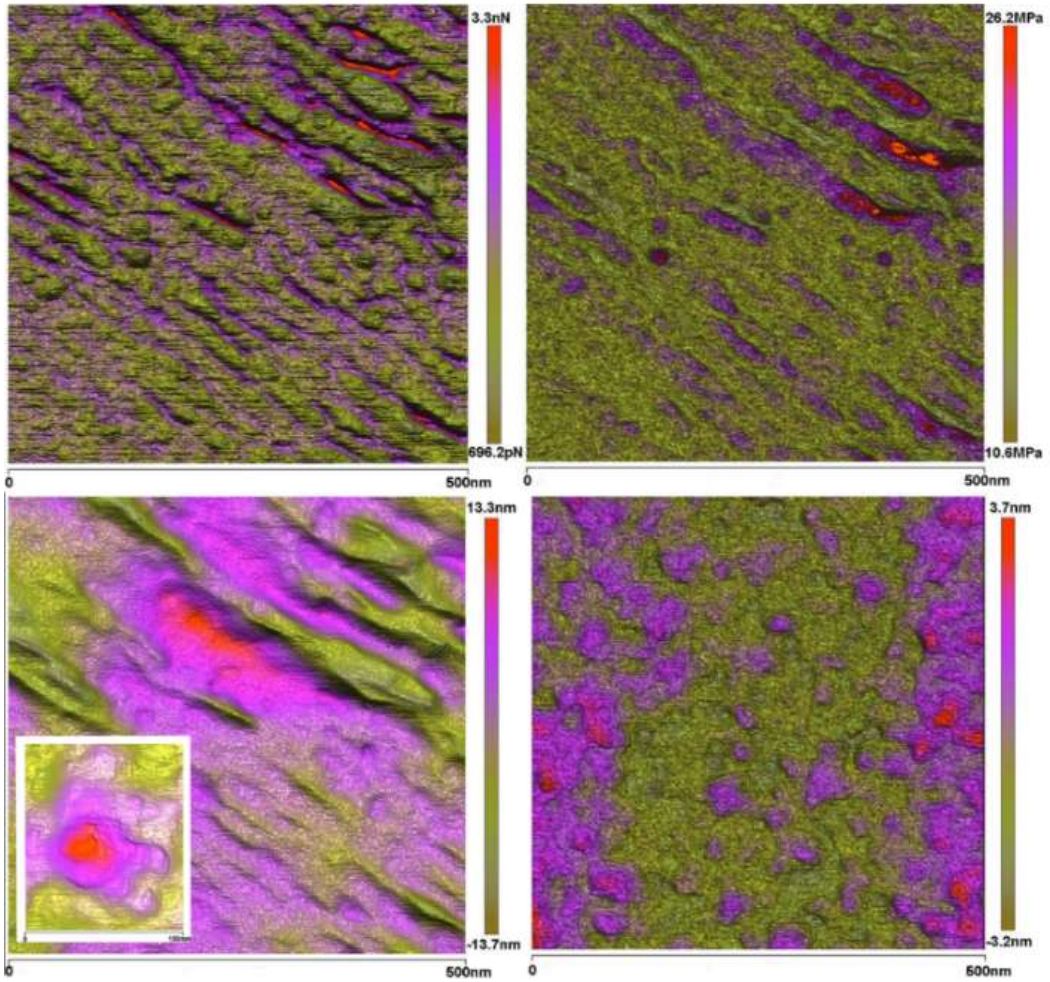

Figure 3.22. AFM images of nanocomposite block-co-polymer PAFMe-PI-*b*-PMMA and the matrix; on the top the modulus (left) and the adhesion (right) studies on PAFMe-PI-*b*-PMMA; on the bottom the height sensor of the nanocomposite (left) with a zoomed volcano, compared with the spotting matrix (right).

Further evidence is given by the DLS analysis of the three polymerization steps, the comparison between PAFMe, PAFMePI and PAFMePI-*b*-PMMA shows that in the case of PAFPI the particle distribution is enlarged with respect to the matrix and the copolymer composite (Fig. 3.23). Therefore, the particles are not uniform after PI for the different chains that are formed between internal polymer, external polymer and polymer that grows form inside to the outside.

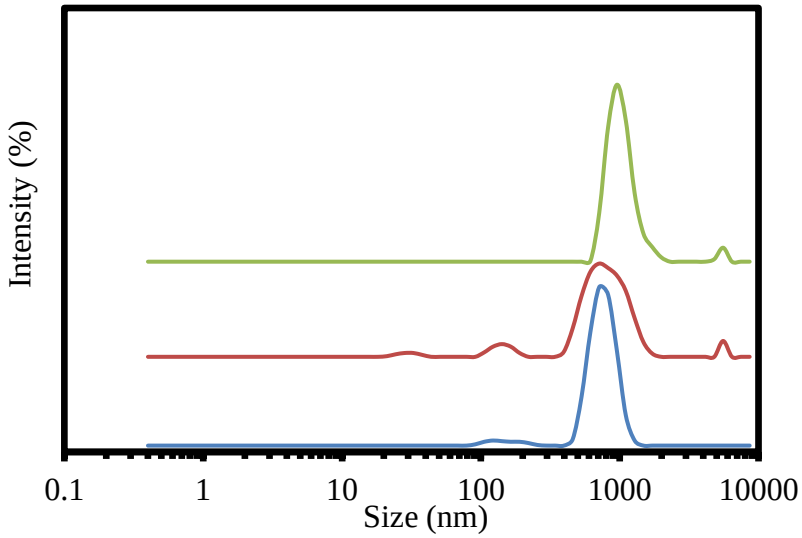

Figure 3.22. DLS analysis of the PAFMe (blue curve), PAFMePI (red curve) and PAFMePI-*b*-PMMA (green curve) in THF dispersion.

3.3| Thermal evolution of polyacrylonitrile in nanochannels MOFs

Compared to traditional porous matrices, MOFs are of particular interest due to their design structures; the size, shape and surface functionality of the nanochannels can be adjusted by modifying the combination of organic ligands and metal ions. These features have attracted scientists to design MOFs for applications in the science of polymeric materials [34]. The polymerization of the monomers encapsulated in nanospaces designed based on MOFs can lead to polymeric materials with desirable structures, which can be considered as tailor-made polymerization systems. Furthermore, the confinement of polymers in nanospaces allows the modification and treatment of polymer chains in conditions that would not be permitted with a bulk polymer.

In this detail, a highly studied polymer is polyacrylonitrile (PAN); this polymer is the most used precursor for the development of carbon fibres. In fact, through heat treatments at different temperatures, this polymer undergoes structural changes that convert the polymer chains into a two-dimensional extension of aromatics carbon atoms similar to graphene (Fig. 3.24) [35].

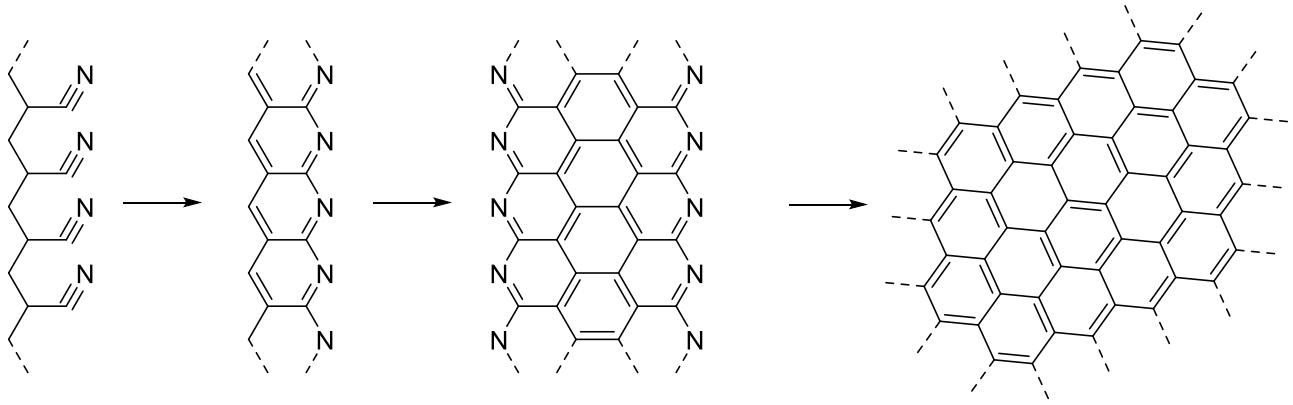

Figure 3.24. Thermal reaction of PAN.

The conversion takes place in three-steps at increasing temperatures and under different conditions: stabilization (200—300 °C), carbonization (400—1300 °C) and graphitization processes (around 1500—3000 °C). During these treatments, the PAN gradually loses nitrogen until it has a predominantly carbon structure. Among the three steps, the most important is the stabilization of the precursors that occurs in bulk PAN at 270 °C; this process can take place both in air and in nitrogen. One of the main problems of this process are intercrosslink reactions, these reactions lead to defects in the ladder polymer, which in the following steps are removed, however, creating cracks and weak points in the carbon fibre structure that reduces its tensile properties. [35] Moreover, the presence of defects decreases the conversion weight yield, as they are removed through degradation in small volatile molecules. To remedy this problem, extensive research has been carried out and one of the most used methods at industrial level is the stretching of polymer chains before heat treatments, in order to reduce the number of defects during stabilization. However, using porous materials with channels it is possible to encapsulate individual PAN chains thus avoiding intercrosslink processes.

Subsequently, the formation and thermal evolution of the PAN within porous channels of MOFs will be illustrated.

3.3.1| Experimental part

The reactors used for the production of the PAN were chosen by looking among the MOFs that present a structure with pores in the channels and with pore size comparable with those of the PAN chains. In particular, two MOFs of aluminium have been chosen, which generally have a high degradation temperature, so they allow the thermal treatment of the PAN inside them. The MOFs chosen were the DUT4 and the DUT5 (Fig. 3.25) synthesized by Kaskel's group [36], these two MOFs have channels with dimensions that allow allocating within them a chain (DUT4) or two chains (DUT5) of PAN. The synthetic procedure used is the same as reported in Kaskel's article and is as follows.

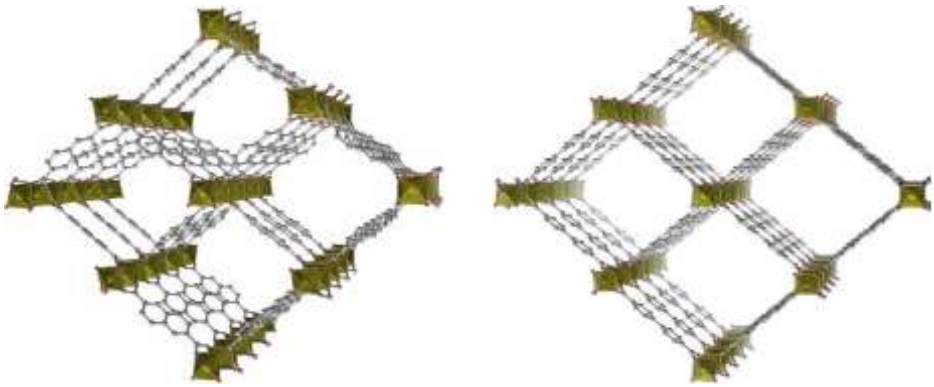

Figure 3.25. Structure of DUT4 (left) and DUT5 (right).

Synthesis of DUT4: 2,6-naphthalene dicarboxylic acid (0.26 g, 1.2 mmol) was dissolved in DMF (30 ml). $Al(NO_3)_3 \cdot 9H_2O$ (0.52 g, 1.4 mmol) was added and the mixture was filled in a 250 ml

Teflon liner, placed in an autoclave, heated to 120 C for 24 h and cooled to room temperature. After the product was separated by centrifugation, the sediment was washed with DMF for three times. The product was dried on air. Yield: 0.43 g (90.5%).

Synthesis of DUT5: 4,4'-biphenyldicarboxylic acid (0.26 g, 1.07 mmol) was dissolved in DMF (30 ml). $Al(NO_3)_3 \cdot 9H_2O$ (0.52 g, 1.4 mmol) was added and the mixture was filled in a 250 ml Teflon liner, placed in an autoclave, heated to 120 C for 24 h and cooled to room temperature. After the product was separated by centrifugation, the sediment was washed with DMF for three times. The product was dried on air. Yield: 0.49 g (95.6%).

To confirm the structure, the MOFs were analysed by powders XRD and the diffraction patterns compared with those reported by Kaskel (Fig. 3.26).

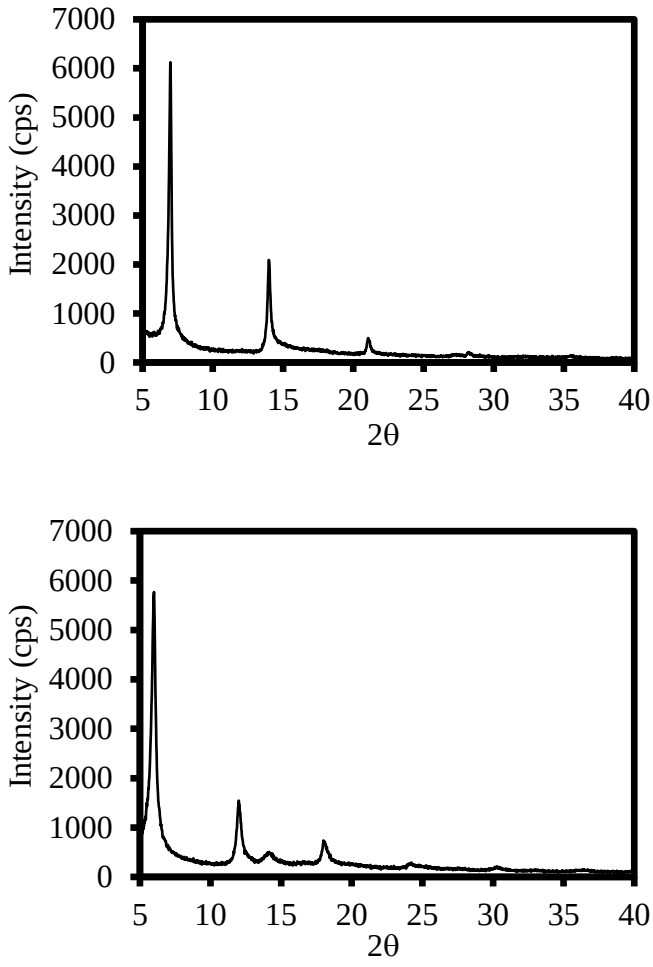

Figure 3.26. XRD analysis of DUT4 (up) and DUT5 (down).

Synthesis of PAN in the MOFs: the MOFs (800 mg) were previously degassed in vacuum at 140 °C for 4 h. At the MOFs were added a solution with AIBN (14 mg) and acrylonitrile (2 ml), the monomers excess was removed in vacuum (8 kPa) at room temperature for 1 h. Subsequently, the mixture was heated at 100 °C for 24 h. After the cooling, the composites were washed with methanol and dried at 80 °C in vacuum.

3.3.2| Results and discussion

After polymerization inside the pores, the composites do not lose their crystallinity as shown by the XRD analysis (Fig. 3.27), the diffractogram of the composite is the same as that of the starting MOF without evidence of new diffraction peaks in particular at 17° typical of the hexagonal cell of the PAN [37]. It is therefore absent some polymer outside the porous matrix. There is a variation in the relative intensities of the peaks; this is due to the presence of the polymer inside the pores, which increases the amount of atoms within the pore, thus modifying the intensity of the peaks.

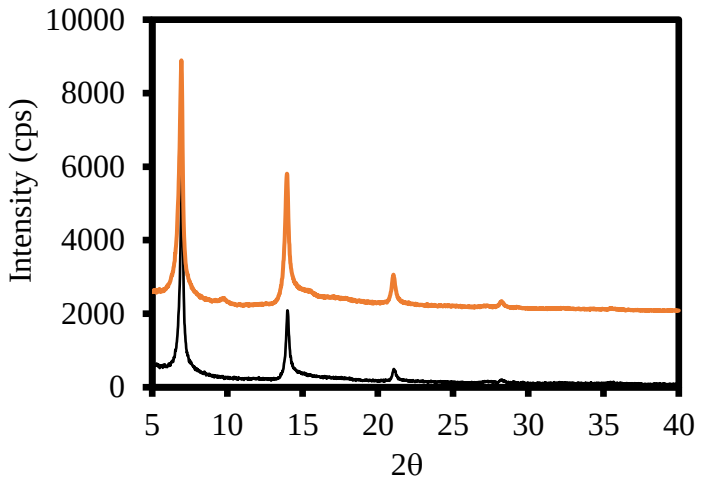

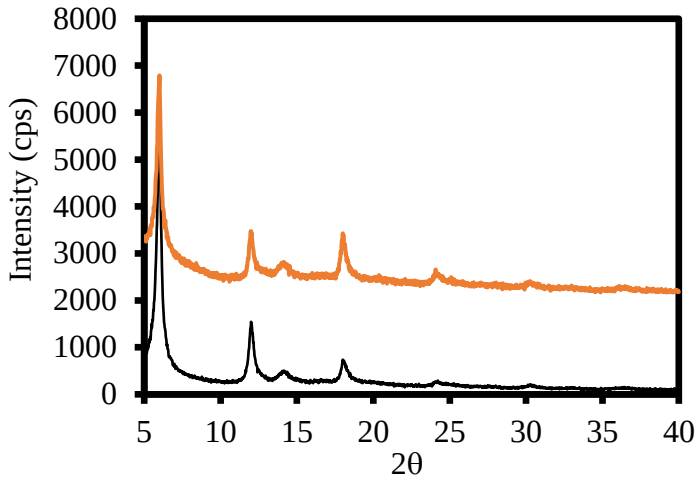

Figure 3.27. XRD pattern of composites (orange curves) compare with the MOFs (black curves). In the up the DUT4 and down the DUT5 systems.

The presence of the polymer in the pores is confirmed by thermogravimetric analyses, which show a weight loss at 350 °C, not present in MOFs (Fig. 3.28), this weight loss is due to the cyclization process with evolution of H_2O. The TGA allows estimating the amount of polymer that is about 10% for DUT4 and 13 % for DUT5. The differential thermal analysis (DTA) confirms the absence of polymer outside (Fig. 3.28). In fact, the presence of polymer outside the MOFs would generate an exothermic reaction that instead is absent in the confined polymer; this is probably due to confinement in these MOFs that can retain the heat released by the cyclization of PAN when it is inside them.

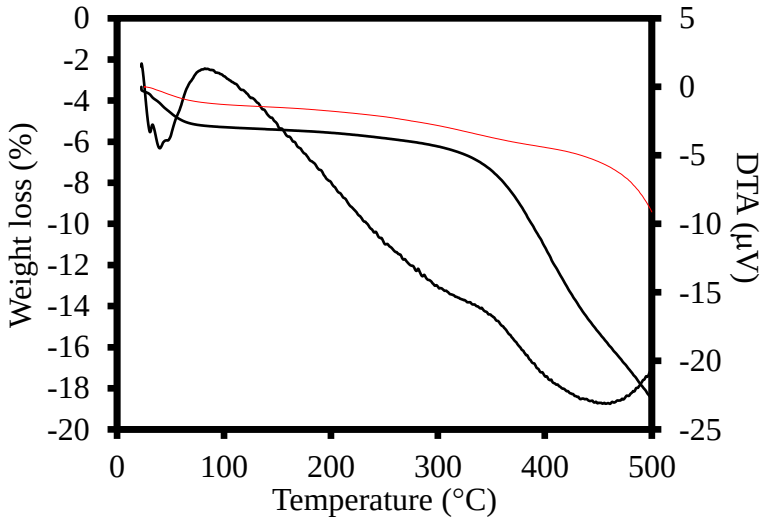

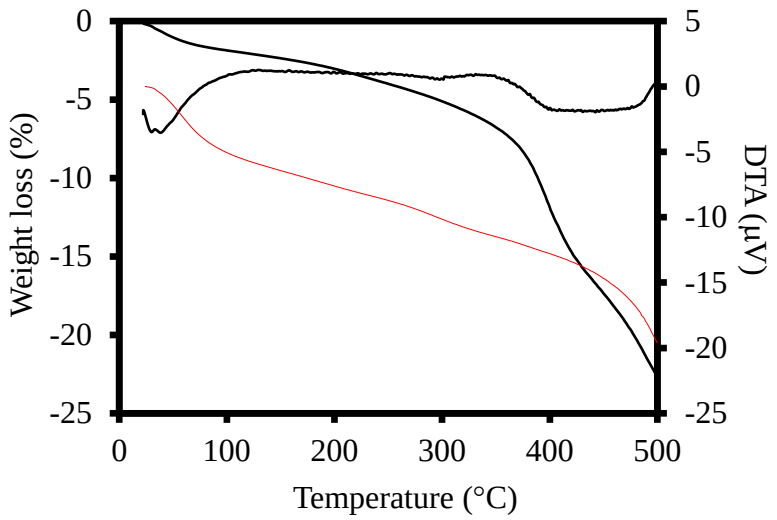

Figure 3.28. TGA and DTA of the composite (black curves) with DUT4 (up) and DUT5 (down). The red curves are the DUT4 and DUT5.

The N_2 adsorption at 77 K (Fig. 3.29) has confirmed the presence of the polymer inside the channels, the adsorption of the two MOFs is clearly decreased compared to before the polymerization, this for the presence of the polymer inside the channels, reducing the space accessible to the gas.

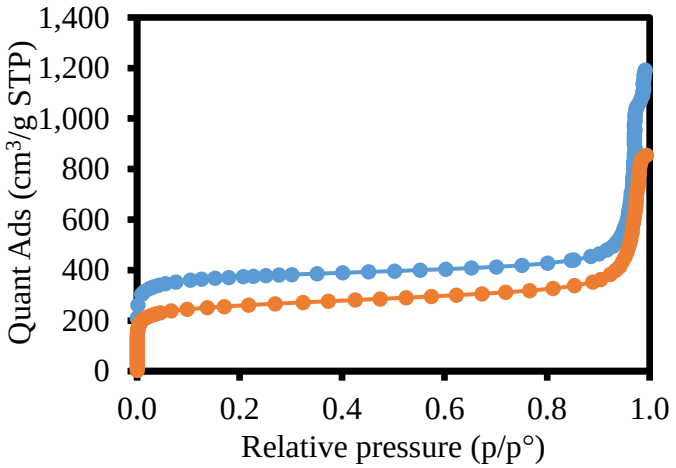

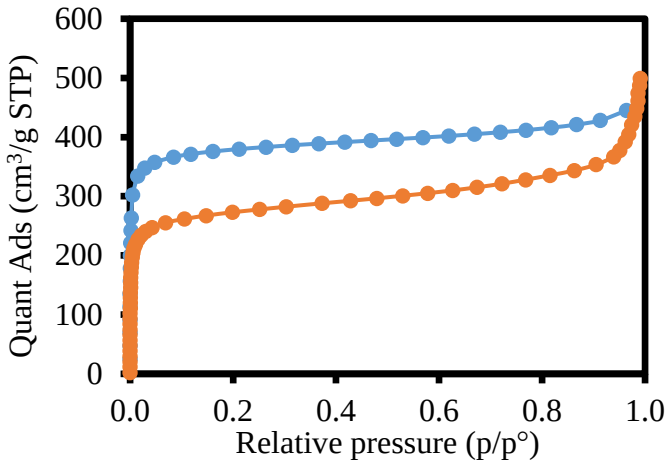

Figure 3.29. N_2 adsorption isotherms at 77 K in the up the DUT4 system and down the DUT5 system. The blue curves are the MOFs and the orange curves are the composites.

Treatment with a 0.05 M EDTA solution for two days allows the removal of frameworks and the isolation of the PAN chains. The polymers isolated from the MOFs show the same typical properties of a radical polymerization, for which the MOFs do not influence the growth of the polymer inside the pores. The isolated polymers have a diffraction pattern equal to that of the bulk PAN (Fig. 3.30). The liquid NMR ^{13}C (Fig. 3.31) allowed to derive the tactics of the polymers; the polymers were typical results of a PAN grown radically and have an atactic conformation.

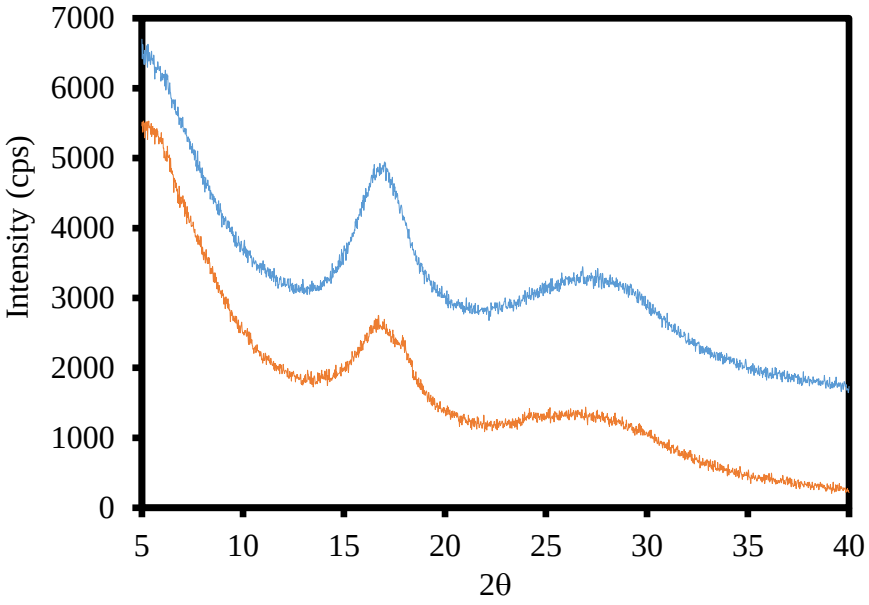

Figurer 3.30. XRD pattern of the PAN isolated from DUT4 (blue curve) and DUT5 (orange curve).

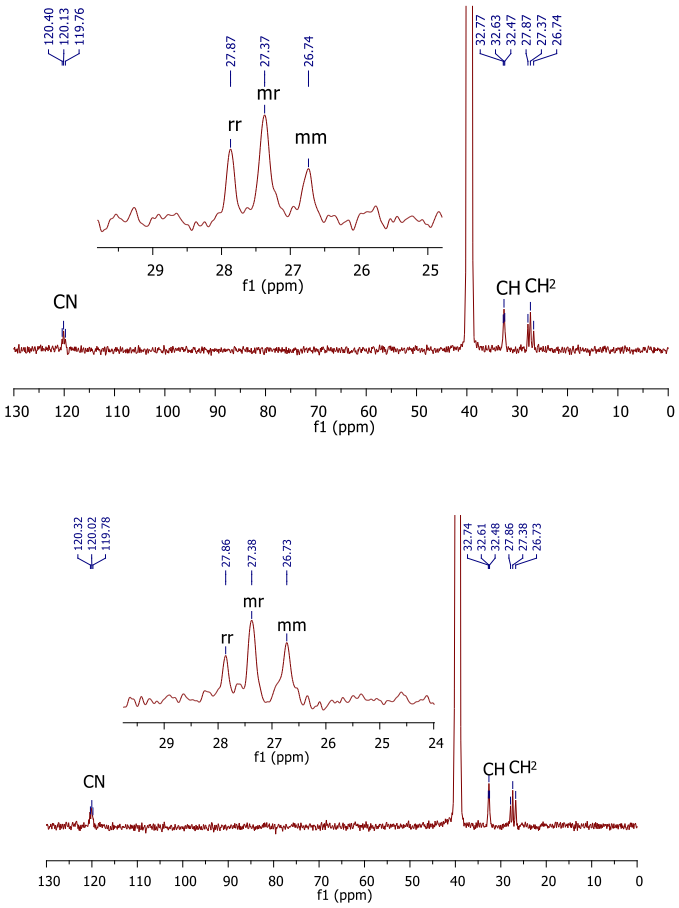

Figure 3.31. ^{13}C liquid NMR in DMSO-d_6 of PAN isolated from DUT4 (up) and DUT5 (down). In evidence, the peaks of CH_2 group with respective dyads.

The ladder polymer was synthesized by heating the composites at 280 °C for 24 h in air. The presence of air is important for obtaining the cyclized form of the stabilization process, as seen in the previous section. After the heat treatment, the structure of MOFs is preserved as evidenced by the maintenance of the diffraction pattern (Fig. 3.32), this is an interesting result, since it indicates the possibility of using this MOFs for the stabilization process of carbon fibres, without the reactor is involved and therefore without creating structures that generate defects in the ladder polymer.

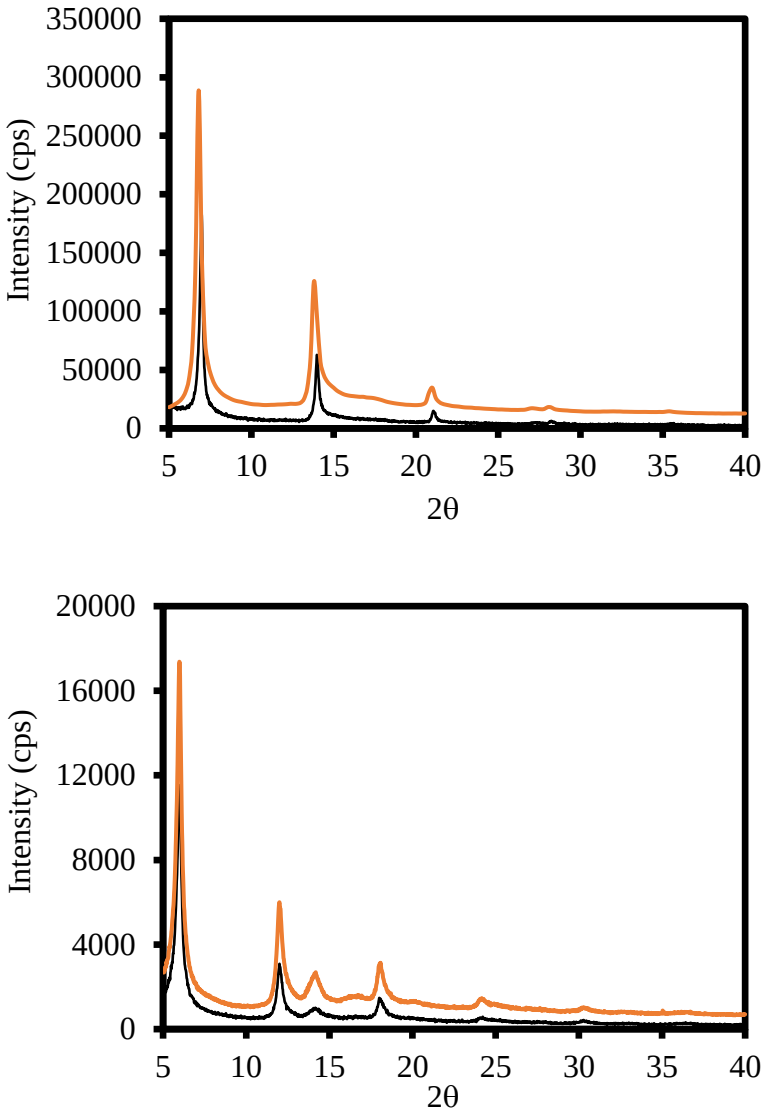

Figure 3.32. XRD pattern of the composites with ladder polymers (orange curves) compared with the DUT4 (up) and DUT5 (down).

The ladder polymers were isolated with the same treatment described for the PAN. The EDX analysis on ladder polymers revealed the presence of a large amount of aluminium (Fig. 3.33) that has not been removed with EDTA treatment. The removal of aluminium was carried out with a 0.1 M HCl treatment confirmed by the EDX analysis performed after treatment (Fig. 3.34).

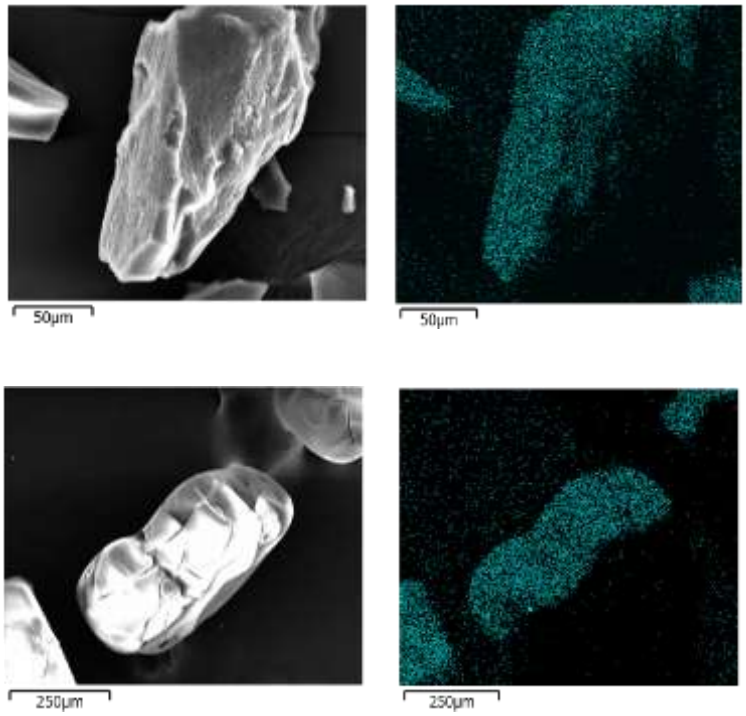

Figure 3.33. SEM imagines and EDX Al mapping of LP isolated from DUT4 (up) and DUT5 (down) before the treatment with HCl.

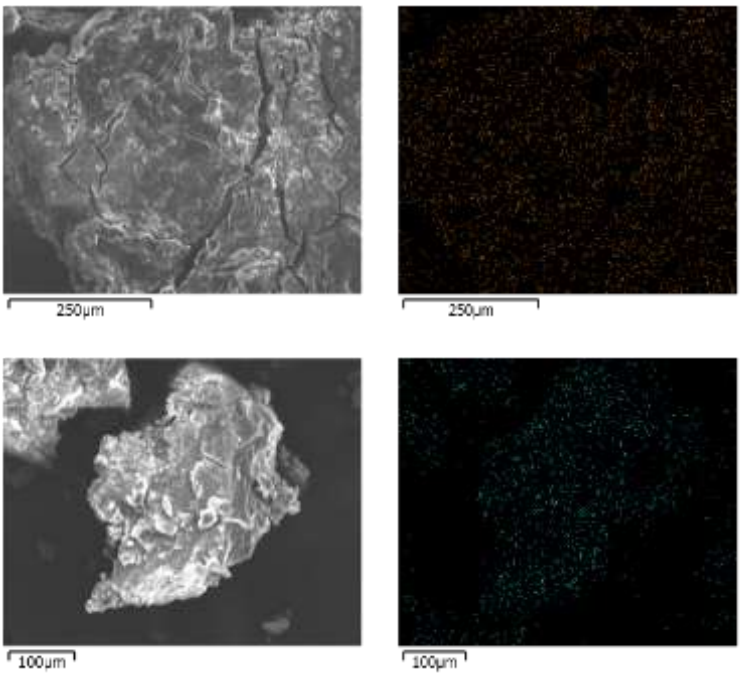

Figure 3.34. SEM imagines and EDX Al mapping of LP isolated from DUT4 (up) and DUT5 (down) after the treatment with HCl.

The structural modification of PAN after heat treatment is detected by the powder diffraction pattern. The diffractogram shows the disappearance of the 17° peak associated with the hexagonal/rhombohedral cell of the PAN and appears a peak enlarged to about 27° typical of the π–π

stacking of aromatics carbon systems (Fig. 3.35) [38]. This peak identifies the plane associated with the Miller indices (002), which indicate the formation of a condensed aromatic structure, which is packed by interaction between π orbitals with a structure similar to that of graphite. If the two ladder polymers are compared with a ladder polymer synthesized in the same conditions but in bulk, it is noted that the bulk ladder polymers still has the peak at 17° identifying the structure of the PAN. Therefore, it is evident how the ladder polymers synthesized in the MOFs have a structure with fewer defects than the synthesized in bulk.

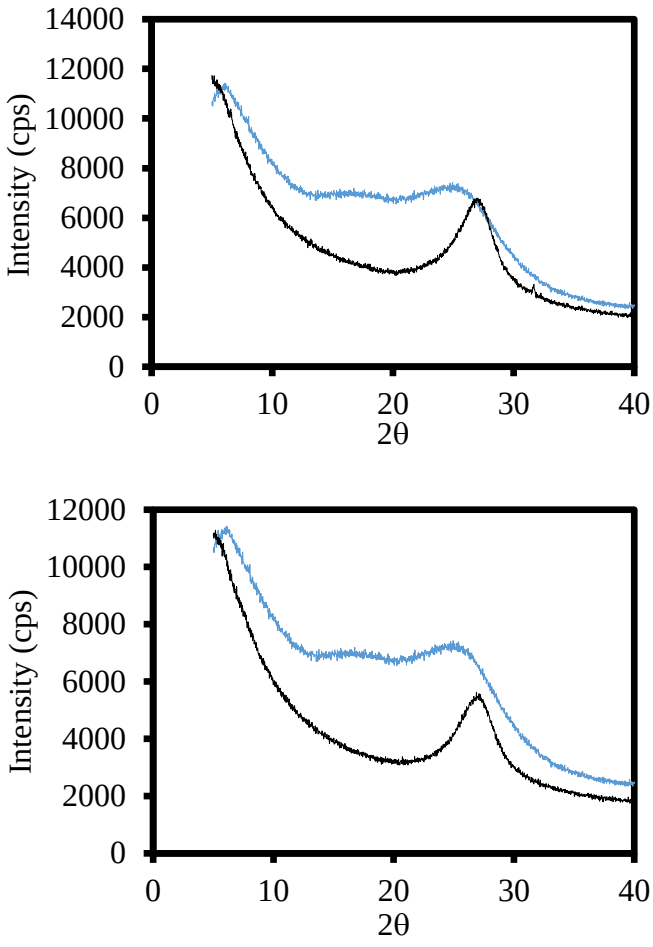

Figure 3.35. XRD patterns of ladder polymers (black lines) isolated from DUT4 (up) and from DUT5 (down). The blue curves are the bulk ladder polymer.

The confirmation of a higher conversion in ladder polymers within MOFs compared to bulk is from the IR spectrum. The IR of the ladder polymers synthesized within the MOFs, show the disappearance of the peak at about 2240 cm^{-1} (Fig. 3.36) typical of the stretching of the C≡N group

characteristic of the PAN. In fact, during the phases of stabilization in air the triple C≡N bond is converted into a double C=N link delocalized on the aromatic structure.

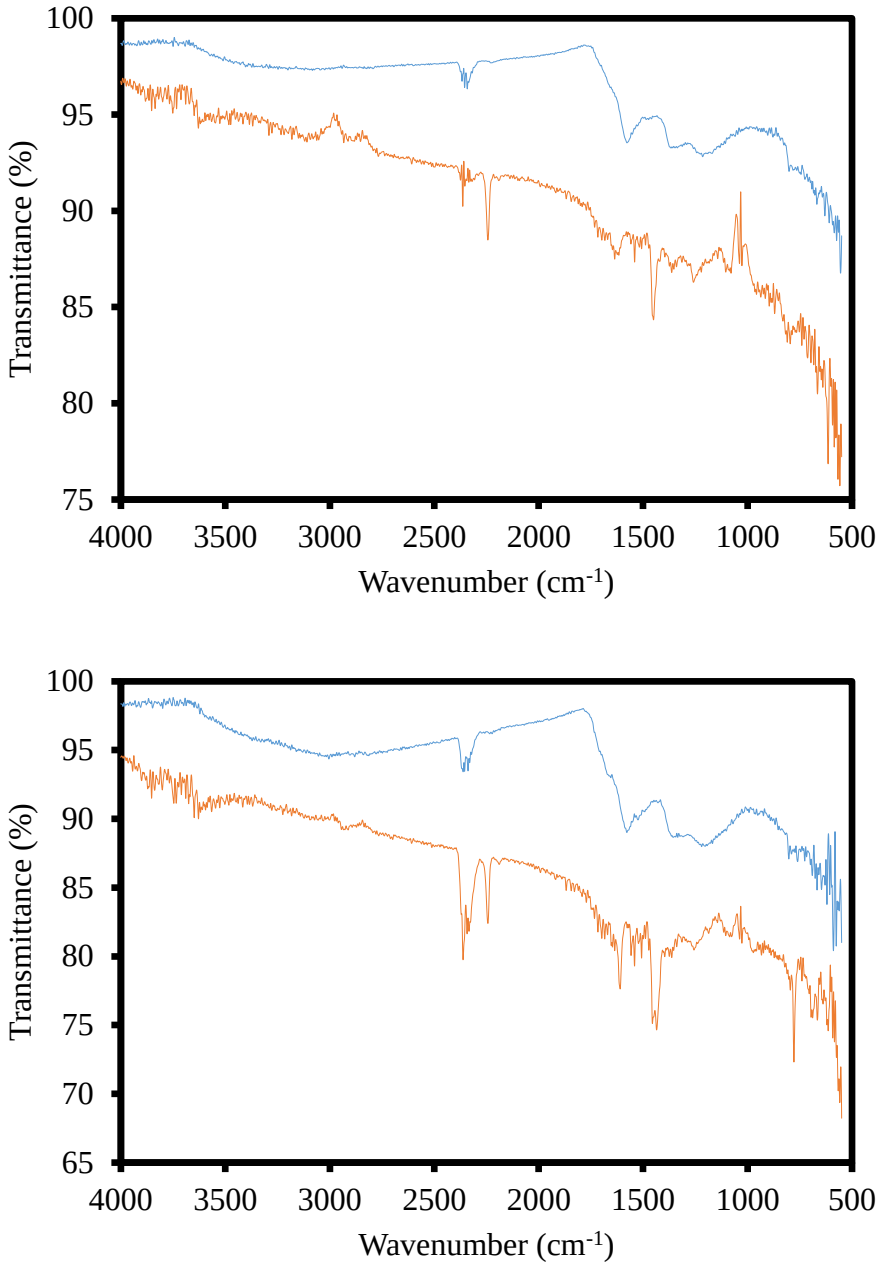

Figure 3.36. IR spectrums of ladder polymers (blue curves) and PAN (orange curves) for the system DUT4 (up) and DUT5 (down).

The Raman spectroscopy is a powerful tool to characterise the nanostructure of carbon materials, since each different carbon material shows its own spectral line shape in their Raman spectra. In addition to this, the spectral line shape of the carbon materials changes drastically depending upon the excitation wavelengths and this dependence can be used as a unique finger-print

for identifying the type of carbon materials [39]. In Raman spectroscopy of the carbon systems, there are two significant peaks one at about 1300 cm^{-1} indicated as D band and one at about 1500 cm^{-1} indicated as G band. These two peaks are associated with the presence of defects; in fact, the G band it is due to the vibration in the plane of the sheets of the fibre, instead the band D is associated to the presence of defects. Usually the intermediate phases of the thermal processes that lead to the carbon fibres are compared through the intensity ratio of these bands, in particular I_D/I_G and comparing the bandwidth. With this premise, the ladder polymers isolated from the MOFs show a more orderly structure than the bulk synthesized ladder polymer. In fact, the Raman spectrum (Fig. 3.37) shows that for the polymers ladder synthesized by the MOFs the relative intensity of the G band with respect to the D band is a little bit intense than the bulk ladder polymers. As far as the bandwidth is concerned, however, the ladder polymers synthesized by the MOFs have a lower bandwidth indicating the lower presence of defects.

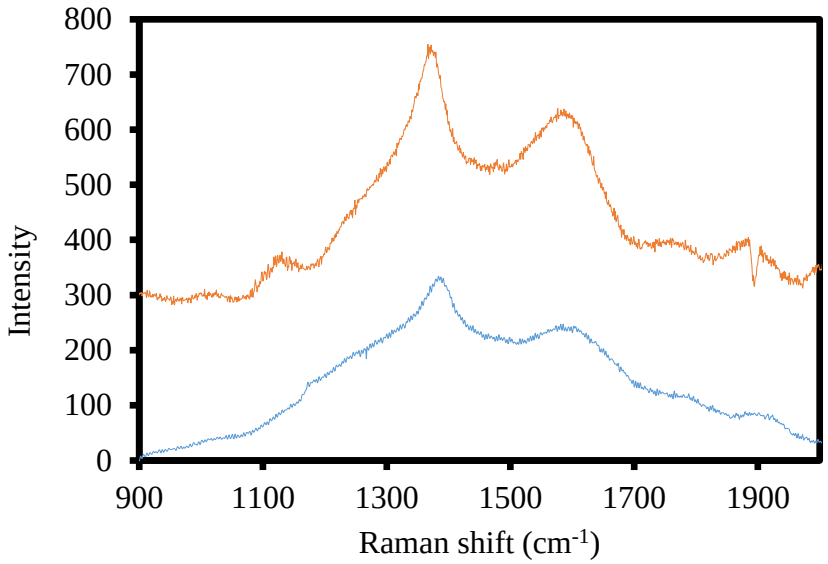

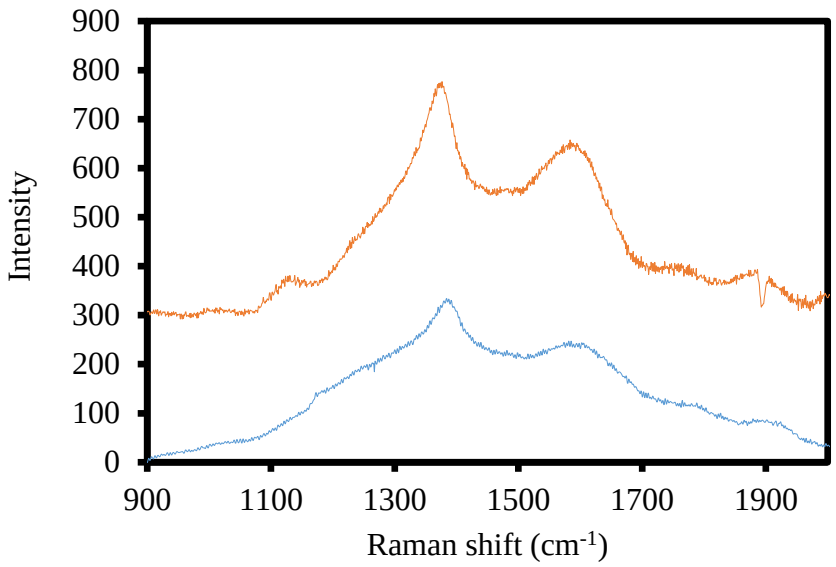

Figure 3.37. Raman spectrums of isolated ladder polymers (orange curves) from DUT4 (up) and DUT5 (down) and bulk ladder polymer (blue curves). Excitation wavelenght 531.9 nm.

The confirmation of the reduced presence of defects is highlighted by the thermogravimetric analysis associated with the mass (TG-MS). The TG-MS analysis at 410 °C (Fig. 3.38) shows that for the polymer synthesized in bulk there is the emission of small organic molecules such as acetonitrile, propene, methacrylonitrile and CO_2, these are associated with the defects that during the heat treatments are burned and expelled from the structure [40]. In the polymers ladder synthesized in the MOFs, however, these molecules are not released during heating, indicating the lower presence of defects.

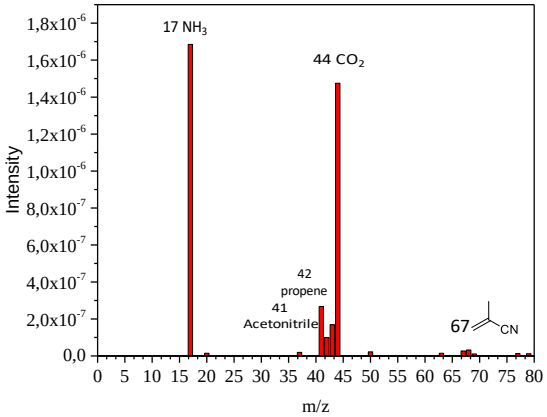

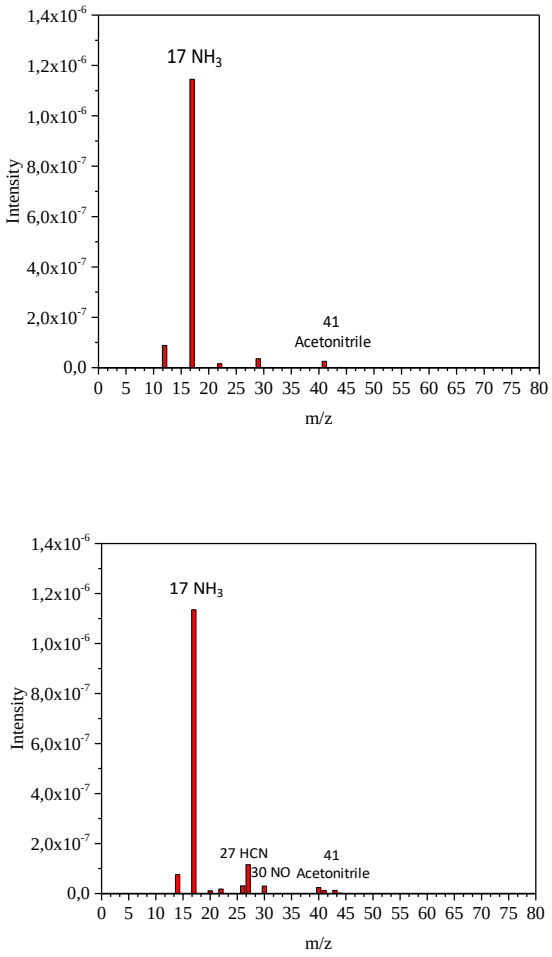

Figure 3.38. TG-MS analysis of bulk ladder polymer (up), and ladder polymers isolated from DUT4 (middle) and DUT5 (down) at 410 °C.

This evolution of gas with higher molecular weights in the case of bulk is further demonstrated by the weight loss of the TGA (Fig. 3.39). In fact, the analysis shows how for the ladder polymers synthesized in the MOFs the weight loss is lower than 900 °C (33 % DUT4 and 29 % DUT5) compared to bulk (40.5 %); confirming a structure with fewer defects if synthesized in nanoreactors.

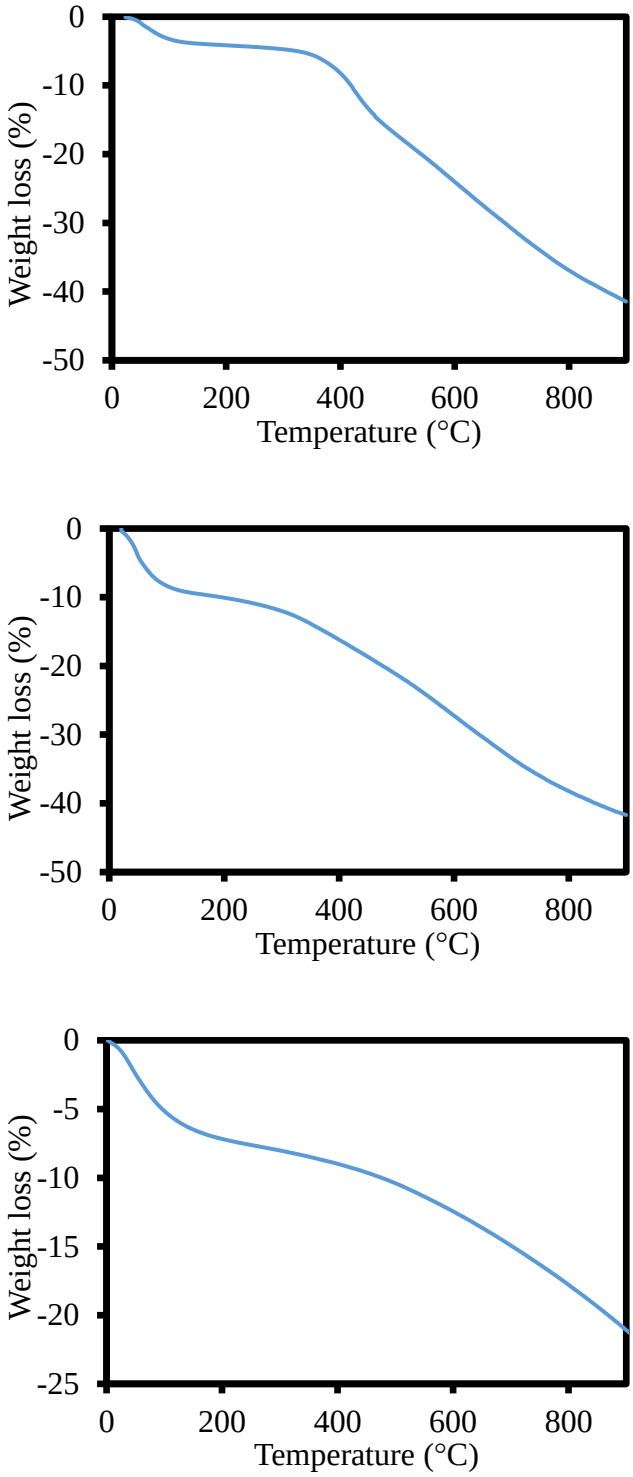

Figure 3.39. TGA of bulk ladder polymer (up), the ladder polymers isolated from DUT4 (middle) and DUT5 (down) until at 900 °C.

The confirmation of the best structure of the ladder polymers synthesized in the MOFs compared to the bulk comes from the SS NMR. The NMR spectra of the three samples have a complex structure in the aromatic part of the peaks associated with the condensed form of the aromatic carbon structure (Fig. 3.40). In addition, in all three samples there is a peak associated with the C=O

bond (176 ppm), relative to the introduction of oxygen during the stabilization phase of the fibres. In the aliphatic area, the bulk ladder polymer shows the presence of aliphatic peaks due to the incomplete aromatization of the structure, which generate the organic molecules found in the TG-MS. The two ladder polymers synthesized in the MOFs instead show a different spectrum in the aliphatic part. The sample synthesized in DUT5 does not show aliphatic peaks, a sign of a complete aromatization of the structure, which confirms the lower weight loss after heating to 900 °C. The sample synthesized in DUT4 instead, still has some peaks associated with an incomplete aromatization. Probably this is due to the size of the pore, which does not allow the chain to rearrange during stabilization, but may also be due to the structure of the ladder polymers which having a distortion caused by the difference in bond length of C=N compared to C=C generates these defects. Another relevant point is the peak at 107 ppm; this peak is associated with isolate double bonds and is present only in the bulk ladder polymer, which confirms the best aromatization process in the ladder polymers synthetized in the MOFs.

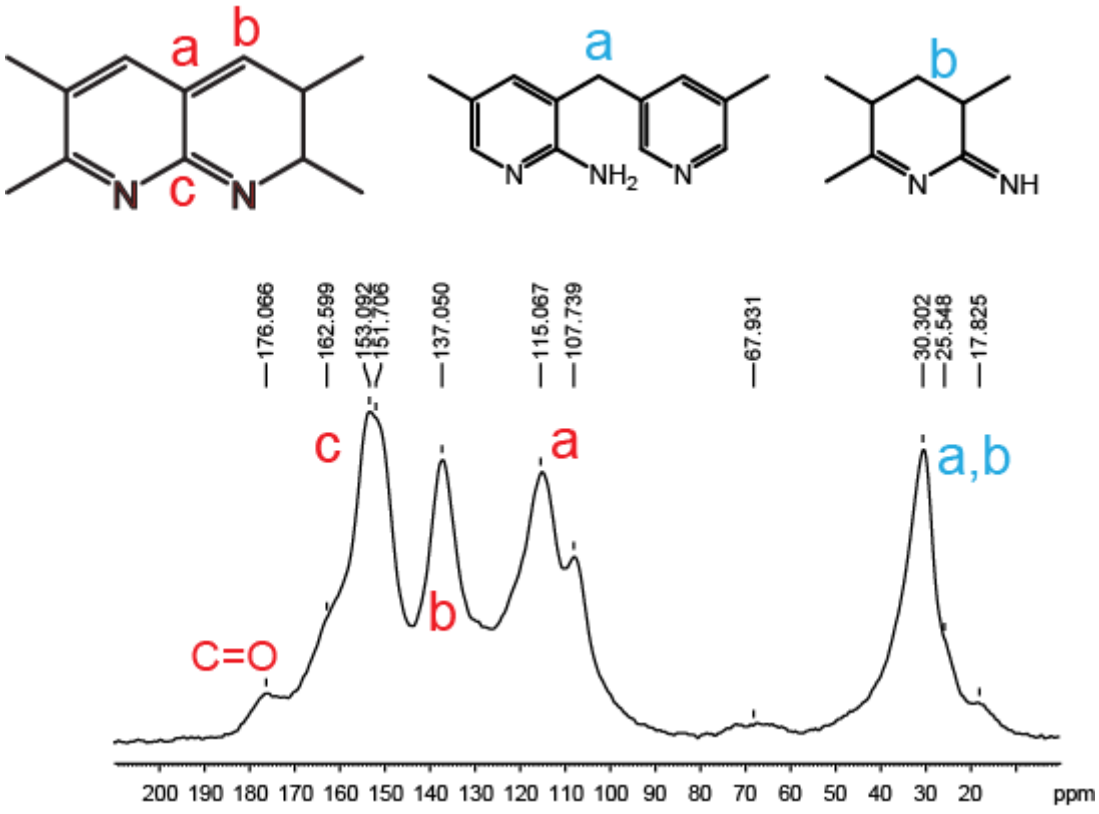

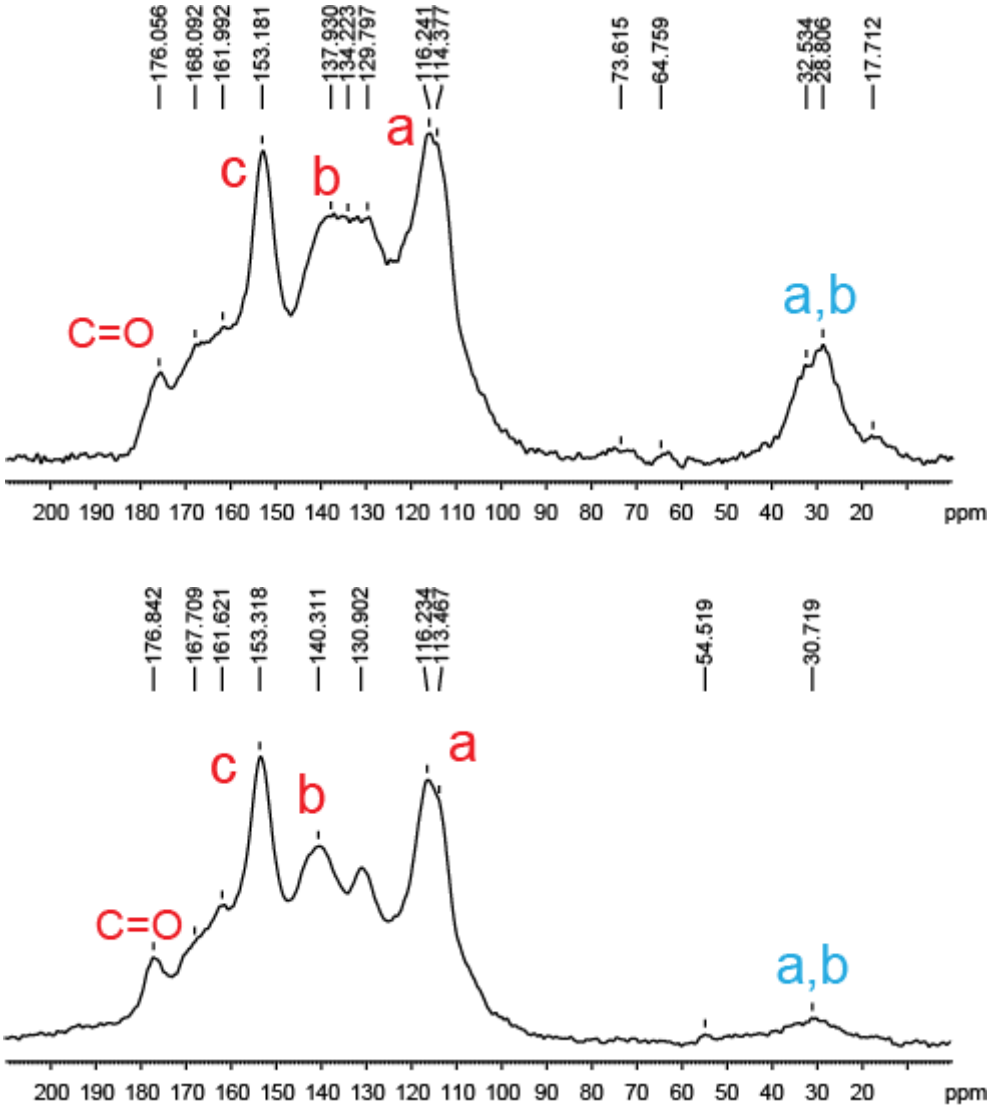

Figure 3.40. ^{13}C CP MAS NMR analysis of the three ladder polymers. In the up the bulk ladder polymers, in the middle the ladder polymer synthetized in the DUT4 and in the down the ladder polymer synthetized in the DUT5.

3.4| Conclusion

A challenge in polymer materials science remains the complete control of the arrangement of monomers to be polymerized into materials in order to improve mechanical

and physical properties of the final product for industrial applications. As for enzymatic catalysis where in regulated molecular nanospace the reaction occur in a stereoselective and chemoselective way, nowadays scientists try again to mimic nature in confined spaces, designing 3D porous hosts for the synthesis of functional polymeric materials with controlled nanostructures that show specific nanospace effects.

In the first part of my work the anionic confined polymerization in nanospaces have been successfully conducted in PAFs systems for the first time. This technique allows the development of new technologies based on purely organic materials. The implementation of a polymerization that allows the fast and easy development of polymers with specific tacticity such as anionic polymerization. The development of block copolymers, which are important polymers at the technological level, just think of the styrene-butadiene rubbers that do not require vulcanization because of the styrene blocks that act as cross-linkers in the material. Moreover, the use of purely organic materials as reactors can be a future development for the production of completely organic nanocomposites going to overcome the problems of chemical affinity that you have with common fillers such as silica nanoparticles. The development of the anchored composite also makes it possible to improve the affinity by creating a chemical bond between filler and polymer, preventing it from being blending. Furthermore, the anchoring has led to polymers with different tacticity than the classic anionic polymerization, which would occur only under certain synthetic conditions, I learn the way to using PAFs as reactors for controlling the growth of the polymer.

In the second part of my work, moreover, the use of thermally stable Al MOFs allowed the use of nanochannels as reactors for the development of the stabilization process of the PAN for the development of carbon fibres with higher yields and fewer defects could affect the final rheological properties of carbon fibre. Moreover, the development of conjugated polymers systems can be used for the implementation of new conductive plastics. This second part of the work is in fact still under development in two directions. The first is the study of the electrical

conduction properties of the ladder polymers synthesized in the MOFs, going to study the behaviour of the charge carriers inside the material. The second one, instead, focuses on the subsequent thermal treatments of the precursor, in order to develop a new synthetic way for the carbon fibres with improved properties compared to those now present.

References

[1] J. F. Brown e D. M. White, *J. Am. Chem. Soc.*, vol. 82, p. 5671, **1960**.

[2] D. M. White, *J. Am. Chem. Soc.*, vol. 82, p. 5678, **1960**.

[3] M. Farina, G. Audisio e G. Natta, *J. Am. Chem. Soc.*, vol. 89, p. 5071, **1967**.

[4] H. R. Allcock, E. N. Silverberg e G. K. Dudley, *Macromolecules*, vol. 27, p. 1033, **1994**.

[5] T. Uemura, R. Nakanishi, S. Mochizuki, S. Kitagawa e M. Mizuno, *Angew. Chem. Int. Ed.*, vol. 55, p. 6443, **2016.**

[6] G. Distefano, A. Comotti, S. Bracco, M. Beretta e P. Sozzani, *Angew. Chem. Int. Ed.*, vol. 51, p. 9258, **2012**.

[7] S. M. Ng, S. I. Ogino e T. Aida, *Macromol. Rapid. Commun.*, vol. 18, p. 991, **1997**.

[8] K. Kageyama, J. Tamazawa e T. Aida, *Science*, vol. 285, p. 2113, **1999**.

[9] P. Sozzani, S. Bracco, A. Comotti, R. Simonutti, P. Valsevia, Y. Sakamoto e O. Terasaki, *Nature Materials*, vol. 5, p. 545, **2006**.

[10] S. A. Johnson, D. Khushalani, N. Coombs, T. E. Mallouk e G. A. Ozin, *J. Mater. Chem.*, vol. 8, p. 13, **1998**.

[11] D. J. Cardin, *Adv. Mater.*, vol. 14, p. 553, **2002**.

[12] T. Bein e P. Enzel, *Angew. Chem. Int. Ed.*, vol. 28, p. 1692, **1989**.

[13] T. Uemura, N. Yanai e S. Kitagawa, *Chem. Soc. Rev.*, vol. 38, p. 1228, **2009**.

[14] T. Uemura, Y. Ono, K. Kitagawa e S. Kitagawa, *Macromolecules*, vol. 41, p. 87, **2008**.

[15] T. Uemura, D. Hiramatsu, Y. Kubota, M. Takata e S. Kitagawa, *Angew. Chem. Int. Ed.*, vol. 46, p. 4987, **2007**.

[16] T. Uemure, T. Kaseda, Y. Sasaki, M. Inukai, T. Toriyama, A. Takahara, H. Jinnai e S. Kitagawa, *Nature Comm.*, vol. 6, p. 1, **2015**.

[17] C. Pei, T. Ben e S. Qiu, *Mater. Horiz.*, vol. 2, p. 11, **2015**.

[18] A. Comotti, S. Bracco, M. Mauri, S. Mottadelli, T. Ben, S. Qiu e P. Sozzani, *Angew. Chem. Int. Ed.*, vol. 124, p. 10283, **2012**.

[19] Y. Yue, C. Zhang, Q. Tang, R. T. Mayes, W. P. Liao, C. Liao, C. Tsouris, J. J. Stankovich, J. Chen, D. K. Hensley, C. W. Abney, D. Jiang, S. Brown e S. Dai, *Ind. Eng. Chem. Res.*, vol. 55, p. 4125, **2016**.

[20] D. W. Lee e B. R. Yoo, *Journ. of Ind. and Eng. Chem.*, vol. 38, p. 1, **2016**.

[21] R. P. Quirk, Q. Zhuo, S. H. Jang, Y. Lee e G. Lizarraga, «Principles of Anionic Polymerization: An Introduction,» in *Application of Anionic Polymerization Research*, Orlando, Florida, R. P. Quirk, **1998**, pp. 2-27.

[22] P. Galka, J. Kowalonek e H. Kaczmarek, *J. Therm. Anal. Calorim.*, vol. 115, p. 1387, **2014**.

[23] V. A. Rozentsvet, A. S. Khachaturov e V. P. Ivanova, *Polymer Science, Ser. A,* vol. 51, p. 870, **2009**.

[24] M. Morton, Anionic Polymerization: Principle and Practice, Academic Press, **1983**.

[25] R. Krishnamoorti, R. A. Vaia e E. P. Giannelis, *Chem. Mater.*, vol. 8, p. 1728, **1996**.

[26] S. Bracco, A. Comotti, P. Valsesia, M. Beretta e P. Sozzani, *CrystEngComm*, vol. 12, p. 2318, **2010**.

[27] S. J. Garibay, M. H. Weston, J. E. Mondloch, Y. J. Colon, O. K. Farha, J. T. Hupp e S. T. Nguyen, *CrystEngComm*, vol. 15, p. 1515, **2013**.

[28] M. Farina, G. Disilvestro e P. Sozzani.Europe Patent 21726 a/84, **1984**.

[29] B. Wesslen e G. Mattsson, *J. of Polym. Sci.: Part A: Polym. Chem.*, vol. 28, p. 1033, **1990**.

[30] D. R. Burfield e K. L. Lim, *Macromolecules*, vol. 16, p. 1170, **1983**.

[31] A. K. Sircar, *Journ. of Therm. Anal.*, vol. 49, p. 293, **1997**.

[32] S. L. Malhotra, L. Minh e L. P. Blanchard, *J. of Macromol. Sci.-Chem.*, vol. A19, p. 579, **1983**.

[33] S. L. Malhotra, C. Baillet e L. P. Blachard, *J. of Macromol. Sci.-Chem.*, vol. A12, p. 1427, **1978**.

[34] T. Uemura, N. Yanai e S. Kitagawa, *Chem. Soc. Rev.*, vol. 38, p. 1228, **2008**.

[35] M. S. A. Rahaman, A. F. Ismail e A. Mustafa, *Polym. Degr. and Stab.*, vol. 92, p. 1421, **2007**.

[36] I. Senkovska, F. Hoffmann, M. Froba, J. Getzschmann, W. Bohlmann e S. Kaskel, *Micropor. and Mesopor. Mat.*, vol. 122, p. 93, **2009**.

[37] X. D. Liu e W. Ruland, *Macromolecules*, vol. 26, p. 3030, **1993**.

[38] L. Zhang, Y. Dai, Y. Kai e R.-G. Jin, *Carbon Letters*, vol. 12, p. 229, **2011**.

[39] H. Okuda, R. J. Young, D. Wolverson, F. Tanaka, G. Yamamoto e T. Okabe, *Carbon*, vol. 130, p. 178, **2018**.

[40] M. Surianarayanan, T. Uchida e M. Wakakura, *Journ. of Loss Prev. in the Proc. Ind.*, vol. 11, p. 99, **1998**.

Conclusion

This work has dealt with the use of porous materials in two different fields but highly studied in this period: the adsorption of gas and the polymerizations confined in nanospaces.

In the first part of the work on adsorption, purely organic materials were synthesized with two different synthetic techniques, generating materials with different chemical-physical characteristics. This part was treated as a screening of organic materials for high-pressure methane storage. Methane is a valid alternative to oil as a fuel due to the low CO_2 emissions. The difficulties in transporting CH_4 using pipelines and LNG have increased the development of CNG technology and technological innovation involves the use of porous materials to improve the efficiency and safety of transport. The synthesized materials are highly efficient from this point of view by storing within them quantities of CH_4 highly superior to those that the common technologies used are able to do. A particular aspect is the production cost of these porous materials that can be synthesized through simple and highly used reactions in industry such as Friedel-Crafts. Moreover, these materials are light and not dense, thus increasing the amount of methane transported without substantially increasing the weight of the container; in addition, they can be pressed in order to reduce their volume inside the transport container without decreasing storage performance. In the second part on adsorption, the main structure of the porous materials has been chemically modified, inserting different functional groups before the synthesis of the material, usually occurs post-synthesis of the material, in order to create specific interactions with different gases. The addition of the functional group has allowed the

creation of three structures with the same skeleton but with substantially different characteristics, leading to three materials that behave differently. The material consisting exclusively of C and H showed a great predisposition to high-pressure storage, due to its high pore capacity. The material with the hydroxyl groups proved to be highly microporous, probably due to a self-assembly during the synthesis phase coordinated by hydrogen bonds, its microporosity allows it to have a great interaction with the low pressure CH_4 bringing it to reach isosteric heat values close to the record. Instead, the material with amino groups showed a great affinity for CO_2, through the interaction between the moment of quadrupole CO_2 and the inert torque of N, this interaction is known and was confirmed for the first time through spectroscopy NMR that showed the interaction between CO_2 and amine at a low temperature.

The use of porous materials for the confinement of reactions among which the polymerizations results in a useful and finer control of the reactions through the use of narrow spaces that prevent the movements of the molecules, going to avoid the use of specific catalysts and to imitate the interaction that is present in the organisms between enzyme and substrate. Biomimetics is highly studied in this period and porous materials can be an approach on this subject. In the first part of the work it was demonstrated for the first time the possibility of performed the anionic polymerization in porous materials, this result open the way for the development of new confined synthetic routes and for the production in confined state of materials that could not be synthesized in other ways, such as block copolymers. After the experimental test of the success of the anionic polymerization, we went beyond using the porous matrix not only as a means for synthesis but also as an activator of the polymerization by previously generating anions in its structure. This opens the door to the development of new types of composite materials where the intimate correlation between the components is further accentuated by the interpenetration of the constituent materials and the entirely carboneous structure that prevent the parts from being blending, a problem found in the polymer composite materials. In the second part of the work on polymerization, instead the use of materials with controlled pores morphology allowed not only the polymerization inside them, generating isolated polymer chains, but also the

thermal transformation of the PAN in the first step for the development of carbon fibres. Carbon fibres are an exceptional material that is now present in many products used in our days. The primary precursor PAN must first be worked through various processes including spinning and stretching of polymer chains. In this work, it has been shown how this can be excluded from the production process by using porous materials consisting of channels that allow the presence of one chain at a time. Moreover, these channels allow the transformation of the polymer to form a ladder polymer with a better structure and with greater efficiency than the transformation into bulk. This leads to higher temperature treatments to carbon fibre with improved mechanical properties and higher yields, but at the same time, a flawless ladder polymer can be implemented in microelectronics, for the production of high performance organic microchips, as is happening for another similar carbonaceous material such as graphene.